IOWA STATE UNIVERSITY
Digital Repository

Retrospective Theses and Dissertations

Iowa State University Capstones, Theses and Dissertations

2006

Ultrafast solvation dynamics in room temperature ionic liquids and protein environments

Lindsay Elizabeth Sanders Headley
Iowa State University

Follow this and additional works at: https://lib.dr.iastate.edu/rtd

 Part of the Physical Chemistry Commons

Recommended Citation
Headley, Lindsay Elizabeth Sanders, "Ultrafast solvation dynamics in room temperature ionic liquids and protein environments " (2006). *Retrospective Theses and Dissertations*. 1261.
https://lib.dr.iastate.edu/rtd/1261

This Dissertation is brought to you for free and open access by the Iowa State University Capstones, Theses and Dissertations at Iowa State University Digital Repository. It has been accepted for inclusion in Retrospective Theses and Dissertations by an authorized administrator of Iowa State University Digital Repository. For more information, please contact digirep@iastate.edu.

www.manaraa.com

Ultrafast solvation dynamics in room temperature ionic liquids and protein environments

by

Lindsay Elizabeth Sanders Headley

A dissertation submitted to the graduate faculty

in partial fulfillment of the requirements for the degree of

DOCTOR OF PHILOSOPHY

Major: Physical Chemistry

Program of Study Committee:
Jacob W. Petrich, Major Professor
Mark S. Hargrove
Mei Hong
Xueyu Song
Hans Stauffer

Iowa State University

Ames, Iowa

2006

UMI Number: 3217275

INFORMATION TO USERS

The quality of this reproduction is dependent upon the quality of the copy submitted. Broken or indistinct print, colored or poor quality illustrations and photographs, print bleed-through, substandard margins, and improper alignment can adversely affect reproduction.

In the unlikely event that the author did not send a complete manuscript and there are missing pages, these will be noted. Also, if unauthorized copyright material had to be removed, a note will indicate the deletion.

UMI®

UMI Microform 3217275

Copyright 2006 by ProQuest Information and Learning Company.

All rights reserved. This microform edition is protected against unauthorized copying under Title 17, United States Code.

ProQuest Information and Learning Company
300 North Zeeb Road
P.O. Box 1346
Ann Arbor, MI 48106-1346

Graduate College
Iowa State University

This is to certify that the doctoral dissertation of

Lindsay Elizabeth Sanders Headley

has met the dissertation requirements of Iowa State University

Signature was redacted for privacy.

Major Professor

Signature was redacted for privacy.

For the Major Program

TABLE OF CONTENTS

ABSTRACT

This dissertation explores solvation dynamics, particularly in room temperature ionic liquids. Using the fluorescent probe coumarin 153, a number of alkylimidazolium-based ionic liquids are studied with various time-resolved spectroscopic techniques. Correlation functions, which track the solvation response, are determined from the time resolved emission spectra. In all cases, including the neutral organic starting materials, there is an initial rapid component of the solvation. Using butylimidazole and 1-butyl-3-methylimidazolium hexafluorophosphate, it is explicitly shown that the correlation functions overlap at early times. This indicates that the organic cation dominates the initial solvation of these liquids, in contrast to previous suggestions.

In addition to experimental studies, the problem of how to theoretically model the dynamics of room temperature ionic liquids is addressed. Two different systems, an aqueous ionic solution and a room temperature ionic liquid, are examined. Their correlation functions are calculated two different ways: using known dielectric data with and without conductivity effects. For both systems, the curves calculated without conductivity fit the experimental curves within experimental error and fit as well as, if not better than, the curves calculated with conductivity, suggesting that a dielectric continuum model can be sufficient for modeling room temperature ionic liquid dynamics.

In anticipation of exploring chiral ionic liquids with chiral fluorescent molecules, the natural product hypericin is separated into its enantiomers. Due to the immediate unavailability of optically pure chiral room temperature ionic liquids, the two hypericin enantiomers are studied in more traditional chiral environments. In all cases, the photophysics of the two enantiomers have no observable differences. This supports the previous conclusion that the extended absorption spectra of racemic hypericin is not due to ground state heterogeneity.

Shifting focus, the prospect of studying solvation dynamics in proteins is addressed. Song (*J. Chem. Phys.* **2002**, *116,* 9359.) has developed a method of theoretically modeling proteins using specific polarizability functions for each amino acid residue. To validate and refine this method experimentally, a complex of apomyoglobin and coumarin 153 is made and characterized. The coumarin 153 binds tightly and preferentially in the empty heme pocket, allowing solvation dynamics to be studied inside the protein.

CHAPTER 1. INTRODUCTION

Room Temperature Ionic Liquids

Room temperature ionic liquids (RTILs) have emerged during the last decade as an increasingly versatile class of solvents.[1-4] Although the first known report of an RTIL synthesis took place in the early 20th century,[5] they were mostly ignored until the early 1980s.[6] Room temperature ionic liquids are just what their name indicates: pure substances (not solutions) that are liquid at room temperature and composed entirely of ions. Any ionic liquid that has a melting point below 100 °C is classified as an RTIL. Generally, the cation is organic and the anion is inorganic. The first RTIL was ethylammonium nitrate, but when they were revisited in the 1980s, alkylimidazolium halogenoaluminates (III) received the most attention.[4,6] However, halogenoaluminates tend to be corrosive and air and moisture sensitive, which greatly hinders their use. Now, a new generation of air and moisture stable RTILs have arisen.[7-8] They commonly use the anions chloride, bromide, tetrafluoroborate, hexafluorophosphate, bis[trifluoromethane-sulfonimide], trifluoromethanesulfonate (triflate), and nitrate, among others. The most common cations are alkylimidazoliums, alkylammoniums, alkylphosphoniums, and alkylpyridiniums. (See Figure 1.1)

These new RTILs have a number of qualities that make them unique and interesting solvents. They tend to be chemically and thermally stable, can be soluble in a range of liquids from water to nonpolar organics, and have negligible vapor pressures. Due to these properties, they have gained popularity in a number of applications. The low vapor pressures and unique solubilities make them interesting as green solvents for synthesis.[9-12] In principle, they are reusable since organic products can simply be removed through distillation. They have also been used as distinct catalyst phases.[13] Most reports of RTILs as synthesis solvents show reaction kinetics not seen in traditional nonpolar organic solvents. There has also been a boom in separation applications. They can be versatile gas chromatography stationary phases,[14-15] liquid-

liquid extraction solvents,[16-17] and ideal liquid matrices for MALDI-MS[18] (matrix-assisted laser desorption/ionization mass spectrometry). As matrices for MALDI, they offer the advantage of being fluid yet viable under vacuum. The hope for the future is to be able to custom-design RTILs for whatever solvation properties are needed in a certain situation. We are not yet at that point, but by studying the solvation dynamics of RTILs on ultrafast time scales, we hope to learn more about how the ions interact with each other and with solutes.

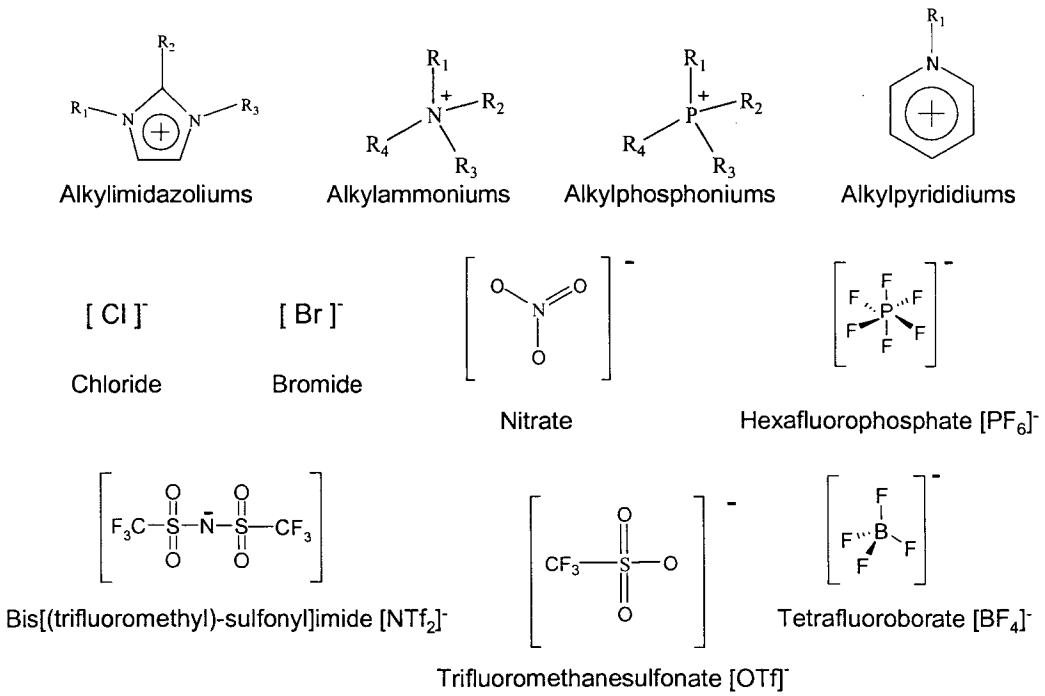

Figure 1.1: Common ions used in room temperature ionic liquids.

Solvation Dynamics

Solvation dynamics is the time-dependent response of a polar solvent to a perturbation on a molecular level. This solvation response is important since it can drastically affect reaction kinetics, especially in the case of electron transfer.[19-20]

Understanding the effects of solvent on reaction rates, yields, and products is a fundamental issue in chemistry. Presumably, if this is understood, chemists would be able to choose or create the ideal solvent for any particular application. Studying solvation dynamics can uncover the importance and roles of various characteristics of fluids, such as hydrogen bonding, polarity, dielectric response, polarizability, and molecular shape and size, among others. Many solvation dynamics experiments covering a wide range of molecular solvents have been conducted over the past two decades.[21-25]

To study solvation dynamics, one must introduce a perturbation in the solvent and monitor the temporal response. The most common way of doing this is electronically exciting a fluorescent probe molecule in the solvent and tracking the fluorescence energy over time. Assuming that there is a significant change in the probe's dipole moment, the solvent will respond to the altered electric field.

This process is depicted in Figure 1.2 (adapted from Ref. 25). We assume in this example that there is a large increase in the probe's dipole upon electronic excitation. Before excitation, the solution is in an equilibrium state. Immediately upon introducing a delta-function pulse of light of sufficient energy, the probe will be in its S_1 excited state. The reorganization (or relaxation) time of the polar solvent is longer than the time it takes for excited state dipole creation. Thus, the system is no longer in equilibrium, and the solvent will respond accordingly. Assuming that the relaxation time is faster than the average fluorescence lifetime of the probe molecules, the solvent will be responding to the dipole as fluorescence occurs. As the solvent stabilizes around the dipole, the S_1 excited state stabilizes as well, decreasing the energy of the fluorescent transition. Using time-resolved spectroscopy, this response can be tracked and used to elucidate solvent motions. See Chapter 2 for experimental details and techniques.

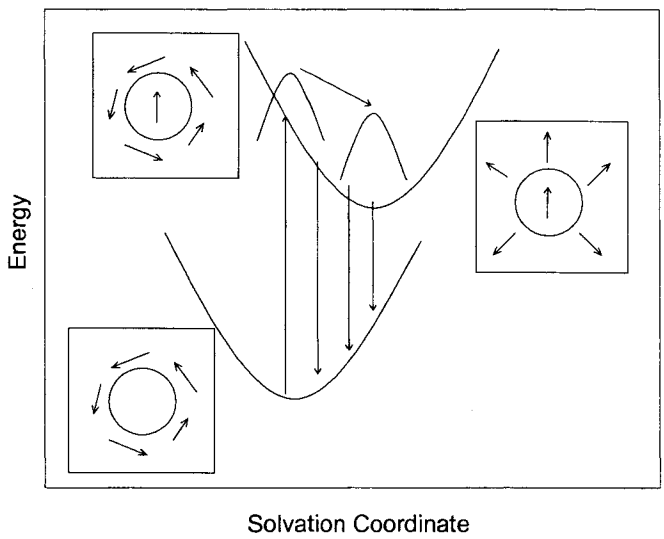

Figure 1.2: Solvation dynamics diagram. The first two electronic energy levels are shown. The boxes depict the probe molecule (circle) and the surrounding solvent dipoles (arrows). When the probe is electronically excited, its dipole moment increases, and the solvent dipoles respond to the new electronic field, lowering the energy of the system.

Fluorescent probes for solvation dynamics studies must be chosen carefully. The most basic requirement is a significant change in dipole upon electronic excitation; without this, there will be no measurable solvation response. Also, the probe needs to exhibit a solvatochromic shift, a shift in emission frequency which is dependent on the environment's polarity. This shift allows one to track the solvation response. A third necessity is an emission lifetime that is longer than the relaxation time, to ensure that the entire response is accounted for. Even when these three requirements are met, there are factors which can obscure the pure solvation response. If the probe exhibits a great deal of intramolecular relaxation, or if the relaxation takes place on the same time scale as solvation, there is no easy way to separate the two contributions. There can also be problems if the emission varies with excitation frequency, indicating the possibility of emitting from more than one state.

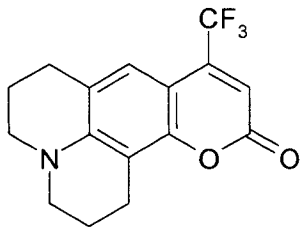

Figure 1.3: Solvation dynamics probe coumarin 153.

Only a handful of molecules have been shown to exhibit the above qualities. The one most widely used today, and the one used in the following investigations, is coumarin 153 (C153) (See Figure 1.3). After exhaustive study, C153 is generally accepted as being an ideal molecule for these studies in many ways.[26] The difference in its dipole moment upon excitation to the first singlet excited state has been estimated to be approximately 7 D.[27-29] This provides a significant perturbation for the solvent. There is a large solvatochromic shift; the emission spectra maximum shifts from 450 nm to 540 nm in going from hexane to methanol. Being a fairly rigid molecule, it has a high quantum yield and a long lifetime in most solvents. C153 certainly fulfills the three most important requirements for a solvation probe.

However, there has been some question about the amount of intramolecular reorganization and the spacing of excited states in this molecule. There have been a handful of notable studies[30-32] which refute the usefulness of C153 as a solvation probe, mainly questioning the assumption that the first excited electronic state is isolated and uncoupled from higher states. Agmon[30] also contends that the apparent solvation shift is actually due to a variation of C153's lifetime with environment, not to a variation of its emission frequency with environment.

Even so, C153 has been widely used, and most researchers in the solvation dynamics field have not observed any anomalous behavior or behavior that would question C153's

utility. Maroncelli and coworkers have been the strongest supporters of C153.[33-34] They have consistently responded to critics, claiming that there is a preferential transition between the S_0 and S_1 electronic states because they have similar transition moments.[34] In response to Agmon's publication, they point out that radiative rate is always dependent on emission frequency, so they will both change with the environment in a consistent manner; hence, the solvation explanation for the shift remains valid.[33] There have also been computational studies indicating that C153 does, indeed, have a fairly isolated transition between the ground and first excited state.[28,35-36] According to experiment, theory, and computational studies, C153 is an ideal solvation probe, and we continue to use it with reliable results.

Previous Studies

The dynamics of RTIL solvation is particularly important because steady-state spectroscopic data show little difference among a large variety of RTILs. Using solvatochromic dyes, such as Reichardt's dye, the "polarities" of RTILs all appear to fall in a narrow range between acetonitrile and methanol.[37-40] According to these data, all RTILs should have similar solvation properties. In practice, this is obviously not the case, since they can be hydrophilic or hydrophobic, soluble or insoluble in nonpolar organics, and able to promote or hinder reactions. To explore these differences, it is necessary to move the focus from statics to dynamics.

A number of studies of RTIL solvation dynamics using C153 have been reported in recent years.[41-49] Typically, these solvents have been described as having biphasic dynamics, meaning that there are two distinct time scales of solvation.[41-43,45] Some researchers prefer to describe the solvation as nonexponential, fitting the correlation function curves to stretched exponentials[44,46] and noting the existance of an ultrafast initial component. Regardless of how the curves are fit, it is clear that RTILs, unsurprisingly, exhibit complex dynamics.

These features are reproduced qualitatively, although not always quantitatively, with a number of different solvation probes including Nile Red,[50] 4-AP,[51] and PRODAN.[52]

The first RTILs studied in this way were based on the commonly used imidazolium cations.[41-42] It was noted that, although the overall solvation is relatively slow as compared to common organic solvents, about half of the dynamics are missed by time-correlated single-photon counting measurements.[44] This, along with the biphasic nature of the observed relaxation, led to various conclusions about the nature of dielectric relaxation in these ionic liquids. An early suggestion was based on conclusions from previous high-temperature molten salt investigations,[53] attributing the faster time component to motions of the generally smaller anions and the slower time component to the bulky cations. This picture was soon modified to acknowledge that the slow component is more likely due to translational motions of both species to preserve electronic neutrality (due to Coulombic forces).[46] This model was corroborated by computer simulations by Shim, et al.,[54] which clearly showed the fast response of the anions to a bimolecular probe.

This relatively simple picture was challenged, however, when Maroncelli, et al.[51] conjectured that the different solvation time scales reflect different types of motions, not a separation between the cation and anion responses. In this model, the slow component is due to structural rearrangements, while the faster component is due to quicker, small-scale motions of the electron cloud and vibrations. While this is probably true, there was still the question of whether one ion dominates the solvation over the other one. Interestingly, it was found that ammoniums and phosphoniums with long-chain alkyl groups do not show the ultrafast relaxation component that is ubiquitous in alkylimidizoliums, regardless of the anion identity.[51] The result suggests to us that the polarizable organic cation is primarily responsible for the amplitude of the initial, rapid component. Chapter 3 presents a novel study that corroborates and develops this conclusion.

Currently, RTIL dynamics have been investigated using a wide range of techniques such as molecular dynamics simulations,[54-55] dielectric spectroscopy,[56] Kerr-effect spectroscopy,[57-59] and time-correlated single-photon counting.[41-51] These studies are starting to clarify RTIL solvation dynamics, but there are still many unanswered questions about the interactions among the ions and the reasons behind the observed solvation kinetics. These questions are what prompted the studies reported in Chapters 3, 4, and 5 of this manuscript.

Solvation Dynamics of Proteins

Besides RTILs, the solvation dynamics of proteins have also been investigated.[60-72] Solvation in proteins is a difficult problem to explore. For theorists, concessions must be made in choosing a representative model. Proteins are unusual dielectric matrices because the dipoles are relatively fixed, hindering complete solvation. Many theorists use a traditional Onsanger-like model of a polar probe surrounded by a dielectric continuum.[60-63] Of course, the polarizabilities and dielectric constants vary within the protein depending on its primary, secondary, and tertiary structures, so this simple approach misses the complexities of the dielectric response. Another possible approach is an atomistic model,[64-67] but this is computationally demanding, and oftentimes long-range effects cannot be explored. Sometimes such a rigorous and complicated treatment is unnecessary.

An alternative approach to studying protein dielectric response lies midway between these extremes. Song[68] has developed a theoretical model that takes into account the 3-D arrangement of the amino acid residues, without having to specify parameters for each atom. In his model, a certain polarizability function is assigned to each of the 20 naturally occurring amino acids. It is assumed that each residue has a constant polarizability regardless of environment. Now, one can study the proteins using 20 polarizability functions instead of assuming a dielectric continuum or having to resort to atomistic simulations.

To complement and perhaps validate this theoretical approach, we have attempted to experimentally study protein dynamics using solvation dynamics techniques. Some experimental studies of protein solvation dynamics have been done in the past,[69-72] and there are some complicating factors. The probe binding site (or the site of a natural probe, such as tryptophan) must be precisely known. If the active pocket is the area of interest in the protein, the probe must have an affinity for and fit reasonably well in the pocket. Also, if a significant fraction of probe molecules bind on the surface of the protein or remain in the bulk solvent, the solvation response will be obscured. Taking these factors and our goals into account, we have characterized a complex between apomyoglobin and coumarin 153 which should work well for exploring Song's polarizability function model. This work is presented in Chapter 6.

Chiral Solutes and Solvents

Room temperature ionic liquids are increasingly being used in analytical separations, especially as stationary phases.[14-15] To expand their use further, it may be possible to use chiral RTILs for separations of chiral molecules. Chiral separation[73-74] is important to numerous areas of research since many biologically and pharmeceutically interesting compounds are chiral. To separate a racemic compound into enantiomerically pure samples requires chiral recognition with the stationary phase. Since RTILs have proven to be viable separation tools, it makes sense to begin investigating chiral RTILs. Solvation is the driving force behind many analytical separation techniques, so we have undertaken a preliminary study of chiral solvation dynamics in RTILs. We attempted to look at a number of chiral RTILs, but we encountered difficulty making them optically pure, so, for now, we report results for more traditional chiral solvents.

The probe we decided to investigate is hypericin (See Figure 1.4). Hypericin is a natural product found in St. John's wort. It has potentially beneficial medical uses due to its

light-activated anti-cancer and anti-viral properties,[75-78] and our lab has previously studied it extensively.[79-84] Hypericin is not a typical solvation probe, but it does have two enantiomers,[85-87] and we were interested to see if their photophysics differed, especially in chiral environments. The study of hypericin enantiomers in cyclodextrin, two proteins, and (s)-(+)-2-butanol, all chiral environments, is presented in Chapter 7.

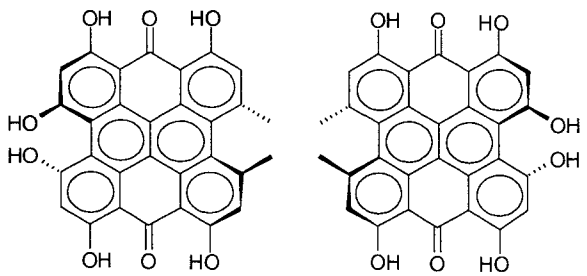

Figure 1.4: Hypericin enantiomers.

Structure of the Dissertation

Following this introduction, there is an experimental methods section which explains many of the techniques and methods of analysis used in the following chapters. Chapter 3 is an early paper on RTILs showing that the polarizable organic piece dominates the fastest solvation component. This work used 1-butyl-3-methylimidazolium with four different anions. Chapter 4 is an extension of this work studying a wider variety of imidazolium cations. Chapter 5 is a study of the RTIL ethylammonium nitrate, for which dielectric information is available, to determine whether a simple dielectric continuum model is sufficient for describing RTIL solvation dynamics. Chapter 6 characterizes the complex of coumarin 153 and apomyoglobin which will be used to experimentally study dielectric relaxation in proteins. Chapter 7 describes preliminary work studying the interactions of

chiral solutes and solvents, possibly to be extended to chiral RTILs, with the chiral probe hypericin. Most papers from our research group are done as a team, so my co-authors deserve much recognition and my sincere gratitude. My contribution to the following work is much of the steady-state and time-correlated single-photon counting data and analysis, measurement of physical properties such as viscosity, and some chemical synthesis, especially of the ethylammonium nitrate used in Chapter 5. Many of the RTILs in Chapter 4 were previously unexplored, and I decided which ones to synthesize and include in the paper. I also contributed to the preparations of the documents by providing many figures, tables, and experimental sections, as well as editing and responding to reviewer's comments.

References

(1) Seddon, K. R. *Nature (Materials)* **2003**, *2*, 363.

(2) *Ionic Liquids as Green Solvents: Progress and Prospects;* Roger, R. D.; Seddon, K. R., Eds.; ACS Symposium Series #856; American Chemical Society: Washington, D.C., 2003.

(3) Ohno, H. *Electrochemical Aspects of Ionic Liquids;* Wiley: Hoboken, NJ, 2005.

(4) Welton, T. *Chem. Rev.* **1999**, *99*, 2071.

(5) Walden, P. P. *Bull. Acad. Imper. Sci. (St. Petersburg)* **1914**, 1800.

(6) Wilkes, J. S.; Levisky, J. A.; Wilson, R. A.; Hussey, C. L. *Inorg. Chem.* **1982**, *21*, 1263.

(7) Wilkes, J. S.; Zaworotko, M. J. *J. Chem. Soc. Chem. Commun.* **1992**, 965.

(8) Fuller, J.; Carlin, R. T.; DeLong, H. C.; Haworth, D. *J. Chem. Soc. Chem. Commun.* **1994**, 299.

(9) Earle, M. J.; Seddon, K. R.; Adams, C. J.; Roberts, G. *Chem. Commun.* **1998**, 2097.

(10) Earle, M. J.; McCormac, P. B.; Seddon, K. R. *Chem. Commun.* **1998**, 2245.

(11) Dyson, P. J.; Ellis, D. J.; Welton, T.; Parker, D. G. *Chem. Commun.* **1999**, 25.

(12) Leadbeater, N. E.; Torenius, H. M. *J. Org. Chem.* **2002**, 67, 3145.

(13) Yao, Q. *Org. Lett.* **2002**, 4, 2197.

(14) Anderson, J. L.; Ding, J.; Welton, T.; Armstrong, D. W. *J. Am. Chem. Soc.* **2002**, 124, 14247.

(15) Anderson, J. L.; Armstrong, D. W. *Anal. Chem.* **2003**, 75, 4851.

(16) Huddleston, J. G.; Rogers, R. D. *Chem. Commun.* **1998**, 1765.

(17) Dai, S.; Ju, Y. H.; Barnes, C. E. *J. Chem. Soc. Dalton. Trans.* **1999**, 1201.

(18) Armstrong, D. W.; Zhang, L. K.; He, L.; Gross, M. L. *Anal. Chem.* **2001**, *73*, 3679.

(19) Maroncelli, M.; MacInnis, J.; Fleming, G. R. *Science* **1989**, *243*, 1674.

(20) Vajda, S.; Jimenez, R.; Rosenthal, S. J.; Fidler, V.; Fleming, G. R.; Castner, E. W. *J. Chem. Soc., Faraday Trans.* **1995**, *91,* 867.

(21) Bagchi, B.; Oxtoby, D. W.; Fleming, G. R. *Chem. Phys.* **1984**, *86*, 257.

(22) Maroncelli, M.; Fleming, G. R. *J. Chem. Phys.* **1987**, *86*, 6221.

(23) Castner, E. W.; Bagchi, B.; Maroncelli, M.; Webb, S. P.; Ruggiero, A. J.; Fleming, G. R. *Ber. Bunsenges. Phys. Chem.* **1988**, *92*, 363.

(24) Maroncelli, M.; Kumar, V. P.; Papazyan, A. *J. Phys. Chem.* **1993**, *97*, 13.

(25) Stratt, R. M.; Maroncelli, M. *J. Phys. Chem.* **1996**, *100*, 12981.

(26) Horng, M. L.; Gardecki, J. A.; Papazyan, A.; Maroncelli, M. *J. Phys. Chem.* **1995**, *99*, 17311.

(27) Samanta, A.; Fessenden, R. W. *J. Phys. Chem. A* **2000**, *104*, 8577.

(28) Cave, R. J.; Castner, E. W. *J. Phys. Chem. A* **2002**, *106*, 12117.

(29) Kanya, R.; Ohshima, Y. *Chem. Phys. Lett.* **2003**, *370*, 211.

(30) Agmon, N. *J. Phys. Chem.* **1990**, *94*, 2959.

(31) Kovalenko, S.A.; Ruthmann, J.; Ernsting, N. P. *Chem. Phys. Lett.* **1997**, *271*, 40.

(32) Flory, W. C.; Blanchard, G. J. *App. Spec.* **1998**, *52*, 82.

(33) Maroncelli, M.; Fee. R. S.; Chapman, C. F.; Fleming, G. R. *J. Phys. Chem.* **1991**, *95*, 1012.

(34) Lewis, J. E.; Maroncelli, M. *Chem. Phys. Lett.* **1998**, *282*, 197.

(35) Kumar, P. V.; Maroncelli, M. *J. Chem. Phys.* **1995**, *103*, 3038.

(36) Hsu, C. P.; Georgievskii, Y.; Marcus, R. A. **1998**, *102*, 2658.

(37) Muldoon, M. J.; Gordon, C. M.; Dunkin, I. R. *J. Chem. Soc., Perkin Trans. 2* **2001**, 433.

(38) Carmichael, A. J.; Seddon, K. R. *J. Phys. Org. Chem.* **2000**, *13*, 591.

(39) Bonhote, P.; Dias, A. P.; Papageorgiou, N.; Kalyanasundarm, K.; Graetzel, M. *Inorg. Chem.* **1996**, *35*, 1168.

(40) Aki, S. N. V. K.; Brennecke, J. F.; Samanta, A. *Chem. Commun (Cambridge)* **2001**, 413.

(41) Karmakar, R.; Samanta, A. *J. Phys. Chem. A* **2002**, *106*, 4447.

(42) Karmakar, R.; Samanta, A. *J. Phys. Chem. A* **2002**, *106*, 6670.

(43) Karmakar, R.; Samanta, A. *J. Phys. Chem. A* **2003**, *107*, 7340.

(44) Arzhantsev, S.; Ito, N.; Heitz, M.; Maroncelli, M. *Chem. Phys. Lett.* **2003**, *381*, 278.

(45) Chakrabarty, D.; Hazra, p.; Chakraborty, A.; Seth, D.; Sarkar, N. *Chem. Phys. Lett.* **2003**, *381*, 697.

(46) Ito, N.; Arzhantsev, S.; Heitz, M.; Maroncelli, M. *J. Phys. Chem. B* **2004**, *108*, 5771.

(47) Arzhantsev, S.; Jin, H.; Baker, G. A.; Ito, N.; Maroncelli, M. In *Femtochemistry VII*; Castleman, A. W.; Ed.; Elsevier: Cambridge, MA, 2005.

(48) Chowdhury, P. K.; Halder, M.; Sanders, L.; Calhoun, T.; Anderson, J. L.; Armstrong, D. W.; Song, X.; Petrich, J. W. *J. Phys. Chem. B* **2004**, *108*, 10245.

(49) Sanders Headley, L.; Mukherjee, P.; Anderson, J. L.; Ding. R.; Halder, M.; Armstrong, D. W.; Song, X.; Petrich, J. W. *J. Phys. Chem. B* **2006**, Submitted.

(50) Saha, S.; Mandal, P. K.; Samanta, A. *Phys. Chem. Chem. Phys.* **2004**, *6*, 3106.

(51) Ingram, J. A.; Moog, R. S.; Ito, N.; Biswas, R.; Maroncelli, M. *J. Phys. Chem B* **2003**, *107*, 5926.

(52) Arzhantsev, S.; Zachariasse, K. A.; Maroncelli, M. *J. Phys. Chem. B* **2006**, Submitted.

(53) Bart, E.; Meltsin, A.; Huppert, D. *J. Phys. Chem.* **1994**, *98*, 3295.

(54) Shim, Y.; Duan, J.; Choi, M. Y.; Kim, H. J.; *J. Chem. Phys.* **2003**, *119*, 6411.

(55) Kobrak, M. N.; Znamenskiy, V. *Chem. Phys. Lett.* **2004**, *395*, 127

(56) Weingartner, H.; Knocks, A.; Schrader, W.; Kaatze, U. *J. Phys. Chem. A* **2001**, *105*, 8646.

(57) Hyun, B. R.; Dzyuba, S. V.; Bartsch, R. A.; Quitevis, E. L. *J. Phys. Chem. A* **2002**, *106*, 7579.

(58) Giraud, G.; Cordon, C. M.; Dunkin, I. R.; Wynne, K. *J. Chem. Phys.* **2003**, *119*, 464.

(59) Shirota, H.; Funston, A. M.; Wishart, J. F.; Castner, E. W. *J. Chem. Phys.* **2005**, *122*, 184512.

(60) Warshel, A.; Russel, S. T. *Q. Rev. Biophys.* **1984**, *17*, 283.

(61) Sharp, K. A.; Honig, B. *Ann. Rev. Biophys. Chem.* **2001**, *19*, 301.

(62) Shutz, C. N.; Warshel, A. *Proteins Struct. Funct. Genet.* **2001**, *44*, 400.

(63) Simonson, T. *Curr. Opin. Struct. Biol.* **2001**, *11*, 243.

(64) Zheng, C.; Wong, C. F.; McCammon, J. A.; Wolynes, P. G. *Chem. Scr.* **1989**, *29A*, 171.

(65) Simonson, T. *Proc. Natl. Acad. Sci. USA* **2002**, *99*, 6544.

(66) Nakamura, H. *Q. Rev. Biophys.* **1996**, *29*, 1.

(67) Brooks, C. L.; Karplus, M.; Pettitt, B. M. *Adv. Chem. Phys.* **1987**, *71*, 1.

(68) Song, X. *J. Chem. Phys.* **2002**, *116*, 9359.

(69) Nandi, N. K.; Bhattacharyya, K.; Bagchi, B. *Chem. Rev.* **2000**, *100*, 2013.

(70) Pierce, D. W.; Boxer, S. G. *J. Phys. Chem.* **1992**, *96*, 5560.

(71) Bashkin, J. S.; McLendon, G.; Mukamel, S.; Marohn, J. *J. Phys. Chem.* **1990**, *94*, 4757.

(72) Homoelle, B. J.; Edington, M. D.; Diffey, W. M.; Beck, W. F. *J. Phys. Chem. B* **1998**, *102*, 3044.

(73) Aboul-Enein, H. Y. *Chiral Separation by Liquid Chromatography and Related Technologies*; Chromatographic Science Series #90; Dekker: New York City, NY,

2003.

(74) *Chiral Separations: Methods and Protocols*; Gubitz, G.; Schmid, M. G., Eds.; Methods in Molecular Biology Series #243; Humana: Totowa, NJ., 2004.

(75) Zhang, W.; Law, R. E.; Hinton, D. R.; Couldwell, W. T. *Cancer Lett.* **1997**, *120*, 31.

(76) Mirossay, A.; Mirossay, L.; Sarissky, M.; Papp, P.; Mojzis, J. *Phys. Res.* **2002**, *51*, 641.

(77) Meruelo, D.; Lavie, G.; Lavie, D. *Proc. Natl. Acad. Sci. USA* **1988**, *85*, 5230.

(78) Lenard, J.; Rabson, A.; Vanderoef, R. *Proc. Natl. Acad. Sci. USA* **1993**, *90*, 158.

(79) Gai, F.; Fehr, M. J.; Petrich, J. W. *J. Am. Chem. Soc.* **1993**, *115*, 3384.

(80) Gai, F.; Fehr, M. J.; Petrich, J. W. *J. Phys. Chem.*. **1994**, *98*, 5784.

(81) Das, K.; Dertz, E.; Paterson, J.; Zhang, W.; Kraus, G. A.; Petrich, J. W. *J. Phys. Chem B* **1998**, *102*, 1479.

(82) Das, K.; Smirnov, A. V.; Wen, J.; Miskovsky, P.; Petrich, J. W. *Photochem. Photobiol.* **1999**, *69*, 633.

(83) Das, K.; Ashby, K. D.; Wen, J.; Petrich, J. W. *J. Phys. Chem. B* **1999**, *103*, 1581.

(84) English, D. S.; Das, K.; Ashby, K. D.; Park, J.; Petrich, J. W. *J. Am. Chem. Soc.* **1997**, *119*, 11585.

(85) Altmann, R.; Etzlstorfer, C.; Falk, H. *Mon. fur Chem.* **1997**, *128*, 361.

(86) Altmann, R.; Etzlstorfer, C.; Falk, H. *Mon. fur Chem.* **1997**, *128*, 785.

(87) Tran, H. T. N.; Falk, H. *Mon. fur Chem.* **2002**, *133*, 1231.

CHAPTER 2. EXPERIMENTAL METHODS AND DATA ANALYSIS

Time-Correlated Single-Photon Counting

Time-correlated single-photon counting (TCSPC) is a time-resolved fluorescence technique widely used for many applications[1-3] including solvation dynamics.[4-6] The basic design in our laboratory is as follows (See Figure 2.1). The light source is a homemade titanium sapphire laser with tunable output from 790 - 900 nm. The most stable mode-locking occurs from 800 – 850 nm. The mode-locked pulses have a repetition rate of 82 MHz, but this frequency is too fast for good resolution and for detecting complete extinction of slower fluorescence lifetimes. To decrease the frequency of the pulses to about one-tenth of its original (8.8 MHz), the beam is passed through a Pockels cell (Model 350-160, Conoptics, Inc.). To time the pulses correctly, the beam is split, with the majority going to the Pockels cell and the rest going to a photodiode connected to the Pockels cell electronics. After pulse selection, the light is frequency doubled to ~400 nm by focusing into a BBO crystal. To ensure vertical polarization, a half-wave plate and a vertical polarizer are placed between the focusing lens and the sample. Fluorescence is detected at a 90° angle from the incident beam. The fluorescence is passed through a polarizer set at the magic angle to ensure that the results are independent of any transition moment anisotropy. The emitted light is filtered to block any scattered incident light and focused into a microchannel plate photomultiplier tube (MCP-PMT) from Hamamatsu (model R3809U-50). Since the MCP-PMT uses microscopic channels instead of larger dynodes found in traditional photomultiplier tubes, the transit time spread is lessened, resulting in narrower instrument functions (see below). If the emission is too intense for the sensitive detector, the excitation intensity can be lessened using neutral density filters.

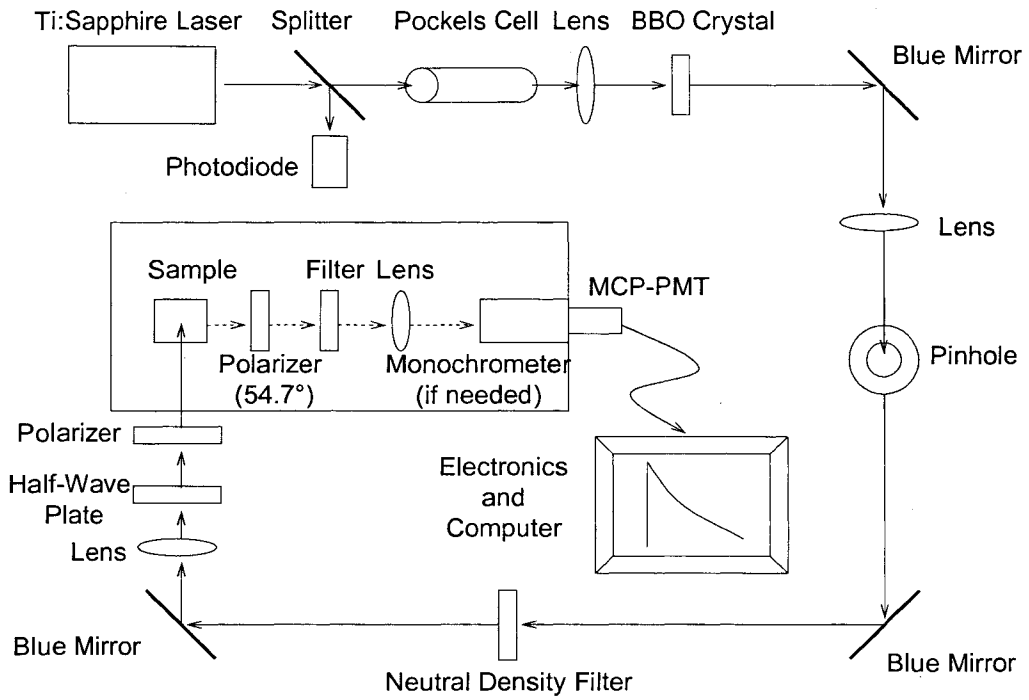

Figure 2.1: TCSPC instrumentation schematic.

To determine fluorescent lifetimes, the system is used as is. The excitation light is filtered up to 430 nm, and all other wavelengths are captured. Fluorescent events can be viewed over a timescale, usually around 11 ns, that is shorter than the time between incident beam pulses. Traces are generally collected up to 10,000 counts in the peak channel. It is important to measure an accurate instrument function to factor out the response time of the electronics and determine the time resolution.[1] This instrument function can change over time due to subtle changes in incident beam quality and electronic jitter. Since data analysis is sensitive to the shape of the instrument function, it is re-checked at least every 30 minutes or between every three runs. To determine the instrument function, the incident light is scattered with a dilute milk or cream solution into the detection system. This scattered light can be intense, so it is important to filter the incident light to protect the detector. The instrument function width for our TCSPC system tends to be between 80 and 120 ps.

For solvation dynamics measurements, data must be taken at discrete wavelengths. A monochromater with a ~4 nm bandpass is used to select for different emission wavelengths. For C153, data is generally taken in increments of 10 nm from 480 – 620 nm, where there is sufficient emission intensity. Instrument functions are taken every 30 minutes or about every three runs. Data are collected over a shorter time-window (typically ~4.5 ns) than for lifetime measurements because solvent relaxation is typically faster than the lifetime; 4.5 ns is usually sufficient for all but the most viscous solvents. Decays are only collected to ~3000 counts in the peak channel due to the large number of runs and lower signal intensity at discrete wavelengths.

TCSPC Data Analysis

To extract the fluorescence decays from the raw data, the decays must first be deconvoluted from the instrument function, according to Equation 2.1.[1] I(t) is the total measured intensity, G(t) is the instrument function, and F(t) is the actual fluorescence decay.

$$I(t) = \int_0^t G(t-T)F(T)dT \tag{2.1}$$

This is best solved with an iterative algorithm. The deconvoluted decays are fit to single, double, or triple exponential functions. Data collection, deconvolution, and exponential fitting can all be done with the same computer program. We have previously used a custom-made program called HomerFit, but we recently upgraded to MAESTRO (Ametek, Inc.). If studying solvation dynamics, time-resolved emission spectra (TRES) can be constructed from the fitting parameters at any time in the experimental timescale. Microcal Origin is a good graphing program for these types of manipulations. The TRES are constructed according to the following equation,

$$S(\lambda,t) = D(\lambda,t)\frac{S_0(\lambda)}{\int_0^\infty D(\lambda,t)dt} \tag{2.2}$$

where $S_0(\lambda)$ is the steady state emission intensity and $D(\lambda,t)$ is the fluorescence decay. Since each spectrum only has a maximum of 15 data points (spaced 10 nm apart), the TRES are fit to a lognormal function (Equation 2.3) to determine where the maximum intensities lie.

$$y = A\exp\left(-0.693\ln\left(\frac{1+\frac{2(x-C)\sinh(B)}{D}}{B}\right)^2\right) \tag{2.3}$$

A is the y-value maximum (the TRES are usually normalized to one); B reflects the asymmetry of the curve, which tends to be around -0.3 for emission spectra; C is the x-value at A (wavenumber at maximum fluorescence intensity); and D is the width of the curve at its base. The frequencies at maximum intensity are used to track the Stokes shift of the emission curves.

Using these frequencies, the normalized correlation function, C(t), can be determined. The correlation function is simply a way to track how the solvation free energy changes with time. Assuming a linear solvation response, this can be determined experimentally.

$$C(t) = \frac{\nu(t)-\nu(\infty)}{\nu(0)-\nu(\infty)} \tag{2.4}$$

$\nu(t)$ are the maxima from the TRES, $\nu(0)$ is usually determined from a time-zero estimation, and $\nu(\infty)$ is the wavenumber at the peak of the steady state emission. The correlation function curves are usually either fit to a sum of exponentials or a stretched exponential. Our lab has used the sum of exponentials functional form.

Time-Zero Emission Spectra

Due to unavoidable time delays in spectroscopic instrumentation, the earliest detected events do not take place at the actual "time-zero" point of fluorescence. Especially with imidazolium RTILs, TCSPC data tend to miss about one-half of the spectral response. Furthermore, with ultrafast techniques, it is possible to catch some intramolecular as well as intermolecular relaxation. This inconsistency will, of course, skew the C(t) results to suggest artificially slow dynamics. Fee and Maroncelli[7] have devised a method of calculating time-zero emission spectra from steady-state data. These spectra represent the state of the system after intramolecular relaxation is complete and before the onset of intermolecular relaxation. Although this separation of intramolecular and intermolecular timescales is a simplification, dielectric relaxation does tend to be significantly slower than intramolecular vibrational relaxation, especially for C153,[8] so it is somewhat reasonable.

This method assumes that there is a single absorbance lineshape and a single fluorescence lineshape for each type of molecule in nonpolar media, and the only changes in these lineshapes are due to an environmentally dependent shift, δ. These nonpolar lineshapes can be determined from steady-state spectra in nonpolar solvents, such as hexane, through the following relationships,

$$g(\nu) \propto \nu^{-1} A_{np}(\nu) \tag{2.5a}$$

$$f(\nu) \propto \nu^{-3} F_{np}(\nu) \tag{2.5b}$$

where $g(\nu)$ and $f(\nu)$ are the nonpolar absorption and emission lineshapes, respectively. $A_{np}(\nu)$ and $F_{np}(\nu)$ are the steady-state absorption (or excitation) and emission spectra in a nonpolar solvent. Since there is a distribution of environments in any polar solvent, the solvent-induced shifts, δ, can be approximateed by a Gaussian.

$$p(\delta) = (2\pi\sigma^2)^{-1/2} \exp[-(\delta - \delta_0)^2 / 2\sigma^2] \tag{2.6}$$

P(δ) is convoluted with the nonpolar absorption lineshape to produce the steady-state absorption spectrum in the solvent of interest:

$$A_p(\nu) \propto \nu \int_{-\infty}^{\infty} g(\nu - \delta) p(\delta) d\delta \tag{2.7}$$

An iterative process can determine the form of p(δ) that most closely recreates the polar absorption spectrum. Once p(δ) is known, it can be used to determine the time-0 spectrum in the polar solvent according to the following equation:

$$F_p(\nu, t = 0; \nu_{ex}) \propto \nu^3 \nu_{ex} \int_{-\infty}^{\infty} g(\nu - \delta) p(\delta) f(\nu - \delta) k(\delta) d\delta \tag{2.8}$$

where k(δ) is the radiative rate function:

$$k(\delta) \propto \frac{\int f(\nu - \delta) \nu^3 d\nu}{\int f(\nu - \delta) d\nu} \tag{2.9}$$

Reorganization Energy

Reorganization energy is the energy needed to structurally readjust the reactants and surrounding solvent molecules to accommodate a reaction. In the case of solvation dynamics, where there is no chemical reaction, the reorganization energy describes the energy used to re-equilibrate the solute and the solvent in response to the intramolecular charge transfer caused by absorbance or fluorescence. This energy generally increases with increasingly polar solvents, and it is a useful complement to solvation dynamics measurements. Reorganization energy has been estimated as being half of the Stokes shift between absorbance and fluorescence (Figure 2.2).[9] This simple picture, however, assumes that spectra are Gaussian and that the shift between the peaks of the curves accurately reflects the actual energy difference between excitation and emission.

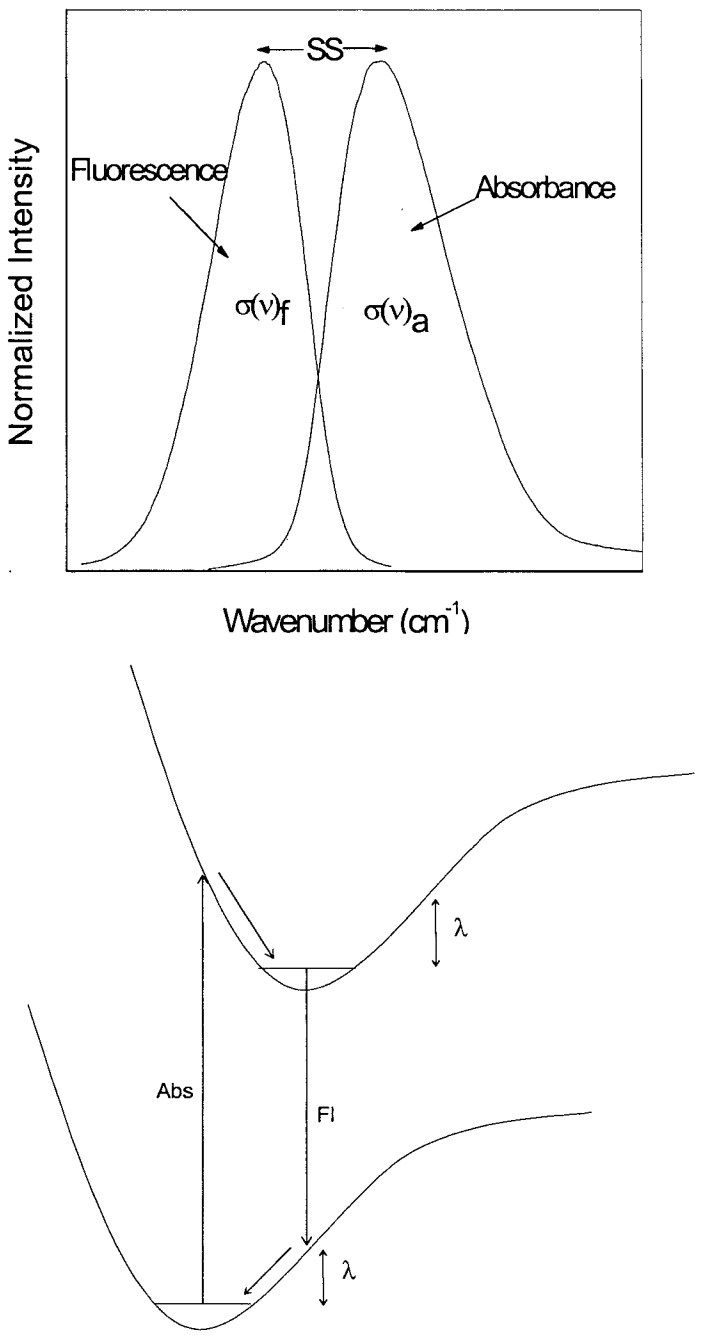

Figure 2.2: Reorganization energy as half the Stokes shift. The top graph shows the experimental Stokes shift between absorbance and fluorescence, and the bottom diagram shows the reorganization energy (λ) on an energy diagram. The bottom curve is the ground state, and the upper curve is the first excited state. This approximation to the reorganization energy assumes Gaussian spectra.

Since spectra are, in general, not Gaussian, Song[10] has developed a method to determine reorganization energy taking the exact lineshapes into account (Equation 2.10).

$$\lambda = \hbar \frac{\int_0^\infty d\nu[\sigma_a(\nu) - \sigma_f(\nu)]\nu}{\int_0^\infty d\nu[\sigma_a(\nu) + \sigma_f(\nu)]} \tag{2.10}$$

σ_a is the steady-state absorption curve, and σ_f is the steady-state fluorescence curve. Before the reorganization energy can be calculated, the excitation and emission spectra must be manipulated to allow their addition and subtraction. They are interpolated and renormalized to give equal spacing between each point, and the intersection of the two curves is forced to zero. If necessary, the curves can be stretched down to zero intensity if there is some constant background from the instrument. This process only tends to change the final result by approximately 1%. Finally, an appropriate number of zeros are added to the high energy end of the emission spectrum and to the low energy end of the excitation spectrum so that the curves can be added and subtracted along their entire lengths. The reorganization energy can now be calculated according to Equation 2.10. The integration is performed from negative infinity to zero rather than from zero to positive infinity to avoid interference from the second harmonic excitation peak.

Synthesis of Room Temperature Ionic Liquids

While working with ethylammonium nitrate, be aware that it is a possible explosive due to its similarity to ammonium nitrate, but I have found no reports of accidental explosions and have had no trouble working with it myself. It can be synthesized simply by slowly adding an equimolar amount of concentrated nitric acid dropwise to 70% ethylamine in water at 0 °C while stirring.[11,12] Care must be taken to start the reaction promptly since

ethylamine quickly evaporates from solution. Once all the nitric acid has been added, the solution is allowed to sit for about ½ hour just to make sure that all the nitric acid has been consumed. To remove the excess ethylamine and bulk water, the product is rotovaped for at least ½ hour at 50-70 °C. A heat gun can be helpful to remove water that condenses in the neck of the flask, although is it not advisable to excessively heat the liquid. The pH is checked with pH paper to ensure that no reactants are left. The pure liquid tends to be around pH 5, although the meaning of pH in ionic liquids is questionable. However, it is still an easy and reliable test for detecting excess acid or base. Any remaining water can be removed by drying under vacuum at 50 °C for at least 24 hours and preferably 48. Finally, before use, the product is forced through a miniature activated silica gel column in a disposable Pasteur pipette. To make the column, some cotton is pushed into the end of a Pasteur pipette, and the pipette is filled with silica to 1-2 cm from the top. The ethylammonium nitrate can be slowly passed through the column using pressure from a pipette bulb. The yield from this step will be approximately 50% due to the absorbent nature of the gel. The dried product is sealed in a desiccator under dry argon since it is very hydroscopic.

All other room temperature ionic liquids we have made in our laboratory begin with the chloride salt. For those made in other laboratories, see the Materials and Methods section of Chapter 3. To make hydrogenated imidazolium chlorides, the imidazole is reacted with an equimolar amount of concentrated hydrochloric acid. Dimethylimidazole is a glassy solid at room temperature, so it must be melted, massed, and dissolved in 2-propanol. The imidazoles are diluted with an equal volume of 2-propanol in a round-bottomed flask. The hydrochloric acid is slowly added dropwise at 0 °C. The reaction is allowed to proceed for 1-2 hours to make sure everything has reacted. The final product is spectroscopically purer if the reaction is done under argon; however, this is not always a necessity.

The 2-propanol and any water is removed by rotovaping at ~50 °C. Also, small amounts of excess HCl can be removed by adding a few small aliquots of water to the RTIL while rotovaping. After observable evaporation has ended, it is advisable to continue evaporating for at least another hour. To remove any excess imidazole, the RTIL is washed with ethyl acetate at least three times in a separatory funnel. The ethyl acetate can be quickly evaporated off in a rotovap. Products are typically dried for 24 hours in a vacuum desiccator under P_2O_5. They can also be dried with silica, similarly to the ethylammonium nitrate.

To substitute the chloride for bis[trifluoromethane-sulfonimide], the RTIL is added to an equimolar amount of lithium trifluoromethanesulfonimide dissolved in water, and the mixture is stirred for 24 hours. Two layers will have formed: the bottom is the hydrophilic RTIL product, and the upper is aqueous lithium chloride. Water in the RTIL can be removed through rotovaping as before. Excess chloride must be removed by washing with multiple aliquots of water and checking purity with the silver nitrate test.

Viscosity Measurements

Since the viscosity of a fluid can alter its solvation behaviors, we often need to report viscosity along with solvation characteristics. We measure solvation using a ViscoLab 4000 (Cambridge Applied Systems) piston-style viscometer. It measures viscosity by determining the amount of magnetic force needed to move a piston of a certain weight vertically through a fluid.[13] Pistons of different weights for various viscosity ranges are available through the company. This viscometer is simple to operate. The piston is placed conical-end down into the instrument's cylindrical sample chamber. Enough fluid is added to fill to the top of the cylinder (~1 mL). The instrument control box will display the viscosity along with the interior temperature of the sample chamber. Temperature can be regulated with the water jacket connected to any standard temperature-controlled water circulator. Heating the fluid

slowly will help ensure temperature equilibration and accurate measurements. Instrumental uncertainties are shown along with the viscosity and temperature readings.

A few precautions will help ensure easy, accurate operation.[13] The piston range must be chosen correctly to avoid anomalous readings. Traces of solvents left in the sample chamber or on the piston can affect accuracy; the sample chamber must be thoroughly cleaned with an appropriate residue-free solvent and wiped dry with a sponge. Care must also be taken not to scratch the inside of the sample chamber with any foreign objects. Besides pipettes and cleaning supplies, this also includes particulate matter in the sample itself. The sample needs to be well-filtered and protected from dust. Air bubbles can also affect accuracy, so liquids must be added slowly, and the viscometer has a purging option to remove bubbles before any measurements are taken.

References

(1) O'Connor, D. V.; Phillips, D. *Time-Correlated Single-Photon Counting*; Academic Press: Orlando, FL, 1984.

(2) Bright, F. V.; Munson, C. A. *Anal. Chim. Acta* **2003**, *500*, 71.

(3) Lakowicz, J. R. *Topics in fluorescence spectroscopy.* Vol. I. Plenom Press: New York, NY, 1992. Ch. 1-2.

(4) Maroncelli, M.; Fleming, G. R. *J. Chem. Phys.* **1987**, *86*, 6221.

(5) Karmakar, R.; Samanta, A. *J. Phys. Chem. A* **2002**, *106*, 6670.

(6) Nandi, N. K.; Bhattacharyya, K.; Bagchi, B. *Chem. Rev.* **2000**, *100*, 2013.

(7) Fee. R. S.; Maroncelli, M. *Chem. Phys.* **1994**, *183*, 235.

(8) Horng, M. L.; Gardecki, J. A.; Papazyan, A.; Maroncelli, M. *J. Phys. Chem.* **1995**, *99*, 17311.

(9) Marcus, R. A. *J. Chem. Phys.* **1963**, *38*, 1858.

(10) Jordanides, X. J.; Lang, M. J.; Song, X.; Fleming, G. R. *J. Phys. Chem. B* **1999**, *103*,

7995.

(11) Weingurtner, H.; Merkel, T.; Kashammer, S.; Schroer, W.; Wiegand, S. *Ber. Bunsenges. Phys. Chem.* **1993**, *97*, 970.

(12) Garlitz, J. A.; Summers, C. A.; Flowers, R. A.; Borgstahl, G. E. O. *Acta. Cryst.* **1999**, *D55*, 2037.

(13) *ViscoLab 3000/4000/4100 Operations Manual*, Cambridge Applied Systems.

CHAPTER 3. DYNAMIC SOLVATION IN ROOM TEMPERATURE IONIC LIQUIDS

A paper published in the *Journal of Physical Chemistry B*[1]

Pramit K. Chowdhury, Mintu Halder, Lindsay Sanders, Tessa Calhoun, Jared L. Anderson, Daniel W. Armstrong, Xueyu Song, and Jacob W. Petrich[2]

Abstract

The dynamic solvation of the fluorescent probe coumarin 153 is measured in five room temperature ionic liquids using different experimental techniques and methods of data analysis. With time-resolved stimulated emission and time-correlated single-photon counting techniques, it is found that the solvation is comprised of an initial rapid component of ~55 ps. In all the solvents, half or more of the solvation is completed within 100 ps. The remainder of the solvation occurs on a much longer time scale. The emission spectra of coumarin 153 are nearly superimposable at all temperatures in a given solvent unless they are obtained using the supercooled liquid, suggesting that the solvents have an essentially glassy nature. The physical origin of the two components is discussed in terms of the polarizability of the organic cation for the faster one and the relative diffusional motion of the cations and the anions for the slower one. A comparison of the solvation response functions obtained from single-wavelength and from spectral-reconstruction measurements is provided. Preliminary fluorescence upconversion measurements are presented against which the appropriateness of

---

[1]Reproduced with permission from *J. Phys. Chem. B* **2004**, *108*, 10245. Copyright 2004 American Chemical Society.

[2]Author to whom correspondence should be addressed.

the single-wavelength method for constructing solvation correlation functions and the use of stimulated emission measurements is considered. These measurements are consistent with the trends mentioned above, but a comparison indicates that the presence of one or more excited states distorts the stimulated emission kinetics such that they do not perfectly reproduce the spontaneous emission data. Fluorescence upconversion results indicate an initial solvation component on the order of ~7 ps.

Introduction

Room-temperature ionic liquids (RTILs) are becoming an increasingly rich area of study.[1,2] They have been used as novel solvent systems for organic synthesis,[3-16] for liquid-liquid extraction,[17,18] in electrochemical studies,[19] and as ultralow volatility liquid matrices for matrix-assisted laser desorption/ionization (MALDI) mass spectrometry.[20] RTILs have other properties that make their application in chemical systems attractive. Some are immiscible with water and nonpolar organic solvents. They are stable to temperatures in excess of 300°C, but they have negligible vapor pressures, thus making them "green" solvents by reducing environmental levels of volatile organic carbons. Their viscosities can easily be varied by changing their cationic or anionic constituents.

Most ionic liquids are said to have similar polarities, close to those of short-chain alcohols.[21-24] The solvatochromic effect of Reichardt's dye[21] and Nile Red[22] as well as of fluorescent probes[23,24] and the Rohrschneider-McReynolds gas-liquid chromatography (GLC) method[25] have been used to characterize ionic liquids by obtaining a general, one-dimensional polarity-based parameter. This approach has not been successful for RTILs because they all fall within the same narrow range of values.[21-24] Yet, two different ionic liquids that have essentially identical "polarity," as measured by such methods, can produce very different results when used as solvents for organic reactions, gas-liquid chromatography, or extractions. Most recently, we have used the solvation parameter model

developed by Abraham, which has been developed to characterize either liquid- or gas-phase interactions between solute molecules and liquid phases.[26-28] This model is based on a linear free energy relationship. The solute retention factor is determined chromatographically for a set of probe solutes, and a multiple linear regression analysis relates it to a set of five parameters that characterize the solvent.[2]

Solvent properties can dramatically influence the rate of chemical reactions. Assuming equilibrium solvation along the reaction coordinate, many of these effects can indeed be explained by classical thermodynamics, as the construction of the above linear free energy relationships attempts. A thermodynamic approach is valid, however, only if the motion of the solvent molecules is very fast compared with the motion along the reaction coordinate, so that the solvent is always in equilibrium with the solute. In particular, the solvent relaxation timescales influence the dynamics of electron transfer, proton transfer, and other charge transfer reactions by exerting a time-dependent dielectric friction. In these cases, reaction rates may be limited by the rate of solvent relaxation.[29,30] A well established method to measure time-dependent solvation is by means of time-resolved fluorescence spectroscopy. After short-pulse excitation, the fluorescence spectrum of a probe solute red shifts in time as the surrounding solvent reequilibrates to the new, excited-state charge distribution. This time-dependent fluorescence shift provides a direct measure of the kinetics of solvation occurring at the microscopic level relevant to chemical reactions.[29]

Before the availability of room temperature ionic liquids, transient solvation by ions was studied by Huppert and coworkers using molten salts[31,32] and by Maroncelli and coworkers using nonaqueous solutions of dissolved ions.[33] The dynamic aspects of solvation by room temperature ionic liquids are becoming an object of experimental and theoretical studies. The dynamic solvation and the reorientational behavior of several probe molecules in different ionic liquids have recently been investigated.[34-39] These workers have shown that the solvation dynamics is biphasic. A molecular dynamics simulation by Shim et al.[40] has

been interpreted in terms of the faster component corresponding to diffusional motion of the anion and the slower component corresponding to collective motion of the anion and the cation. In addition, Hyun et al.[41] and Giraud et al.[42] have used the optical Kerr effect to study the low-frequency vibrational motions (< 200 cm^{-1}) of these solvents.

In this article, we address the dynamic aspects of solvation by RTILs using Stokes shift data of the fluorescent probe, coumarin 153 (Figure 3.1), from the subpicosecond to the nanosecond time regimes. We investigate four RTILs based on the 1-butyl-3-methylimidazolium cation, $BMIM^+$, and either the Cl^-, BF_4^-, PF_6^-, or the $(CF_3SO_2)_2N^-$ anions (Figure 3.1). They are typically referred to as [$BMIM^+$][Cl^-], [$BMIM^+$][BF_4^-], [$BMIM^+$][PF_6^-], and [$BMIM^+$][NTf_2^-], respectively. We compare these RTILs with the organic subunits, butylimidazole and methylimidazole. A fifth ionic liquid studied is [$NHEt_3^+$][TFA^-], triethylammonium trifluoroacetate. Major conclusions are that the rapid initial phase of solvation arises from the cation and that the simulations of Shim et al.[40] may not provide an appropriate comparison for large organic fluorescent solvation probes, such as coumarin 153. In the course of this work, comparisons are made between different methods of constructing the solvation correlation function and of obtaining the solvation data itself. Consequently, this work addresses aspects of methodology nearly as much as the problem of solvation by RTILs.

The plan of the article is as follows. After a description of the various experimental and data-treatment methods, we present the results. It became apparent during the course of the investigation that they depend sometimes rather significantly on the type of experiment or data treatment used. The discussion section is separated into three parts. The first is a short consideration of the steady-state spectra of the RTILs. The second deals with the early stages of this work, where the long-time behavior (up to 4 ns) of RTILs was studied by time-correlated single-photon counting and the early events by stimulated emission, the latter of which employed a particular method of constructing the solvation correlation function using

a single probe wavelength. Although these methods produced results obeying reasonable trends, it became apparent that neither measurement of stimulated emission nor single-wavelength analysis was adequate. The third part of the discussion provides a comparison with results from upconversion measurements that offer a more traditional and direct measure of spontaneous emission. Salient points are summarized in the conclusions section.

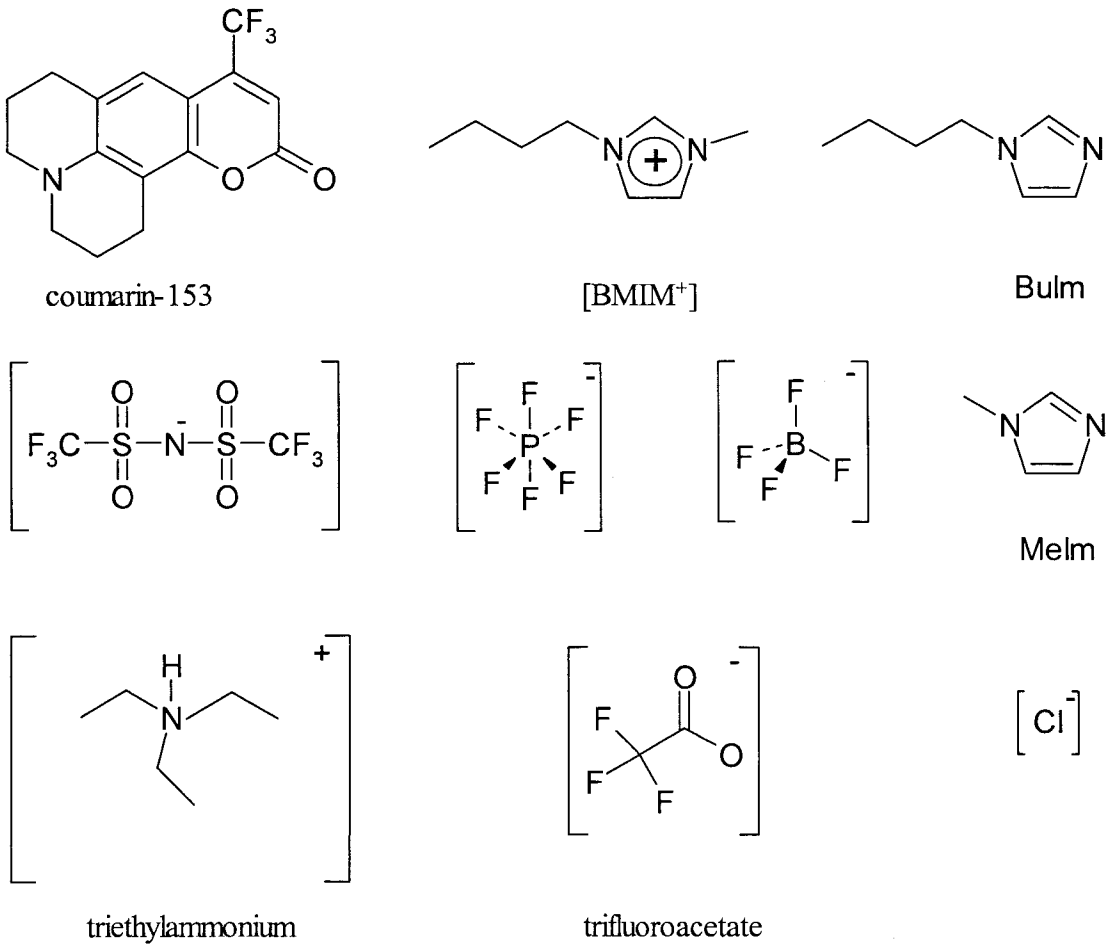

Figure 3.1: The solvation probe, coumarin 153; 4 RTILs ([$BMIM^+$][Cl^-], [$BMIM^+$][BF_4^-], [$BMIM^+$][PF_6^-], and [$BMIM^+$][NTf_2^-]) formed from the 1-butyl-3-methylimidazolium cation and the four anions indicated ([NTf_2^-] is $(CF_3SO_2)_2N^-$); one RTIL formed from the triethylammonium cation and trifluoroacetate ([$NHEt_3^+$][TFA^-]); and butylimidazole and methylimidazole.

Materials and Methods

Room Temperature Ionic Liquids. 1-Butyl-3-methylimidazolium chloride [$BMIM^+$][Cl^-] is produced by refluxing equimolar amounts of 1-methylimidazole with 1-chlorobutane at 70 °C for 72 hours. The resulting [$BMIM^+$][Cl^-] is washed with ethyl acetate and dried under vacuum. 1-Butyl-3-methylimidazolium tetrafluoroborate [$BMIM^+$][BF_4^-] is produced by mixing 10 grams [$BMIM^+$][Cl^-] (0.057 mol) in ~100 mL acetone. 6.29 grams (0.057 mol) of sodium tetrafluoroborate is added and stirred for 24 hours. The resulting sodium chloride is filtered off and the acetone removed under vacuum. 1-Butyl-3-methylimidazolium hexafluorophosphate [$BMIM^+$][PF_6^-] is produced by dissolving 164.49 grams (0.94 mol) [$BMIM^+$][Cl^-] in ~250 mL water, reacting an equimolar amount (0.94 mol) of hexafluorophosphoric acid (HPF_6), and stirring for 24 hours. The resulting [$BMIM^+$][PF_6^-] is washed with water until the washings are no longer acidic. The IL is then dried under vacuum. Hexafluorophosphoric acid is corrosive, toxic and should be handled with care. 1-Butyl-3-methylimidazolium bis[(trifluoromethyl)-sulfonyl]imide, [$BMIM^+$][NTf_2^-], is produced by dissolving 34.0 grams (0.118 mol) N-lithiotrifluoromethanesulfonimide in ~150 mL water and mixing with 20.67 grams (0.118 mol) [$BMIM^+$][Cl^-] also dissolved in ~150 mL water. The mixture is stirred for 12 hours. The aqueous portion is removed and the resulting ionic liquid washed with water and then dried under vacuum. All RTILs produced using the [$BMIM^+$][Cl^-] salt are subjected to the silver nitrate test to ensure no chloride impurities remain in the samples. [$NHEt_3^+$][TFA^-] is prepared by adding a slight molar excess of trifluoroacetic acid dropwise to triethylamine in a 50 mL round bottom flask. The mixture is then heated at 40 °C and stirred for 2 hours. Excess trifluoroacetic acid is removed under vacuum, and the remaining ionic liquid is dried using a silica gel column and then stored under P_2O_5.

Spectroscopic Measurements and Data Analysis. Butylimidazole (>98% purity) and methylimidazole (>99% purity) were obtained from Aldrich (St. Louis, MO) and dried over molecular sieves (type 4A) before use. During spectroscopic measurements, the quartz cuvettes are kept tightly sealed so as to prevent moisture from being absorbed by the ionic liquids. The temperature dependent measurements are carried out in a thermoelectric temperature controlled cuvette holder (Quantum Northwest, WA), permitting regulation over the range -40-100 °C. All ionic liquids are carefully dried before optical measurements were performed. Silica gel of 60-200 mesh is activated at 150 °C. A small silica gel column is prepared using a Pasteur pipette and the pure ionic liquid is added to the column. Depending on the viscosity of the ionic liquid, a bulb is used to force the ionic liquid through the silica gel column. Once the ionic liquid emerges from the column, it is stored in a dessicator under P_2O_5 until further use. The RTILs are subsequently dried over molecular sieves: Type 4A, GRADE 514, 8-12 Mesh and with effective pore size of 4 angstroms.

Steady-state Measurements. Steady-state excitation and emission spectra are recorded with a SPEX Fluoromax with a 4-nm bandpass and corrected for detector response. A 1-cm pathlength quartz cuvette is used for the measurements. The steady-state spectra can be used to compute the reorganization energy, λ, by means of [43]:

$$\lambda = \hbar \frac{\int_0^\infty d\upsilon [\sigma_a(\upsilon) - \sigma_f(\upsilon)]\upsilon}{\int_0^\infty d\upsilon [\sigma_a(\upsilon) + \sigma_f(\upsilon)]} \tag{3.1}$$

The $\sigma_{a,f}$ are the absorption (or excitation) and emission spectra, respectively, on a wavenumber scale. The reorganization energy is widely used as a measure of the strength of interactions between a chromophore and its surrounding dielectric media in solvation dynamics studies. It is usually taken as half of the Stokes shift. This estimation is accurate if the excitation and emission spectra are Gaussian, but it becomes unreliable if they are not.

The actual computation of λ is accomplished by first manipulating the emission and excitation spectra to permit their addition and subtraction. This requires normalized spectra consisting of equally spaced points. We interpolate and renormalize them so as to obtain spectra having 20-cm^{-1} spacing between each point and then shift the crossing point of the two curves so that it lies at 0 cm^{-1}. The spectral baselines are then corrected by subtracting the lowest intensity and renormalizing. This manipulation is motivated by the low intensity emission near 800 nm and questions concerning the utility of the correction factors of our fluorimeter in this region. In any case, baseline subtraction is minor and changes the final result by approximately 1%. An appropriate number of zeros is added to the high energy end of the emission spectrum and to the low energy end of the excitation spectrum so that the curves can be added and subtracted along their entire breadths. λ may now be calculated according to Equation 1. In practice, however, the integration is more conveniently performed from negative infinity to zero instead of from zero to positive infinity to avoid interference from transitions to higher-lying excited states. Taking these limits of integration is permitted as long as there is mirror image symmetry between the emission and excitation spectra. Time-resolved spectra are treated similarly, but the emission data first must be continued down to zero intensity, since it is impractical to obtain time- and spectrally-resolved data out into the wings of the emission spectrum. This continuation is done simply by connecting the last two points of the available data with straight lines that extend to zero. These new curves consisting of the data points and the straight lines are interpolated in the same way as the steady state excitation curve. The value of λ is sensitive to the way in which the spectrum is continued. We have used both straight-line and log-normal continuations, but have opted for the simplest. The errors introduced in the continuation are effectively canceled when time-dependent λ's are compared with each other (as opposed to the steady-state λ's) as they are in Table 3.1, which furnishes λ at 100 and 4000 ps. The rest of the process proceeds as above. All data manipulations were performed with Microcal Origin 7.0.

Time-resolved Measurements. The laser source for the time-correlated single-photon counting measurements was a home-made mode-locked Ti-sapphire laser, tunable from 780 to 900 nm with a repetition rate of 82 MHz. The fundamental from the Ti-sapphire oscillator was modulated by a Pockels cell (Model 350-160, Conoptics Inc) to reduce the repetition rate to about 8.8 MHz and was subsequently frequency doubled by focusing tightly into a 0.4-mm BBO crystal. The resulting blue light, which had a central wavelength of 425 nm, provided the excitation source. The fluorescence decays were collected at the magic angle (polarization of 54.7° with respect to the vertical). Emission was collected through a single monochromator (ISA H10) fitted with a slit having an 8 nm band pass. A half-wave plate before a vertical polarizer ensured the polarization of the excitation light. The instrument response function of the apparatus had a full-width–at-half-maximum (FWHM) of 80 ps. A cuvette of 1-cm pathlength was used for the time-resolved measurements of C153 in the different solvents. To construct the time resolved spectra, a series of decays (~3000 counts in the peak channel) were collected over as much of the fluorescence spectrum as possible and were fit to a maximum of three exponentials, yielding fits with chi-squared values ~1. Transient spectra were reconstructed from these fits by normalizing to the steady state spectra of the samples according to the equation[29]:

$$S(\lambda,t) = D(\lambda,t)\frac{S_0(\lambda)}{\int_0^\infty D(\lambda,t)} \tag{3.2}$$

$D(\lambda,t)$ is the wavelength-resolved fluorescence decay; $S_0(\lambda)$, the steady-state emission intensity at a given wavelength. We have employed the traditional approach of fitting the time-resolved spectra to a log-normal line-shape function, from which we extract the peak frequency, $\nu(t)$, as a function of time. The solvation dynamics were described by the normalized correlation function as follows[29]:

$$C(t) = \frac{\nu(t) - \nu(\infty)}{\nu(0) - \nu(\infty)} \tag{3.3}$$

$\nu(0)$ is the frequency at zero time, that is, immediately after excitation. $\nu(\infty)$ is the frequency at "infinite time," the maximum of the steady state fluorescence spectrum. The decays used to construct the time resolved emission spectra were typically collected over a range of wavelengths from 470 nm to 610 nm at intervals of 10 nm: unless otherwise indicated, a total of fifteen transients were used to construct the time-resolved emission spectra, from which the C(t) were obtained.

Transient Absorption (Stimulated Emission) Measurements. The instrument function of our time-correlated single-photon counting system has a FWHM of 80 ps. In order to investigate more rapid phenomena, better time resolution was required. This was provided by a home-made regeneratively amplified Ti:sapphire system,[44,45] providing 130-fs pulses, which we used to perform pump-probe transient stimulated emission measurements. Samples were excited at 407 nm. ($[BMIM^+][Cl^-]$ was not investigated with this system because our rotating sample holder is not temperature controlled and because the solvent slowly solidifies at room temperature.)

The use of stimulated emission to measure solvation requires special conditions—notably that excited-state (and ground-state) absorption does not contaminate the signal. Such a situation should not be assumed to be the norm. Ernsting and coworkers[46] have studied the time-dependent spectra of coumarin 153. Their results suggested that the spectral regions near 480 and 560 nm are free of absorbing species. This was fortuitous because Gardecki and Maroncelli[47] indicated that 480 and 560 nm could be used for coumarin 153 to construct single-wavelength solvation correlation functions. Such a situation seemed to be optimal experimentally since laboratories are more typically equipped to perform transient

absorption than fluorescence upconversion experiments and because a single-wavelength analysis is not as time-consuming as one requiring data collection over a range of wavelengths. Several research groups have discussed and employed the single-wavelength solvent correlation function, $C_{SW}(t)$.[47-49] As a result, we measured stimulated emission kinetics at 480 nm and 560 nm, and typically collected over a full time scale of 100 ps.

To have a picture of the solvation over the entire time scale, starting from "time zero" (as defined by the 130-fs pulses of the transient absorption apparatus) to about 4 ns, the longest time scale we investigated with our photon-counting system, we spliced the data from the two experiments together and constructed the single-wavelength solvation response function at the probe wavelength of 480 nm. The decay curves from the stimulated emission and the photon-counting measurements were first fit to multiexponential functions. The data points were taken from the fitted stimulated emission kinetics for the first 100 ps and from from the fitted photon-counting experiments for 100 ps to 4 ns. The spliced curves were normalized according to the following equation[47]:

$$F'(\nu,t) = F(\nu,t)\exp\left\{+K_{tot}^{\infty}t\right\} \tag{3.4}$$

where $F(\nu, t)$ is the spliced emission curve and $\exp\left\{+K_{tot}^{\infty}t\right\}$ is the population factor. For normalization, we used the inverse of the average fluorescence lifetime ($1/\langle\tau_F\rangle$), obtained from measuring the fluorescence decay while collecting light from most of the emission band, to approximate K_{tot}. An average lifetime is employed since the fluorescence decay is not well described by a single exponential. Once the population factor was taken into account, the normalized single wavelength solvation response curve, $C_{SW}(t)$, was constructed:

$$C_{SW}(t) = \frac{F'(\nu_{SW},t) - F'(\nu_{SW},\infty)}{F'(\nu_{SW},0) - F'(\nu_{SW},\infty)} \tag{3.5}$$

Fluorescence Upconversion Measurements. The system used for fluorescence upconversion measurements is the same amplified Ti:sapphire referred to above. The fundamental output from the amplifier (815 nm) is doubled by a type-I LBO crystal (2 mm). The frequency doubled blue pulses (407 nm) are separated from the fundamental by a dielectric mirror coated for 400 nm and are focused onto a rotating cell containing the sample using a 5-cm convex lens. The remaining fundamental is used as the gate to upconvert emission. Fluorescence is collected by an LMH-10x microscopic objective (OFR Precision Optical Products) coated for near UV transmission. The gate and the emission are focused by a quartz lens (12 cm) onto a type-I 0.4-mm BBO crystal (MgF_2 coated, cut at 31° and mounted by Quantum Technology, Inc). The polarization of both the gate and excitation source is controlled with a set of zero-order half-wave plates for 800 nm and 400 nm, respectively. The upconverted signal is then directed into an H10 (8 nm/mm) monochromator (Jobin Yvon/ Spex Instruments S. A. Group) with a 5-cm convex lens coupled to a Hamamatsu R 980 PMT equipped with a UG11 UV-pass filter and operated at maximum sensitivity. The PMT output is amplified in two stages (total by a factor of 25, 5 for each stage) by a Stanford research Systems SR-445 DC-300 MHz amplifier with input terminated at 500 Ω and was carefully calibrated after a long (1-2 hours) warm-up. Photon arrival events are registered with a SR-400 gated photon counter operated in CW mode with a threshold level of -100 mV. This signal is fed into a boxcar averager. A part of the blue pulse train is used to normalize pump beam fluctuations. A translation stage (Compumotor) with a resolution of 0.06 mm/step is used to delay the exciting pulses, and a computer with Keithley Metrabyte (DAS 800) interfacing card drives the motor. The instrument response function is obtained by collecting the cross-correlation function of the blue and red pulses; the resulting third harmonic intensity is plotted against delay time. The cross-correlation functions typically have a FWHM of ~1 ps. This instrument response is a little over three times as broad as that obtained with our unamplified system.[50,51] We attribute this to the absence of compensating

prisms after frequency doubling, the presence of the rotating sample cell, and perhaps a nonideal optical geometry, which nevertheless permits the facile interchange between pump-probe transient absorption and fluorescence upconversion measurements. All curves are fit and deconvoluted from the instrument function using an iterative convolute and compare least-squares algorithm.

Results

Table 3.1 summarizes most of the results obtained in this study. (Upconversion results will be discussed separately.) Figure 3.2 presents excitation and emission spectra of coumarin 153 in the three ionic liquids for which we were able to obtain spectra above and below their melting points (while the ionic liquids still remained fluid). The significant feature is that the emission spectra of coumarin 153 are superimposable at all temperatures in a given solvent unless the spectra are obtained using the supercooled liquid.

Figure 3.3 presents two typical wavelength-resolved decay profiles of coumarin 153 in $[BMIM^+][NTf_2^-]$. Figure 3.4 gives the solvation correlation functions, $C_{SR}(t)$, constructed from the time-correlated single-photon counting data using the spectral reconstruction method. The single-wavelength solvent response functions, $C_{SW}(t)$, obtained at 480 nm from combining the stimulated-emission and the photon-counting results are shown in Figure 3.5. These results are direct measurements of the early rapid solvation process in these ionic liquids, at least 50% of which is completed in the first 100 ps. In general, this method reports a fast solvation component of 40-70 ps, which is considerably longer than the < 5 ps suggested by Maroncelli and coworkers[37,39] based on their estimation of the resolution of their time-correlated single-photon counting apparatus. The significance and accuracy of our result will be discussed in more detail at the end of this section. A comparison of the solvation correlation functions obtained from the single-wavelength and the spectral reconstruction methods is given in Figure 3.6 and in Table 3.1 in order to check the

appropriateness of using the stimulated emission data to measure the initial rapid phase of solvation. The agreement between the two methods is often quite good, as in the cases of $[BMIM^+][Cl^-]$ at 70°C, $[BMIM^+][BF_4^-]$, and butylimidazole. It is rather poor in the cases of $[BMIM^+][PF_6^-]$ and $[BMIM^+][NTf_2^-]$ (not shown). The agreement in general appears poorer upon comparison of the average solvation times in Table 3.1 than when visually inspecting the form of the correlation functions. This is because the curves fail to superimpose in the long-time region, where even low-amplitude slow dynamics can contribute considerably to the average. Even in this long-time region, however, the form of the two correlation functions may remain similar, as can be seen by comparing the data for $[BMIM^+][Cl^-]$ at 70°C and $[BMIM^+][BF_4^-]$.

Fluorescence upconversion measurements provide an independent gauge of the time scale for this initial rapid process. Whereas stimulated emission (i.e., transient absorption) measurements are sensitive to both emitting and absorbing species, fluorescence measurements report only on spontaneous emission and thus provide a more straightforward means of probing the solvation behavior of interest. Upconversion data are provided in Figures 3.7-3.9 for $[BMIM^+][PF_6^-]$, butylimidazole, and methanol. For each of the solvents, the transients obtained using the two methods are compared at 480 and 560 nm, the wavelengths suggested for use in single-wavelength analysis for coumarin 153.[47] For each solvent, there are deviations arising from excited-state absorbance at these wavelengths, which distort the time scale for solvation.

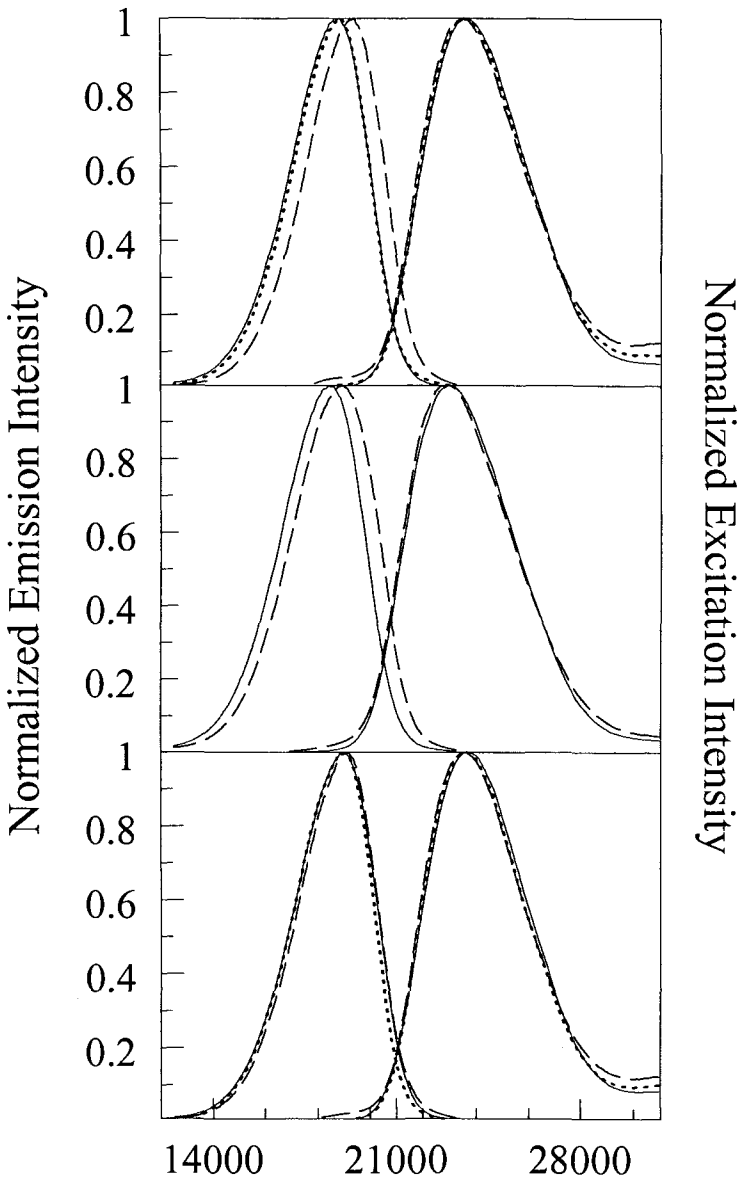

Figure 3.2: Excitation and emission spectra of coumarin 153 in [$BMIM^+$][PF_6^-] at 90°C (solid) λ = 2662 cm^{-1}, 25°C (dotted) λ = 2592 cm^{-1}, and -10°C, supercooled (dashed) λ = 2272 cm^{-1}; [$BMIM^+$][Cl^-] at 70°C (solid) λ = 2582 cm^{-1}, and 30°C, supercooled (dashed) λ = 2294 cm^{-1}; [$BMIM^+$][NTf_2^-] at 90°C (solid) λ = 2649 cm^{-1}, 25°C (dotted) λ = 2607 cm^{-1}, and -10°C, supercooled (dashed) λ = 2466 cm^{-1}. All samples were excited at 420 nm. For excitation spectra, the emission monochromator was set at 600 nm.

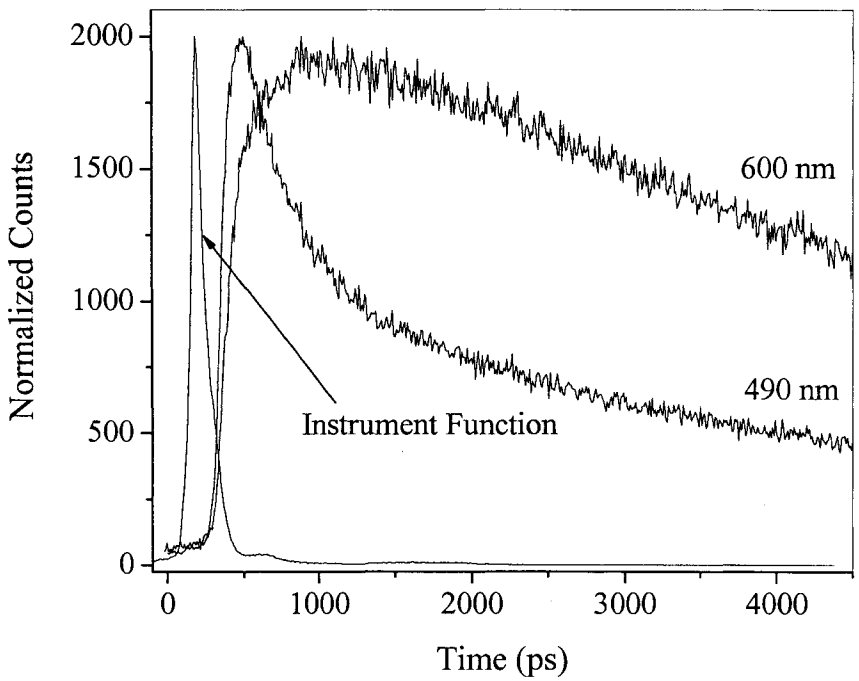

Figure 3.3: Representative wavelength-resolved decays for C153 [$BMIM^+$][NTf_2^-] at 490 and 600 nm. A typical instrument function profile is included. The trace at 600 nm reveals the growth of a solvent relaxed state (which is absent in the profile at 490 nm). The decays used to construct the time resolved emission spectra were typically collected over a range of wavelengths from 470 nm to 610 nm at intervals of 10 nm: a total of fifteen time-resolved fluorescence traces were used to construct the time-resolved emission spectra, from which the C(t) were obtained.

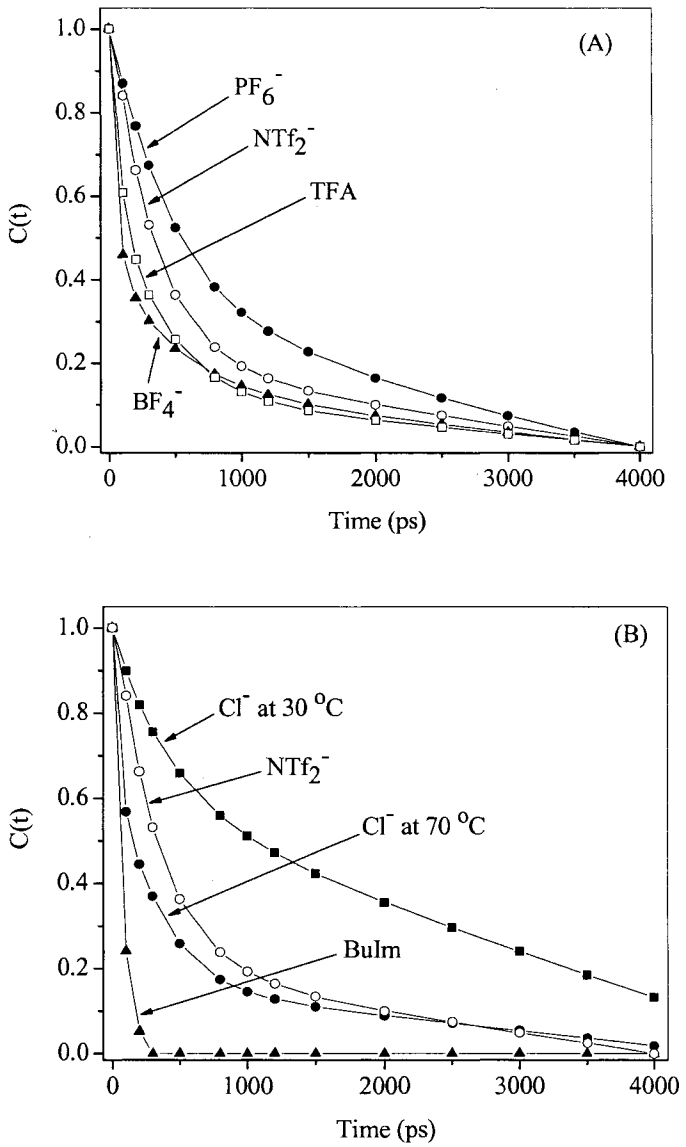

Figure 3.4: $C_{SR}(t)$ curves and corresponding fits for C153 in (A) $[BMIM^+][NTf_2^-]$ (hollow circles) [C(t) = 0.72 exp(-t/350 ps) + 0.28 exp(-t/1670 ps)], $[BMIM^+][PF_6^-]$ (solid circles) [C(t) = 0.36 exp(-t/360 ps) + 0.64 exp(-t/1360 ps)], $[BMIM^+][BF_4^-]$ (solid triangles) [C(t) = 0.62 exp(-t/60 ps) + 0.38 exp(-t/1100 ps)], and $[NHEt_3^+][TFA^-]$ (hollow squares) [C(t) = 0.58 exp(-t/120 ps) + 0.37 exp(-t/940 ps)] and (B) $[BMIM^+][Cl^-]$ at 30°C (solid squares) [C(t) = 0.24 exp(-t/270 ps) + 0.76 exp(-t/2530 ps)], $[BMIM^+][Cl^-]$ at 70°C (solid circles) [C(t) =0.63 exp(-t/120 ps) + 0.37 exp(-t/1290 ps)], $[BMIM^+][NTf_2^-]$ (hollow circles), and butylimidazole (solid triangles) [C(t) = exp(-t/70 ps)].

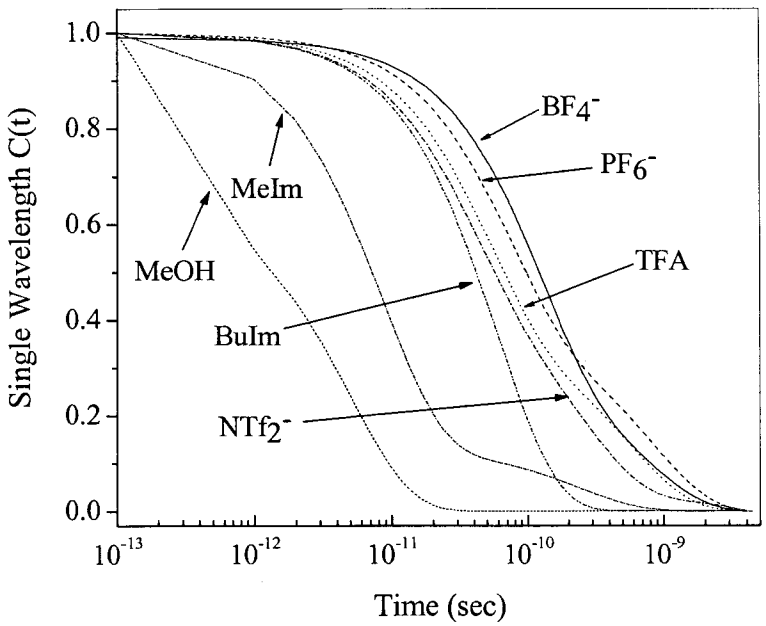

Figure 3.5: $C_{SW}(t)$ for C153 obtained at 480 nm at room temperature. The plots are stimulated emission kinetics obtained over 100 ps with 130-fs pulses and, where necessary, time-correlated single-photon counting data obtained over 4 ns with an 80-ps instrument function. The two traces were spliced together at 100 ps in order to present a continuous trace of the solvation dynamics. Global fits to the $C_{SW}(t)$ are summarized in Table 3.2. The $C_{SW}(t)$ for methanol is presented as a "control" experiment, yielding an average solvation time of 3.5 ps. That the fast solvation components of the $BMIM^+$ liquids resemble that of butylimidazole and that the fast component is seen to become more rapid as the solvent is changed to methylimidazole or to methanol suggests that the ~55-ps event in the ionic liquids is a plausible result. See, however, the correlation functions obtained from fluorescence upconversion data: Figures 3.7, 3.8, and 3.10.

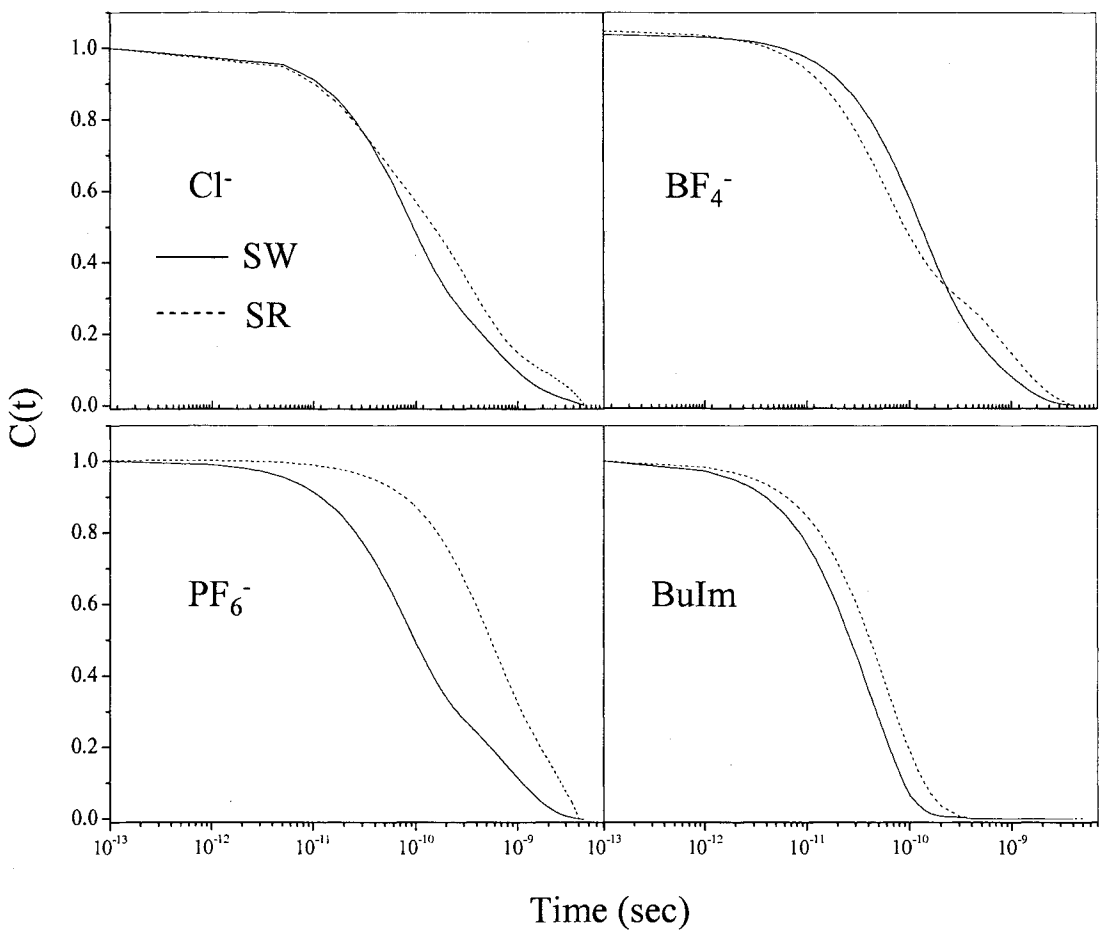

Figure 3.6: A comparison of the solvation correlation functions obtained from the single-wavelength (solid lines), $C_{SW}^{480nm}(t)$, and the spectral reconstruction (dashed lines), $C_{SR}(t)$, methods. All data were obtained from time-correlated single-photon counting experiments. A complete comparison is given in Tables 3.1 and 3.2. The agreement ranges from very good for [$BMIM^+$][Cl^-] at 70°C and [$BMIM^+$][BF_4^-] to poor for [$BMIM^+$][PF_6^-].

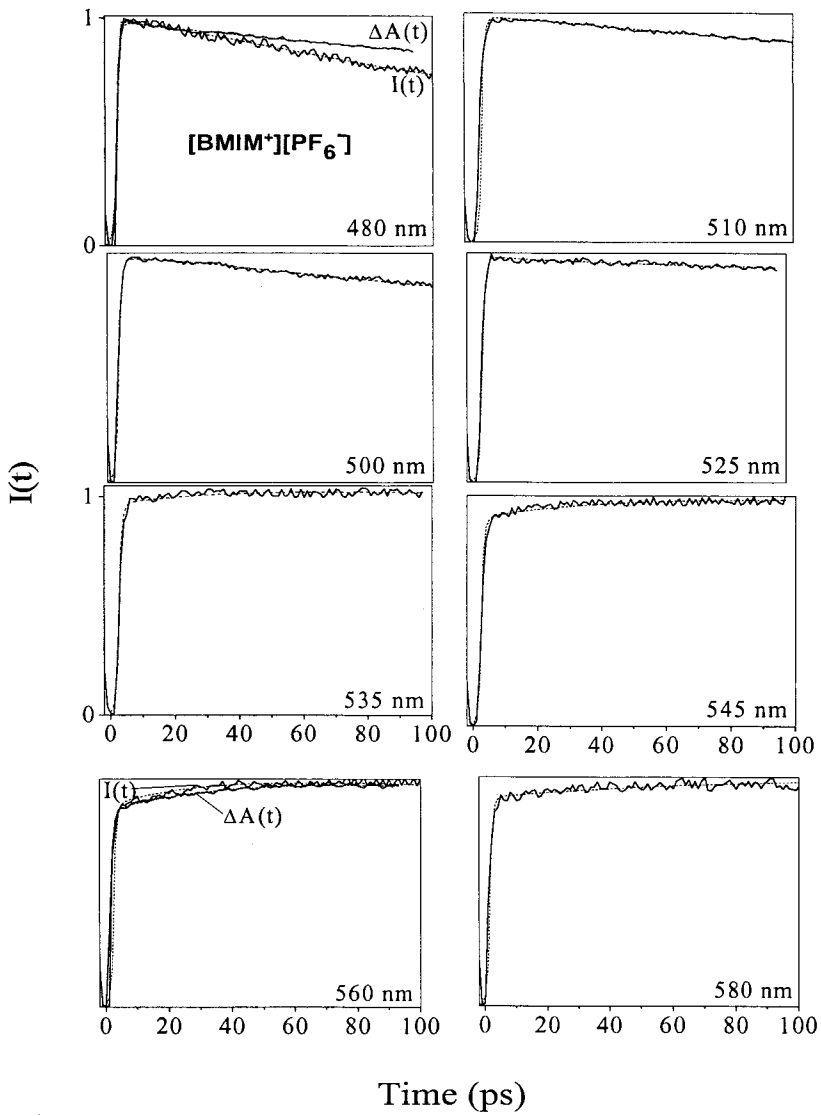

Figure 3.7: Normalized upconversion traces, I(t), for C153 in [$BMIM^+$][PF_6^-] at different wavelengths. ΔA(t) is the kinetic trace for the pump-probe stimulated experiment at the corresponding wavelength. All upconversion traces are fitted globally with time constants of 5, 210, and 5100 ps.

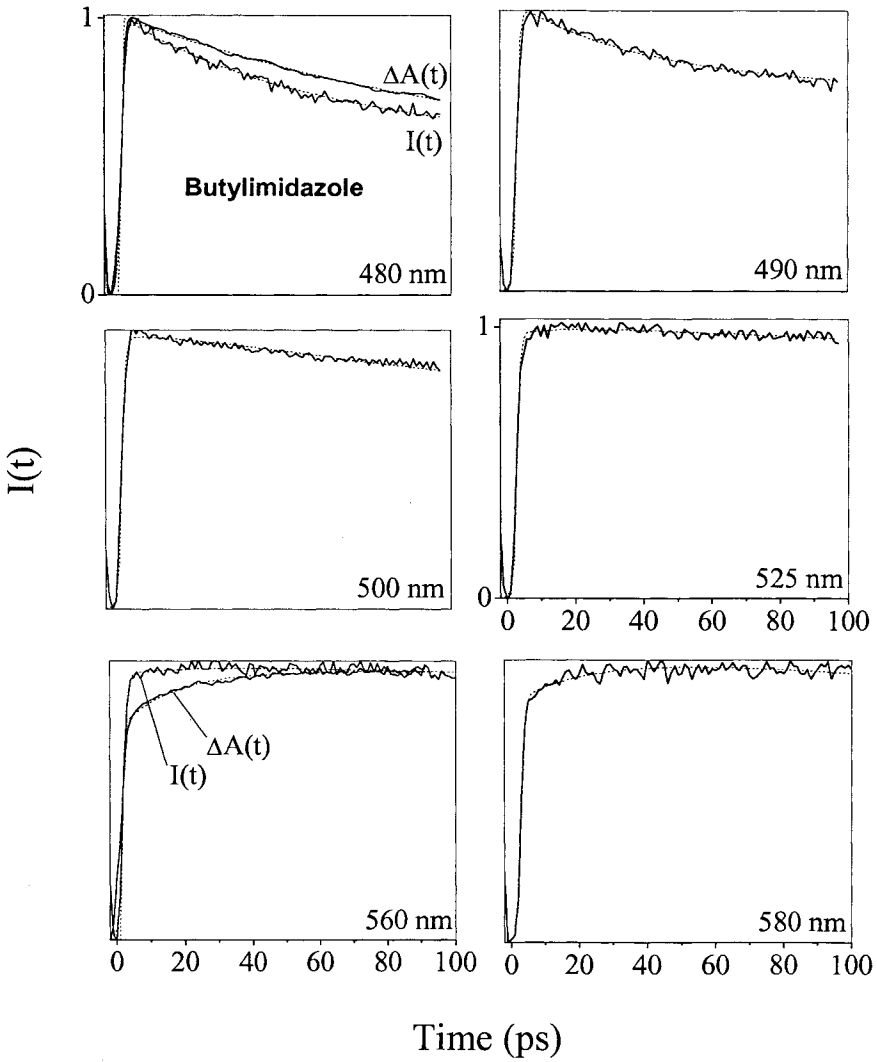

Figure 3.8: Normalized upconversion traces, I(t), for C153 in butylimidazole at different wavelengths. ΔA(t) is the kinetic trace for the pump-probe stimulated experiment at the corresponding wavelength. All upconversion traces are fitted globally with the following time constants: 28, 102, and 4700 ps.

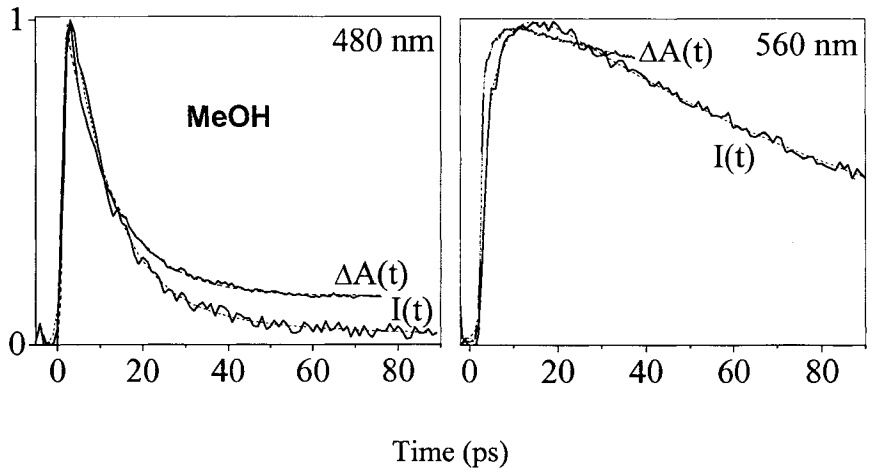

Figure 3.9: Normalized upconversion traces, I(t), for C153 in MeOH at the 480 and 560 nm along with the stimulated emission traces, ΔA(t), obtained at the same wavelengths.

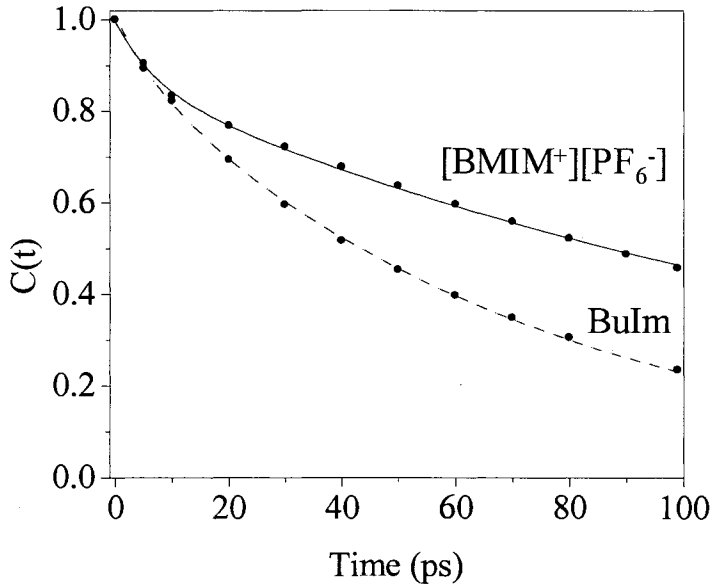

Figure 3.10: Solvation correlation functions, $C_{SR}(t)$, for $[BMIM^+][PF_6^-]$ (solid line) and butyl imidazole (dashed line). The correlations functions are well described by the following forms:

$[BMIM^+][PF_6^-]$: 0.14 exp(-t/7 ps) + 0.86 exp(-t/160 ps);
butylimidazole: 0.09 exp(-t/7 ps) + 0.91 exp(-t/72 ps).

It is likely that the relative amplitude of the short component in these correlation functions is reduced with respect to those obtained from stimulated emission measurements owing to the poorer time resolution of ~1 ps.

Table 3.1: Spectral characteristics of coumarin 153 in some RTILs

Ionic Liquid [a]	m.p. (°C)[b]	η (cP)	$\langle\nu\rangle_{abs}$ (cm^{-1})[d]	$\langle\nu\rangle_{em}$ (cm^{-1})[d]	λ (cm^{-1}) [e]	$\lambda_{100\ ps}$ (cm^{-1}) [f,g]	$\lambda_{4000\ ps}$ (cm^{-1}) [f,g]	$\langle\tau\rangle_{SR}$ (ns) [h]	$\langle\tau\rangle_{SW}$ (ns) [i]
$[BMIM^+][Cl^-]$ (30°C)	65	11000[c]	23490	18570	2294	1940	2112	2.0	1.7
$[BMIM^+][Cl^-]$ (70°C)	65	334[c]	23540	18090	2582	2285	2627	0.53	0.33
$[BMIM^+][PF_6^-]$ (20°C)	-8	371[c] 312[b]	24080	18420	2592	2015	2313	1.0 1.4 ± 0.3 [j] 1.8 ± 0.4 [k] 3.35 ± 0.02 [l] 6.47 ± 0.20 [s]	0.38
$[BMIM^+][BF_4^-]$ (20°C)	-82	154[c] 233[b]	23670	18350	2481	1968	2203	0.46 1.44 [m] 2.13 [n]	0.31
$[BMIM^+][NTf_2^-]$ (20°C)	-4	52[b]	24110	18530	2607	1965	2180	0.72 0.28 ± 0.04 [o] 0.48 ± 0.07 [p] 0.56 ± 0.08 [q] 0.38 ± 0.06 [r]	0.17
butylimidazole (20°C)		< 50	24040	18700	2622	2263	2344	0.070	0.041
methylimidazole (20°C)		< 50	24000	18330	2672	2484	2480	0.050	0.025
$[NHEt_3^+][TFA^-]$ (20°C)			26100	19450	2836	2451	2764	0.42	0.27

[a] For abbreviations, see the caption to Figure 3.1. Although the melting point of $[BMIM^+][Cl^-]$ is ~65°C,[57] it usually takes several days at room temperature before it solidifies.

[b] From reference.[57]

[c] From reference.[52]

[d] $< \nu > = \frac{\int_0^\infty \nu I(\nu) d\nu}{\int_0^\infty I(\nu) d\nu}$, computed using 70% of the emission and excitation spectra in order to exclude the contributions from absorption to states higher than S_1 in energy.

[e] Computed from Equation 3.1. See text and reference.[43]

[f] The reorganization energies at 100 and 4000 ps are computed as discussed in the experimental section. Note that because of the limited data set used to obtain the time resolved spectra, the λ at 4000 ps deviate from the steady-state values, for which in most cases we would expect them to be approximately the same.

[g] The fractional amount of solvation at 100 ps, for example, can be determined by $f_{100\,ps} = \frac{\lambda_{100\,ps} - \lambda_i}{\lambda_{4000\,ps} - \lambda_i}$, where λ_i is the intramolecular contribution to the reorganization energy. Maroncelli and coworkers have addressed the estimation of λ_i by proposing methods to compute the "zero-time" spectrum arising only from solvation.[58]

[h] Average solvation times obtained from the spectral reconstruction data, computed from the fit parameters given in the caption to Figure 3.4. The comparison of the average solvation times is made using only data accumulated from time-correlated single-photon counting data. Errors in the solvation times are ~± 15%.

[i] Average solvation times obtained from the single-wavelength data, computed from the fit parameters given in the caption to Figure 3.5. The average time is computed from the spliced picosecond and nanosecond experiments.

[j] 25 °C using 4-aminophthalimide (4-AP).[37]

[k] 25 °C using coumarin 102.[37]

[l] 25 °C using coumarin 153.[38]

[m] 20 °C using 6-propionyl-2-dimethylaminonaphthalene (Prodan).[35]

[n] At room temperature using coumarin 15. [34]

[o] 25 °C using coumarin 153. The average solvation time is computed from parameters obtained from a stretched exponential fit.[39]

[p] 20 °C using coumarin 153.[36]

[q] 20 °C using Prodan.[36]

[r] 20 °C using 4-AP.[36]

[s] 298 K using Prodan.[53]

Table 3.2: Global fitting of the initial rapid phase of $C_{SW}(t)$ of some RTILs [a]

Ionic Liquid	η (cP) [b]	a_1	τ_1 (ps)	τ_2 (ps)
$[BMIM^+][BF_4^-]$ (20°C)	154 [52] 233 [57]	0.39	55	1000
$[NHEt_3^+][TFA^-]$ (20°C)		0.61	55	650
$[BMIM^+][PF_6^-]$ (20°C)	371 [52] 312 [57]	0.62	55	2250
$[BMIM^+][NTf_2^-]$ (20°C)	52 [57]	0.73	55	1500
butylimidazole (20°C)	< 50	0.98	55	120
methylimidazole (20°C)	< 50	0.80	8.5	190
methanol (20°C)	0.59	0.35	0.32	5.2

[a] $C_{sw}(t)$ obtained from 480-nm stimulated emission data as described in the text are fit to a sum of exponentials, $C_{sw}(t) = a_1 \exp(-t/\tau_1) + a_2 \exp(-t/\tau_2)$, where $a_1 + a_2 = 1$. In all cases (except the last two solvents) the rapid solvation component is fixed at 55 ps. Given the 100-ps full scale used in most cases (for $[NHEt_3^+][TFA^-]$, a 400-ps scale was used), the longer-lived components should not be regarded as accurate estimations of the slower solvation phase. The $C_{sw}(t)$ are displayed in Figure 3.5.

[b] We have no viscosity information for $[NHEt_3^+][TFA^-]$ and have not been able to obtain any for butylimidazole or methylimidazole from either the literature or the supplier.

Disussion

Steady-State Spectra. Steady-state spectra taken as a function of temperature are presented in Figure 3.2 for three RTILs. Spectra obtained at temperatures above the melting point are nearly superimposable. These three solvents can be supercooled easily. Once the temperature is lowered below the melting point, crystallization occurs slowly. In the case of $[BMIM^+][Cl^-]$, it can occur over a period of several days. Upon supercooling, a significant change in the spectra is observed, which is manifest essentially in their position. There is less solvent relaxation, which we have quantified by means of the reorganization energy, λ (Table 3.1 and Figure 3.2). In the case of $[BMIM^+][Cl^-]$, λ decreases from 2582 cm^{-1} at 70°C to 2294 cm^{-1} for the supercooled liquid at 30°C. This shift suggests that the solvent is essentially "glassy" in the supercooled state. For $[BMIM^+][Cl^-]$, supercooling increases the average solvation time by about a factor of four. An interesting aspect of the spectra is that the change in reorganization energy between the normal (90°C) and the supercooled liquids (-10°C) is much smaller for $[BMIM^+][NTf_2^-]$ than for $[BMIM^+][Cl^-]$ and $[BMIM^+][PF_6^-]$: $\Delta\lambda$ = 183, 288, and 390 cm^{-1}, respectively (see the caption to Figure 3.2). That the change is the smallest for $[BMIM^+][NTf_2^-]$ may be attributed to it having the lowest viscosity of the three solvents: upon supercooling, it is immobilized to a lesser degree than $[BMIM^+][Cl^-]$ or $[BMIM^+][PF_6^-]$. We were unable to perform the same temperature dependent analysis with the BF_4^- solvent because it melts at -82°C and our apparatus did not permit us to obtain such a temperature. Maroncelli and coworkers[37,39] have recently shown that ionic liquids conform to standard glass behavior by fitting their kinetic data to stretched exponentials and by showing that it varies linearly with viscosity.

Stimulated Emission, Time-Correlated Single-Photon Counting, and Single-Wavelength Analysis. Inspection of Table 3.1 indicates that there is a considerable disparity in the values of the average solvation times obtained from different laboratories using the spectral

reconstruction method. Reasonable agreement is obtained between our result for $[BMIM^+][PF_6^-]$ and those of Maroncelli and coworkers using 4-AP and coumarin 102.[37] There is also reasonable agreement between our result for $[BMIM^+][NTf_2^-]$ and those of Karmakar and Samanta using coumarin 153 and Prodan.[36] Some of the disparity may be attributed to the number of counts collected in the fluorescence decay, which affects the signal-to-noise ratio, and to the full-scale time window used, which determines how accurately the long-time component is determined. In our case, we use ~4 ns, which is smaller than that used by other groups. A more significant origin of the discrepancies may arise from the preparation and purity of the ionic liquids themselves. Trace amounts of water and chloride impurities are known to have large effects on the viscosities and densities of RTILs [52]. Notably, Bright and coworkers[53] report that the average solvation time of Prodan in $[BMIM^+][PF_6^-]$ decreases from 6.5 to 3.9 ns as the water content is increased from <50 ppm to 1.8 wt %. Since the focus of this article is not to obtain a *quantitative* comparison of the long-time behavior of the RTILs, these differences do not cause excessive concern. They should, however, give an indication to future workers of the spectrum of results that have been obtained with an eye to assuring reproducibility when examining the glassiness of the RTILs.

Of more immediate interest in this work is the initial rapid phase of solvation in the ionic liquids. Several previous studies[34-39] have suggested, and our results indicate (Figures 3.4 and 3.5), that more than 50% of solvation relaxation is very rapid. The origin of these fast solvent fluctuations is not clear. We have hypothesized that the fast relaxations result from the organic cations. In order to test this idea, we attempted to compare the solvation dynamics of butylimidazole with those of the four ionic liquids bearing the BMIM cation. A comparison of $[NHEt_3^+][TFA^-]$ with triethylamine was, unfortunately, not possible because triethylamine quenches excited-state coumarin by electron transfer.[54] We attempted other comparisons with RTILs formed from butylpyridinium and pyridinium organic cations with

BF_4^- and NTf_2^-. These also presented complications in the excited-state kinetics that prevented a further comparison of solvation dynamics of the RTILs with their organic counterparts. The organic solvent, butylimidazole, has a solvation time of between 40-70 ps (Figures 3.4 and 3.5, Tables 3.1 and 3.2). Butylimidazole has a very low viscosity, and amplitudes of the fast components of the solvation times for the ionic liquid counterparts seem to scale with viscosity, as indicated by Figure 3.5 and Table 3.2. The latter presents the results of a global fitting analysis to the $C_{SW}(t)$ functions (except where indicated). In this procedure, the $C_{SW}(t)$ were fit to two decaying exponential components where the smallest time constant was fixed to agree roughly with that of butylimidazole, 55 ps. The amplitudes of the two components and the time constant of the longer were permitted to vary. A 55-ps component was present in all the fits. Such a value seems reasonable given that the time constant and the average solvation time for butanol, obtained by fluorescence measurements, are 47 and 63 ps, respectively.[55] Another point of comparison is provided by the $C_{SW}(t)$ of methylimidazole (Figure 3.5 and Table 3.2), which is dominated by a rapid component of 8.5 ps. The time constant and average solvation time for methanol, as measured by fluorescence techniques, are 2.3 and 5.0 ps, respectively.[55] Our $C_{SW}(t)$ for coumarin 153 in methanol (Figure 3.5) obtained from stimulated emission kinetics is described by an average solvation time of 3.5 ps. This suggests that ionic liquids based on the methylimidazolium cation will have much faster initial solvation components owing to the shortening of the aliphatic chain from butyl to methyl, just as the solvation by the alcohols is faster for methanol than for butanol. A more direct test of this hypothesis will require measurements of the solvation times of different RTILs at the same viscosity as well as a comparison with ionic liquids based on other cations.

On the other hand, another interpretation of the origin of the initial fast component has resulted from a recent computer simulation. Shim et al.[40] place a dipolar excitation on a model diatomic solute in a RTIL. They observe fast initial relaxation apparently arising from

translations of the anions. Given the small size of the model solute and the large changes in net charge, the motions of the resulting concentrated anionic charges may dominate the relaxation. In the experimental solvation dynamics studies of organic dye molecules such as coumarin 153 in RTILs, the charge distribution change is scattered across the whole probe molecule, which is most likely well solvated by the cations given the hydrophobic nature of C153 in the ground state. We suggest, therefore, that the most possible scenario is that the cation motions dominate the contribution of the initial fast relaxation upon excitation, which is consistent with our experimental observations. In order to elucidate the nature of the fast relaxations, a realistic model of C153 in RTILs will be needed.

Analysis Based Upon Fluorescence Upconversion Results. Finally, we wish to comment on the relative merits of using stimulated emission measurements, single wavelength construction of C(t), and direct fluorescence measurements. The comparison provided here, in particular the data presented in Figures 3.6-3.9, indicate that while the stimulated emission measurements provide a good qualitative picture of the dynamics, they deviate considerably from the fluorescence upconversion measurements. We have already noted the discrepancies in the subnanosecond and nanosecond time regimes using single wavelength and "complete" spectral data from photon-counting measurements (Figure 3.6). The fluorescence upconversion measurements permit us to make this comparison in the picosecond time regime. Examination of the traces at 480 and 560 nm indicates that there is at least one absorbing species that contributes to the stimulated emission signal. In the absence of absorption, the two techniques should give identical results. But in fact, for $[BMIM^+][PF_6^-]$ and butylimidazole, excited-state absorption causes the stimulated emission kinetics at 480 and 560 nm to decay and rise, respectively, slower than those of their spontaneous emission counterparts. This translates into an overestimation of the time scale for solvation by a factor of ~8. Deviations are also apparent for methanol. In particular, while the fluorescence

upconversion trace in methanol decays essentially to zero, the stimulated emission trace levels off at about 40 ps to a steady-state value of about 20% of the initial signal intensity, again indicating the presence of one or more absorbing states.

Figure 3.10 presents the $C_{SR}(t)$ for $[BMIM^+][PF_6^-]$ and buytlimidazole obtained from the data in Figures 3.7 and 3.8, respectively. These solvation correlation functions can both be fit to the same initial rapid component of 7 ps; and, as such, the role of the organic cation suggested by the stimulated emission studies is corroborated. A more comprehensive comparison is, however, required and is currently being undertaken.

Conclusions

Our results are generally consistent with those of previous workers,[34-39] but there are significant discrepancies in the average solvation times reported for some ionic liquids, most likely arising from the determination of the longer-lived dynamics. Solvation times obtained from the spectral resolution and the single wavelength methods are compared. Our stimulated emission experiments with subpicosecond time-resolution are the first to probe directly the initial rapid solvation component that had been suggested in the earlier studies. They yield a time constant in the range of 40-70 ps (Figure 3.5, Table 3.2). Nevertheless, fluorescence upconversion measurements indicate that the presence of excited-state absorption increases this time by approximately a factor of 8 from its value as obtained by monitoring spontaneous emission directly. Consequently, while stimulated emission measurements can be useful in indicating general trends, direct measurements of spontaneous emission and use of spectral reconstruction methods are required for quantitative work. These results lead one to inquire into the nature and the number of the excited states contributing to this absorption since their presence could profoundly affect the interpretation of solvation dynamics data, although studies to date have argued that this is not the case.[56] Finally, a comparison of the solvation times in the 1-butyl-3-methylimidazolium ionic liquids

with that of butylimidazole itself (and methylimidazole) leads us to consider the role of the polarizability of the cationic partner in giving rise to the initial rapid solvation component.

Acknowledgements

DWA was supported by NIH grant RO1 GM53825-08. We thank Dr. Ranjan Das for technical assistance in collecting the fluorescence upconversion data. Mark Maroncelli provided stimulating comments, and we thank him for sharing his Kerr-gated fluorescence data with us before publication.

References

(1) Seddon, K. R. *Nature (Materials)* **2003**, *2*, 363.

(2) Anderson, J. L.; Ding, J.; Welton, T.; Armstrong, D. W. *J. Am. Chem. Soc* **2002**, *124*, 14247.

(3) Wilkes, J. S.; Zaworotko, M. J. *J. Chem. Soc., Chem. Commun.* **1992**, 965.

(4) Adams, C. J.; Earle, M. J.; Roberts, G.; Seddon, K. R. *Chem. Commun.* **1998**, 2097.

(5) Earle, M. J.; McCormac, P. B.; Seddon, K. R. *Chem. Commun. (Cambridge)* **1998**, 2245.

(6) Dyson, P. J.; Ellis, D. J.; Parker, D. G.; Welton, T. *Chem. Commun. (Cambridge)* **1999**, 25.

(7) Leadbeater, N. E.; Torenius, H. M. *J. Org. Chem.* **2002**, *67*, 3145.

(8) Mann, B. E.; Guzman, M. H. *Inorg. Chim. Acta* **2002**, *330*, 143.

(9) Wasserscheid, P.; Keim, W. *Angew. Chem., Int. Ed.* **2000**, *39*, 3772.

(10) Reynolds, J. L.; Erdner, K. R.; Jones, P. B. *Org. Lett.* **2002**, *4*, 917.

(11) Welton, T. *Chem. Rev.* **1999**, *99*, 2071.

(12) Nara, S. J.; Harjani, J. R.; Salunkhe, M. M. *Tetrahedron Lett.* **2002**, *43*, 2979.

(13) Yao, Q. *Org. Lett.* **2002**, *4*, 2197.

(14) Fletcher, K. A.; Pandey, S.; Storey, I. K.; Hendricks, A. E.; Pandey, S. *Anal. Chim. Acta*

2002, *453*, 89.

(15) Grodkowski, J.; Neta, P. *J. Phys. Chem. A* **2002**, *106*, 5468.

(16) Handy, S. T.; Zhang, X. *Org. Lett.* **2001**, *3*, 233.

(17) Huddleston, J. G.; Rogers, R. D. *Chem. Commun.* **1998**, 1765.

(18) Dai, S.; Ju, Y. H.; Barnes, C. E. *J. Chem. Soc., Dalton Trans.* **1999**, 1201.

(19) Dickinson, V. E.; Williams, M. E.; Hendrickson, S. M.; Masui, H.; Murray, R. W. *J. Am. Chem. Soc.* **1999**, *121*, 613.

(20) Armstrong, D. W.; Zhang, L.-K.; He, L.; Gross, M. L. *Anal. Chem.* **2001**, *73*, 3679.

(21) Muldoon, M. J.; Gordon, C. M.; Dunkin, I. R. *J. Chem. Soc., Perkin Trans. 2* **2001**, 433.

(22) Carmichael, A. J.; Seddon, K. R. *J. Phys. Org. Chem.* **2000**, *13*, 591.

(23) Bonhote, P.; Dias, A.-P.; Papageorgiou, N.; Kalyanasundaram, K.; Graetzel, M. *Inorg. Chem.* **1996**, *35*, 1168.

(24) Aki, S. N. V. K.; Brennecke, J. F.; Samanta, A. *Chem. Commun, (Cambridge)* **2001**, 413.

(25) Armstrong, D. W.; He, L.; Liu, Y.-S. *Anal. Chem.* **1999**, *71*, 3873.

(26) Abraham, M. H.; Whiting, G. S.; Doherty, R. M.; Shuely, W. J. *J. Chromatogr. A* **1990**, *518*, 329.

(27) Abraham, M. H.; Whiting, G. S.; Andonian-Haftvan, J.; Steed, J. W. *J. Chromatogr. A* **1991**, *588*, 361.

(28) Abraham, M. H.; Whiting, G. S.; Doherty, R. M.; Shuely, W. J. *J. Chromatogr. A* **1991**, *587*, 213.

(29) Maroncelli, M.; Fleming, G. R. *J. Chem. Phys.* **1987**, *86*, 6221.

(30) Vajda, S.; Jimenez, R.; Rosenthal, S. J.; Fidler, V.; Fleming, G. R.; Castner, E. W. *J. Chem Soc. Faraday Transactions* **1995**, *91*, 867.

(31) Huppert, D.; Ittah, V.; Kosower, E. M. *Chem. Phys. Lett.* **1989**, *159*, 267.

(32) Ittah, V.; Huppert, D. *Chem. Phys. Lett.* **1990**, *173*, 496.

(33) Chapman, C. F.; Maroncelli, M. *J. Phys. Chem.* **1991**, *95*, 9095.

(34) Karmakar, R.; Samanta, A. *J. Phys. Chem. A* **2002**, *106*, 4447.

(35) Karmakar, R.; Samanta, A. *J. Phys. Chem. A* **2002**, *106*, 6670.

(36) Karmakar, B.; Samanta, A. *J. Phys. Chem. A* **2003**, *107*, 7340.

(37) Ingram, J. A.; Moog, R. S.; Ito, N.; Biswas, R.; Maroncelli, M. *J. Phys. Chem. B* **2003**, *107*, 5926.

(38) Chakrabarty, D.; Hazra, P.; Chakraborty, A.; Seth, D.; Sarkar, N. *Chem. Phys. Lett.* **2003**, *381*, 697.

(39) Arzhantsev, S.; Ito, N.; Heitz, M.; Maroncelli, M. *Chem. Phys. Lett.* **2003**, *381*, 278.

(40) Shim, Y.; Duan, J.; Choi, M. Y.; Kim, H. J. *J. Chem. Phys.* **2003**, *119*, 6411.

(41) Hyun, B.-R.; Dzyuba, S. V.; Bartsch, R. A.; Quitevis, E. L. *J. Phys. Chem. A* **2002**, *106*, 7579.

(42) Giraud, G.; Gordon, C. M.; Dunkin, I. R.; Wynne, K. *J. Chem. Phys.* **2003**, *119*, 464.

(43) Jordanides, X. J.; Lang, M. J.; Song, X. Y.; Fleming, G. R. *J. Phys. Chem. B* **1999**, *103*, 7995.

(44) English, D. S.; Zhang, W.; Kraus, G. A.; Petrich, J. W. *J. Am. Chem. Soc.* **1997**, *119*, 2980.

(45) English, D. S.; Das, K.; Zenner, J. M.; Zhang, W.; Kraus, G. A.; Larock, R. C.; Petrich, J. W. *J. Phys. Chem. A.* **1997**, *101*, 3235.

(46) Kovalenko, S. A.; Ruthmann, J.; Ernsting, N. P. *Chem. Phys. Lett.* **1997**, *271*, 40.

(47) Gardecki, J. A.; Maroncelli, M. *J. Phys. Chem. A* **1999**, *103*, 1187.

(48) Nagarajan, V.; Brearley, A. M.; Kang, T.-J.; Barbara, P. F. *J. Chem. Phys.* **1987**, *86*, 3183.

(49) Changenet-Barret, P.; Choma, C. T.; Gooding, E. F.; DeGrado, W. F.; Hochstrasser, R. M. *J. Phys. Chem. B* **2000**, *104*, 9322.

(50) Das, K.; Smirnov, A. V.; Wen, J.; Miskovsky, P.; Petrich, J. W. *Photochem. Photobio.* **1999**, *69*, 633.

(51) Smirnov, A. V.; Das, K.; English, D. S.; Wan, Z.; Kraus, G. A.; Petrich, J. W. *J. Phys. Chem. A* **1999**, *103*, 7949.

(52) Seddon, K. R.; Stark, A.; Torres, M.-J. Viscosity and density of 1-alkyl-3-methylimidazolium ionic liquids. In *Clean Solvents: Alternative Media for Chemical Reactions and Processing.*; ACS Symposium Series, 2002; Vol. 819; pp 34.

(53) Baker, S. N.; Baker, G. A.; Munson, C. A.; Chen, F.; Bukowski, E. J.; Cartwright, A. N.; Bright, F. V. *Ind. Eng. Chem. Res.* **2003**, *42*, 6457.

(54) Castner, E. W., Jr.; Kennedy, D.; Cave, R. J. *J. Phys. Chem. A* **2000**, *104*, 2869.

(55) Horng, M. L.; Gardecki, J.; Papazyan, A.; Maroncelli, M. *J. Phys. Chem.* **1995**, *99*, 17311.

(56) Lewis, J. E.; Maroncelli, M. *Chem. Phys. Lett.* **1998**, *282*, 197.

(57) Carda-Broch, S.; Berthod, A.; Armstrong, D. W. *Anal. Bioanal. Chem.* **2003**, *375*, 191.

(58) Fee, R. S.; Maroncelli, M. *Chem. Phys.* **1994**, *183*, 235.

CHAPTER 4. DYNAMIC SOLVATION OF NONGLASSY IMIDAZOLIUM IONIC LIQUIDS ON SHORT TIME SCALES

A paper submitted to *The Journal of Physical Chemistry B*[1]

Lindsay Sanders Headley, Prasun Mukherjee, Jared L. Anderson, Rongfang Ding, Mintu Halder, Daniel W. Armstrong, Xueyu Song, and Jacob W. Petrich[2]

Abstract

Steady-state and time-resolved Stokes shift data for the probe coumarin 153 in two imidazoles, six imidazolium-based ionic liquids, and several other solvents are presented. These results are consistent with our original suggestion (*J. Phys. Chem. B* **2004**, *108,* 10245-10255) that initial solvation is dominated by the organic moiety of the ionic liquid, and they show that for the imidazole-based liquids initial solvation is in all cases very rapid. Solvation by methylimidazole and butylimidazole is complete in 100 ps; and all the imidazolium ionic liquids demonstrate similarly rapid initial solvation. Owing to the importance of determining the amount of initial solvation that is missed in a given experiment with finite time resolution, we discuss a method of estimating the intramolecular contribution to the reorganization energy. This method yields 1426 cm^{-1} and is compared with an alternative but equivalent method.

---

[1]Reproduced with permission from *J. Phys. Chem. B*, submitted for publication. Copyright 2006 American Chemical Society.

[2]Author to whom correspondence should be addressed.

Introduction

Room temperature ionic liquids (RTILs) are comprised of an organic cation and an inorganic anion. They have been used as novel solvent systems for organic synthesis,[1-14] liquid-liquid extraction,[15-17] in electrochemical studies,[18] and as ultralow volatility liquid matrices for matrix-assisted laser desorption/ionization (MALDI) mass spectrometry.[19] RTILs have many properties that make their applications in chemical systems attractive. Some are immiscible with both water and nonpolar organic solvents. They are stable to temperatures in excess of 300°C, but they have negligible vapor pressures, thus making them "green" solvents by reducing environmental levels of volatile organic carbons. Their viscosities can easily be varied by changing their cationic or anionic constituents. Their growing utility requires a detailed and fundamental understanding of their behavior.

Early treatments of solvation by ionic fluids were provided by Huppert and coworkers using molten salts[20,21] and by Maroncelli and coworkers using nonaqueous solutions of dissolved ions.[22] More recently, solvation by RTILs has been studied by fluorescence techniques by Karmakar and Samanta[23-25] and by Maroncelli and coworkers.[26-31] Karmakar and Samanta have argued that the solvation dynamics is biphasic, with a short component corresponding to diffusional motion of the anion and a long component corresponding to the collective motion of the anion and the cation. Maroncelli and coworkers, however, have insisted on the nonexponential nature of the solvation dynamics and on the glassiness of the RTILs. Several groups[32-37] have used the optical Kerr effect to study ionic liquids. Finally, Weingärtner and coworkers[38,39] and Richert and coworkers[40] have investigated the dielectric relaxation of ionic liquids.

Previously, we had suggested that the organic cation determined the early time solvation behavior of these materials.[41] This conclusion was based on a comparison of the behavior of an ionic liquid based on an imidazolium cation and the uncharged organic counterpart, butylimidazole. Castner and coworkers[37] have subsequently performed similar

studies comparing an ionic liquid with its isoelectronic neutral binary counterpart using femtosecond optical Kerr effect spectroscopy.

Here we present steady-state and time-resolved Stokes shift data for the probe coumarin 153 in two imidazoles, six imidazolium-based ionic liquids, and several other solvents (Figure 4.1 and Table 4.1). These results are consistent with our original suggestion, and show that for the imidazole-based liquids initial solvation is in all cases very rapid. Since there is always some finite time resolution associated with the measurement of a dynamic Stokes shift, it is important to know how much of the Stokes shift has been missed in the measurement, or, alternatively, what fraction of the total solvation has been completed at a given time. Fee and Maroncelli[42] have discussed this question at length and have indicated a method of estimating a "zero-time" emission spectrum, which reflects a vibrationally equilibrated emissive state that has not yet experienced any Stokes shift resulting from solvent motion. We propose a method for estimating the intramolecular contribution to the reorganization energy, which is an alternative but equivalent means of obtaining the same information.

Materials and Methods

Ionic Liquids. All the ionic liquids are prepared via their chloride salts. 1-Methylimidazolium chloride, 1-butylimidazolium chloride, and 1,2-dimethylimidazolium chloride were synthesized by adding a 1:1 molar ratio of hydrochloric acid dropwise to a round bottom flask containing 1-methylimidazole, 1-butylimidazole, or 1,2-dimethylimidazole in ~100 mL of 2-propanol. After stirring for 2 hours at room temperature, the solvent was removed using rotary evaporation. The bis[(trifluoromethyl)-sulfonyl]imide (NTf_2^-) ionic liquids were synthesized by dissolving the chloride ionic liquids in 100-150 mL water. One molar equivalent lithium trifluromethanesulfonimide was dissolved in 50 mL of water and added to the chloride salt. After stirring for 2 hours, the

lower ionic liquid layer was washed with at least three 30 mL portions of water. A silver nitrate test was used to verify the removal of any excess chloride salt. The resulting ionic liquids were dried overnight in a vacuum desiccator under P_2O_5. Triethylammonium chloride was purchased from Alfa Aesar. Triethylammonium NTf_2^- was made using the same anion exchange as described above.

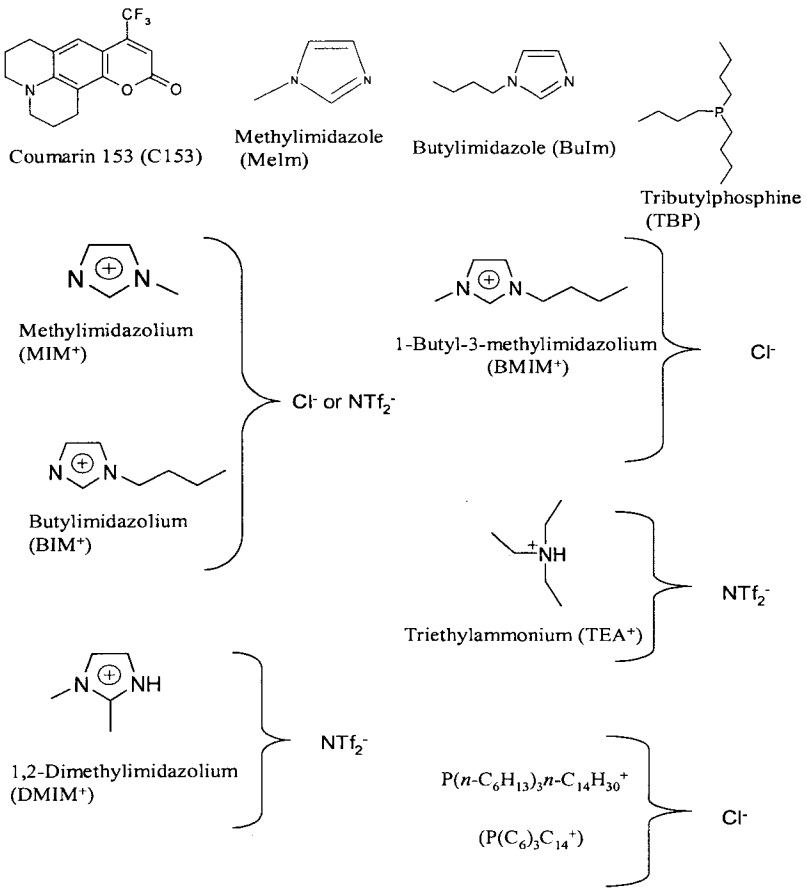

Figure 4.1: Structures of the solvation probe, coumarin-153, along with methylimidazole (MeIm), butylimidazole (BuIm), and tributylphosphine (TBP). Structures are also provided for the RTILs studied: the methylimidazolium cation [MIM^+], butylimidazolium cation [BIM^+], 1,2-dimethylimidazolium cation [$DMIM^+$], 1-butyl-3-methylimidazolium cation [$BMIM^+$], triethylammonium cation [TEA^+], and the corresponding anions. The phosphonium ionic liquid, [$P(C_6)_3C_{14}^+$][Cl^-], was investigated by Maroncelli and coworkers.[29]

Viscosity measurements for TBP, $[TEA^+][NTf_2^-]$, $[BIM^+][NTf_2^-]$, $[DMIM^+][NTf_2^-]$, $[MIM^+][NTf_2^-]$, and $[BIM^+][Cl^-]$ were taken with a ViscoLab 4000 piston-style viscometer from Cambridge Applied Systems. The digital read-out provided the viscosity and interior temperature along with measurement errors. The viscosity of the TBP was measured in a glove bag under argon. Measurements were taken at various pressures to ensure that the viscosity reading was not significantly affected by the positive pressure inside the glove bag. Viscosity measurements for MeIm, BuIm, and $[MIM^+][Cl^-]$ were provided by Professor E. W. Castner, Jr. (Rutgers) using a Cambridge Applied System model ViscoLab 4100 automated viscometer (SPL480 sensor with Thermal Jacket). Temperature was controlled with a Lauda Refrigerating Circulator Models RMT-6, accurate to 0.01 K.

Steady-state Measurements. Steady-state excitation and emission spectra were recorded with a SPEX Fluoromax with a 4-nm bandpass and were corrected for detector response. A 1-cm pathlength quartz cuvette was used for the measurements. During spectroscopic measurements, the quartz cuvettes were kept tightly sealed to prevent moisture from being absorbed by the ionic liquids. The steady-state spectra can be used to compute the reorganization energy, λ, by means of[43]

$$\lambda = \hbar \frac{\int_0^\infty d\nu[\sigma_a(\nu) - \sigma_f(\nu)]\nu}{\int_0^\infty d\nu[\sigma_a(\nu) + \sigma_f(\nu)]} \tag{4.1}$$

The $\sigma_{a,f}$ are the absorption (or excitation) and emission spectra, respectively, on a wavenumber scale. The reorganization energy is widely used as a measure of the strength of interactions between a chromophore and its surrounding dielectric media in solvation dynamics studies. It is usually taken as half of the Stokes shift. This estimate is accurate if the excitation and emission spectra are Gaussian, but it becomes unreliable if they are not.

Time-resolved Measurements. The laser source for the time-correlated single-photon counting measurements was a home-made mode-locked Ti-sapphire laser, tunable from 780 to 900 nm with a repetition rate of 82 MHz. The fundamental from the Ti-sapphire oscillator was modulated by a Pockels cell (Model 350-160, Conoptics Inc) to reduce the repetition rate to about 8.8 MHz and was subsequently frequency doubled by focusing tightly into a 0.4-mm BBO crystal. The resulting blue light, which had a central wavelength of 425 nm, provided the excitation source. The fluorescence decays were collected at the magic angle (polarization of 54.7° with respect to the vertical). Emission was collected through a single monochromator (ISA H10) fitted with a slit having an 8- nm band pass. A half-wave plate before a vertical polarizer ensured the polarization of the excitation light. The instrument response function of the apparatus had a full-width–at-half-maximum (FWHM) of ≤ 100 ps. A 1-cm pathlength quartz cuvette was used for all the time-resolved measurements. To construct the time-resolved spectra, a series of decays (~3000 counts in the peak channel) were collected over as much of the fluorescence spectrum as possible, typically from 470 nm to 610 nm at 10 nm intervals. They were fit to a maximum of three exponentials. Transient spectra were reconstructed from these fits by normalizing to the steady state spectra:

$$S(\lambda,t) = D(\lambda,t)\frac{S_0(\lambda)}{\int_0^\infty D(\lambda,t)} \tag{4.2}$$

$D(\lambda,t)$ is the wavelength-resolved fluorescence decay, and $S_0(\lambda)$ is the steady-state emission intensity at a given wavelength. We have employed the traditional approach of fitting the time-resolved spectra to a log-normal function, from which we extract the peak frequency, $\nu(t)$, as a function of time.

The solvation dynamics were described by the normalized correlation function:

$$C(t) = \frac{\nu(t) - \nu(\infty)}{\nu("t = 0") - \nu(\infty)} \tag{4.3}$$

ν("t = 0") is the frequency at zero time, calculated using the method described by Fee and Maroncelli.[42] $\nu(\infty)$ is the frequency at "infinite time," the maximum of the steady-state fluorescence spectrum. $\nu(t)$ is determined by taking the maxima from the lognormal fits as the emission maximum. In most of the cases, however, the spectra are broad, so there is some uncertainty in the exact position of the emission maxima. Thus, we have considered the range of the raw data points in the neighborhood of the maximum to estimate an error for the maximum obtained from the lognormal fit. Depending on the width of the spectrum (i.e., "zero-time", steady-state, or time-resolved emission spectrum), we have determined the typical uncertainties as follows: "zero-time" ~ steady-state ($\sim \pm$ 100 cm^{-1}) < time-resolved emission ($\sim \pm$ 200 cm^{-1}). We use these uncertainties to compute error bars for the computed C(t). Some representative error bars are given in Figure 4.3. Some representative steady-state, "zero-time," and 100-ps spectra are presented in Figure 4.2. Finally, in generating the C(t), the first point was obtained from the "zero time" spectrum. The second point was taken at the maximum of the instrument response function, which, having a full-width at half-maximum of $\leq$ 100 ps, was taken to be ~100 ps. Fractional solvation at 100 ps was calculated using f (t = 100 ps) = 1 – C (t = 100 ps).

Results and Discussion

Solvation by Imidazoles and Imidazoliums. Figure 4.3 presents the experimentally obtained solvation relaxation correlation functions for two imidazoles and several imidazolium-based ionic liquids. There is a very rapid early phase of solvation in all of these solvents, which is consistent with our previous suggestion that the organic cation dominates the early-time solvation behavior.[41] Table 4.1 indicates that the solvation dynamics correlate well with viscosity, and Figure 4.4 compares the average solvation time against the solvent viscosity on a logarithmic scale. Maroncelli and coworkers have used such a linear correlation to argue

for translational ionic motion.[30] While it is reasonable that there is indeed such translational motion in ionic liquids, we do not find the linearity of a log-log plot as compelling evidence for the role of such motion in the solvation process.

Phosphine and Phosphonium. Maroncelli and coworkers[29] have studied the solvation of several nonpolarizable, long-chain ionic liquids, in particular $[N(n\text{-}C_4H_9)_3CH_3^+][Tf_2N^-]$ and $[P(C_6)_3C_{14}^+][Cl^-]$. For these solvents, in contrast to the imidazolium-based liquids, there is no ultrafast solvation response and consequently the entire solvation response can be measured. Based on our earlier comparison of $[BMIM^+][PF_6^-]$ and butylimidazole, we undertook a study of tributylphosphine (TBP) in order to compare its behavior with that of $P(C_6)_3C_{14}^+$ (Figure 4.1). We anticipated that the nonpolarizable butyl sidechains of TBP would give rise to slow solvation dynamics. Notwithstanding its small viscosity, 2.2 cP, the fractional solvation at 100 ps of 1.0 and average solvation time of 0.08 ns seem surprising. The steady-state reorganization energy of TBP is, however, 2100 cm^{-1} as opposed to ~1400 or 1700 cm^{-1}, which one obtains from nonpolar CCl_4 or from zero-time spectra of initially "unsolvated" chromophores (see below). TBP behaves more like a polar molecule than one would expect and is consequently not a good model for the organic counterpart of $P(C_6)_3C_{14}^+$.

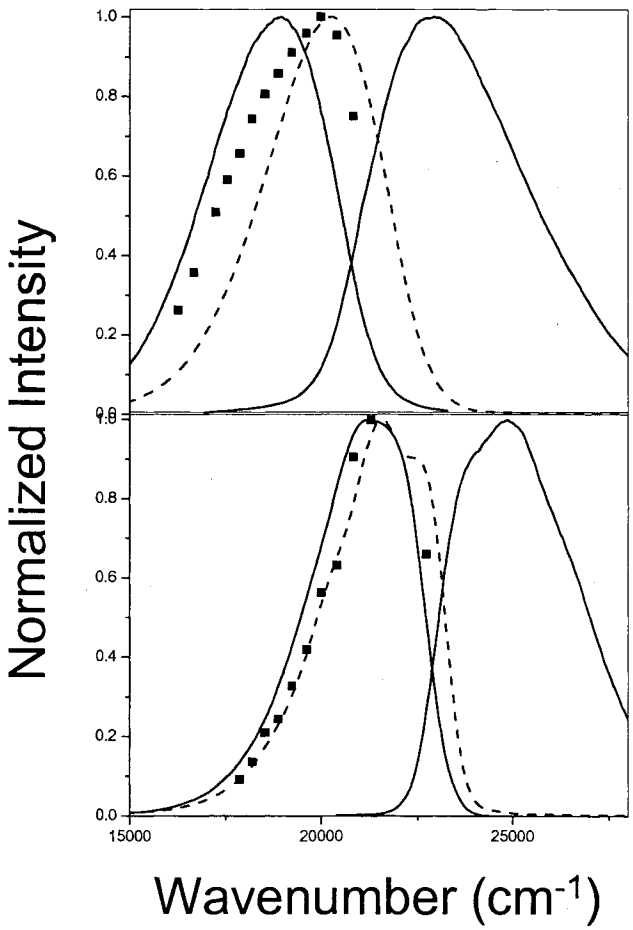

Figure 4.2: Fluorescence emission and excitation curves for $BMIM^+Cl^-$ at 30°C (top) and TBP (bottom). The solid lines are the steady state data, the dashed lines are the calculated time-zero emission curves, and the scattered dots are the TRES data at our instrument's shortest collection time. Steady state excitation wavelengths were 420 nm for $[BMIM^+][Cl^-]$ and 400 nm for TBP. The emission monochromator was set to 600 nm for $[BMIM^+][Cl^-]$ and 500 nm for the TBP.

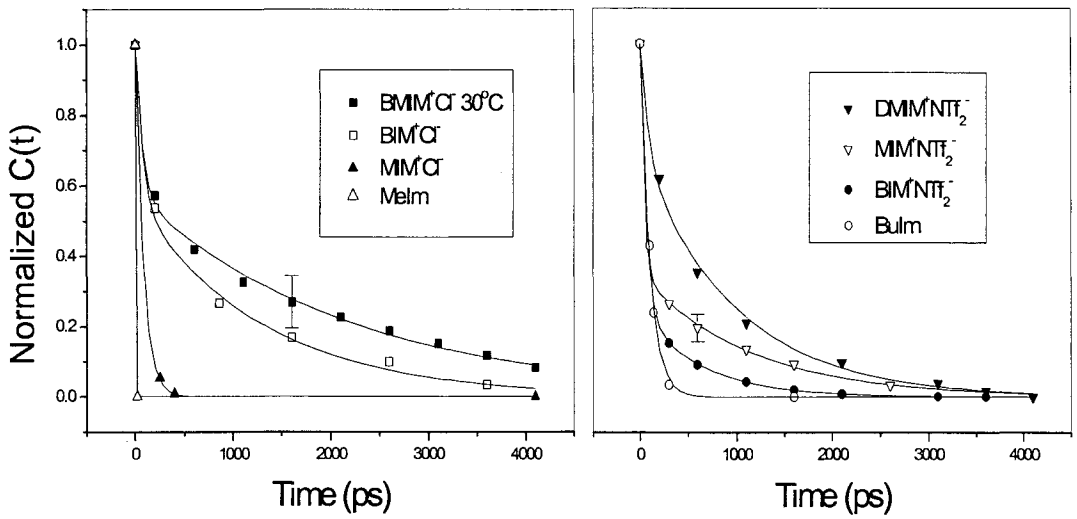

Figure 4.3: Solvation correlation functions, C(t), for the imidazole-based solvents. Two exponentials were sufficient to describe the data. A representative error bar is shown for $[BMIM^+][Cl^-]$ and $[MIM^+][NTf_2^-]$.

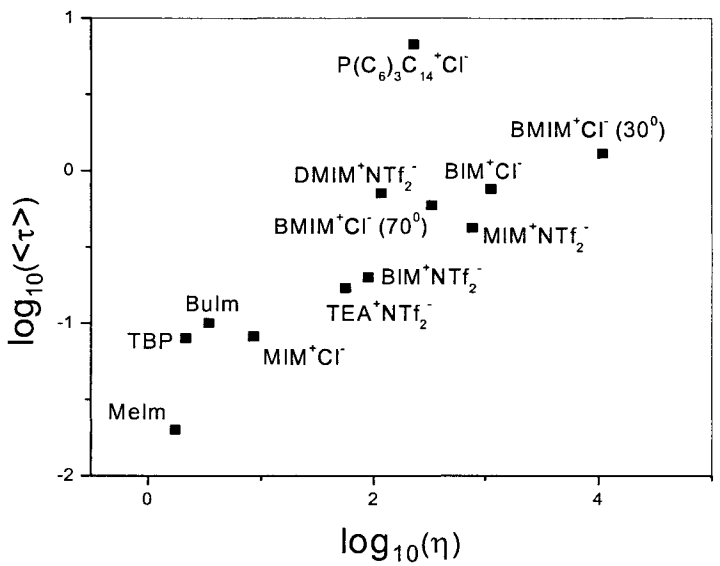

Figure 4.4: Log-log plot of the average solvation times against the viscosities of the ionic liquids and corresponding organic solvents. There is a good correlation between the two properties. The phosphonium solvent lies off the line described by the imidazoliums. It is not expected that different solvent types yield different slopes on such plots.[30]

Table 4.1: Spectral Characteristics of Coumarin 153 in Various RTILs.

RTIL[a]	η (cP)	$\langle\nu\rangle_{abs}$ (cm^{-1}) [b]	$\langle\nu\rangle_{em}$ (cm^{-1}) [b]	$\lambda_{"t=0"}$ (cm^{-1}) [c]	λ (cm^{-1}) [c]	$f_{100\ ps}$ [d]	$\langle\tau\rangle_{SR}$ (ns)
MeIm	1.76 ± 0.02 [e]	24000	18330	1305	2672	1.0	< 0.02
TBP	2.18 ± 0.01	25100	21030	1870	2082	1.0	0.080
BuIm	3.50 ± 0.06 [e]	24040	18700	1416	2622	0.57	0.10
MIM^+Cl^-	8.7 ± 0.2 [e]	23450	17430	1584	2530	1.0	0.082
$TEA^+NTf_2^-$ [f]	56.7 ± 0.2	23690	17920	1710	2565	0.77	0.17
$BIM^+NTf_2^-$	90.03 ± 1.5	23210	18070	1662	2482	0.65	0.20
$DMIM^+NTf_2^-$	117.3 ± 0.9	22190	18020	1783	2220	0.30	0.71
$P(C_6)_3C_{14}^+Cl^-$ [g]	230 [h]	--	--	--	--	0	6.7 [g]
$BMIM^+Cl^-$ (70 °C)	334 [i]	23540	18090	1694	2582	0.21	0.59
$MIM^+NTf_2^-$	776.3 ± 3.1	22980	18190	1746	2348	0.64	0.42
BIM^+Cl^-	1130 ± 20	22940	18270	1823	2413	0.39	0.76
$BMIM^+Cl^-$ (30 °C)	11000 [i]	23490	18570	1659	2294	0.36	1.3

[a] For abbreviations, see the caption to Figure 4.1. Unless indicated, the parameters reported are for 20°C.

[b] $\langle\nu\rangle = \frac{\int_0^\infty \nu I(\nu)d\nu}{\int_0^\infty I(\nu)d\nu}$, computed using 70% of the emission and excitation spectra in order to exclude the contributions from absorption to states higher than S_1 in energy.

[c] Computed from Equation 4.1.

[d] There are instances where the fractional solvation does not track the viscosity as expected. We attribute this to our definition of "100 ps," as indicated in the Experimental Section.
[e] These viscosities were kindly measured for us by personnel in Professor E. W. Castner Jr.'s laboratory before we had acquired our own viscometer.
[f] $[TEA^+][NTf_2^-]$ is included for completeness. We hoped to compare it with the chloride salt, which proved impossible since the latter melts at 261°C.
[g] From Ref. 29.
[h] From Ref. 53.
[i] From Ref. 54.

Determination of the Intramolecular Contribution to the Reorganization Energy, λ. In order to estimate the intramolecular contribution to the reorganization energy of C153 and to establish a classical model for C153 in studies of solvation dynamics (that is, a rigid solute molecule with a charge distribution change), we performed a regression analysis of C153 in nine solvents with various dielectric constants.[44] The initial charge distribution change was estimated from a semi-empirical quantum chemistry calculation.[45,46] The total experimental reorganization energy is estimated from the emission and excitation spectra (Equation 4.1). The solvent contribution to the reorganization energy is calculated from the charge distribution change and the solvent static and optical dielectric constants using the boundary element method with a realistic molecular surface of C153.[46] See Table 4.2.

A linear regression analysis between the calculated λ and the total experimental λ yields a slope of 1.25. The intercept gives the intramolecular contribution of λ as 1426 cm^{-1}, given the calculated value of 40 cm^{-1} for the solvent's contribution to the reorganization energy for CCl_4 (Figure 4.5). From such an analysis we can rescale the charge distribution change by a factor of 1.12 and take the intramolecular reorganization energy contribution as 1426 cm^{-1}. In principle, the intramolecular contribution to λ can be obtained by measurement of the gas phase spectra. Ernsting and coworkers have presented such measurements for coumarin 153 at 383 K.[47] Computation of λ from their gas phase data yields 2230 cm^{-1}, which is considerably in excess of the value we measure in CCl_4, suggesting that the coumarin in the gas phase measurement may have been complexed to solvent molecules or other coumarin molecules. In our previous work, we used the above analysis to define the fractional solvation, f(t), in terms of reorganization energies.[41] Now that we have calculated the "zero-time" values and incorporated them into the solvation correlation function, f(t) at a given time can simply be obtained from:

$$f(t) = 1 - C(t) \tag{4.4}$$

Values of f(t = 100 ps) are given in Table 4.1.

Finally, if the above estimate of intramolecular reorganization energy is reasonable we can use the dielectric constant of ionic liquids measured by Weingärtner and coworkers[39] to estimate the reorganization energy of ionic liquids. For example, 1-butyl-3-methylimidazolium tetrafluoroborate has a static dielectric constant of 11.7; our theoretical estimation of the reorganization energy yields 2400 cm^{-1}. The experimental measurements give 2481 cm^{-1};[41] therefore, the C153 model we use appears to be appropriate for studies of solvation dynamics.

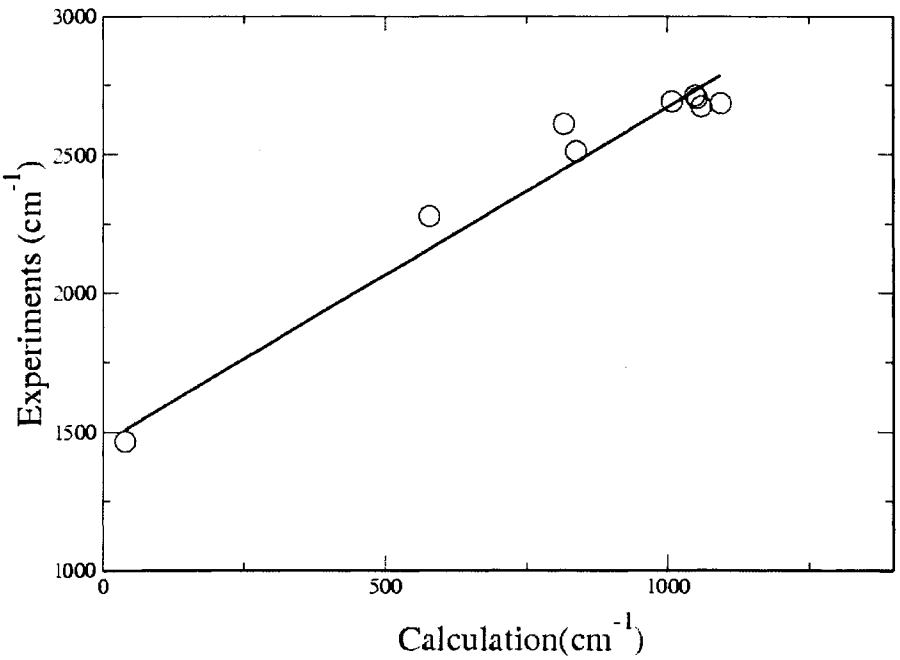

Figure 4.5: Plot of the reorganization energy obtained from fluorescence emission and excitation spectra using Equation 4.1 against the reorganization energy obtained from calculations. The intercept, 1426 cm^{-1}, provides the intramolecular contribution of the reorganization energy for coumarin 153.

Table 4.2: Solvent Reorganization Energies (cm^{-1}) for Coumarin 153

Solvents	ϵ_0	n_D	λ, expt.	λ, calc.
acetone	20.56	1.359	2685	1095
acetonitrile	35.94	1.433	2713	1049
butyronitrile	20.7	1.384	2673	1060
CCl_4	2.23	1.46	1466	40
chloroform	4.81	1.444	2276	577
dichloromethane	8.93	1.424	2512	837
dimethylformamide	36.71	1.431	2704	1053
dimethylsulfoxide	46.45	1.479	2692	1008
tetrahydrofuran	7.58	1.4035	2610	815

Conclusions

The picture we originally put forward for solvation by ionic liquids was that the organic cation determined the early time solvation behavior of these materials.[41] This conclusion was based on a comparison of the behavior of an ionic liquid based on an imidazolium cation and the uncharged organic counterpart, butylimidazole. In other words, because the organic cation carries most of the permanent dipole moment, is more polarizable, and is nearer to the solute, it seems reasonable that it contributes the most to early-time solvation events. The additional solvation data for the imidazoles and the imidazolium ionic liquids presented here are consistent with this idea. Solvation by methylimidazole and butylimidazole is complete in 100 ps; and all the imidazolium ionic liquids demonstrate similarly rapid initial solvation. Also consistent with this idea is that Maroncelli and coworkers[29] observe no ultrafast solvation component in long-chain, nonpolar ionic liquids such as $[N(n\text{-}C_4H_9)_3CH_3^+][NTf_2^-]$ and $[P(C_6)_3C_{14}^+][Cl^-]$. We still do not completely understand, however, the rapid solvation afforded by the uncharged neutral, TBP. It is most likely at least partially attributable to its low viscosity and to the fact that it is expected to be more polar than its ionic liquid counterpart. $P(C_6)_3C_{14}^+$ can be thought of as having its positive charge spherically distributed about it, while TBP, having only three alkyl groups, assumes a pyramidal configuration and can be thought of as being a polar molecule.

Several theoretical investigations have been undertaken of ionic liquids.[48-51] In a recent computer simulation, Shim et al.[49] place a dipolar excitation on a model diatomic solute in a RTIL. They observe a fast initial relaxation and suggest that it arises from translations of the anions. Given the small size of the model solute and the large changes in net charge, the motions of the resulting concentrated anionic charges may dominate the relaxation. In the experimental solvation dynamics studies of organic dye molecules such as coumarin 153 (C153) in RTILs, the charge distribution change is smeared across the whole probe molecule, which is most likely well solvated by the bulky organic cations given the

hydrophobic nature of C153 in the ground state. This suggests, therefore, that the most probable scenario is that the cation motions dominate the contribution of the initial fast relaxation upon excitation. In order to elucidate the nature of the fast relaxations, a realistic model of C153 in RTILs will be needed. Znamenskiy and Kobrak have recently performed molecular dynamics simulations of the dye betaine-30 in [$BMIM^+$][PF_6^-].[50] They obtain radial distribution functions indicating the proximity of the 1-butyl-3-methylimidazolium ring to the dye, which is consistent with our experimental observations for coumarin 153. The solvation relaxation is argued to arise from the translation and diffusional motion of ions.

Simulations by Kobrak and Znamenskiy[51] have also indicated collective cation-anion motion on subpicosecond time scales, which again argues against a purely anionic subpicosecond solvation response. The existence of collective motion is not inconsistent with our suggestion of the role of the organic cation. Indeed, the motions of cations and anions must be correlated in order to ensure local electrical neutrality, a constraint imposed by the strong coulombic interaction between ions. This is well documented by experimental measurements of radial distribution functions and by computer simulations.[52] What is especially relevant about the ion pairs is not whether they exist but how long they exist.

Finally, we have discussed a means of computing the reorganization energy due to intramolecular vibrations. The value obtained, 1426 cm^{-1}, is commensurate with that obtained from computing the reorganization energy from the "zero-time" spectra, 1659 ± 170 cm^{-1}, which speaks to the appropriateness of our method as well as to the robustness of the "zero-time" method.

Acknowledgements

We thank Professor E. W. Castner, Jr. for providing us with some initial viscosity measurements and for helpful conversations. Professors R. Richert, M. Maroncelli, and H.

Weingärtner kindly provided preprints of their work. We also thank Mr. Jeffrey Crank for providing us with the [TEA^+][NTf_2^-] and Ms. Tessa Calhoun for collecting and analyzing the C153 spectra used in the intramolecular reorganization energy calculations.

References

(1) Wilkes, J. S.; Zaworotko, M. J. *J. Chem. Soc., Chem. Commun.* **1992**, 965.

(2) Adams, C. J.; Earle, M. J.; Roberts, G.; Seddon, K. R. *Chem. Commun.* **1998**, 2097.

(3) Earle, M. J.; McCormac, P. B.; Seddon, K. R. *Chem. Commun. (Cambridge)* **1998**, 2245.

(4) Dyson, P. J.; Ellis, D. J.; Parker, D. G.; Welton, T. *Chem. Commun. (Cambridge)* **1999**, 25.

(5) Leadbeater, N. E.; Torenius, H. M. *J. Org. Chem.* **2002**, *67*, 3145.

(6) Mann, B. E.; Guzman, M. H. *Inorg. Chim. Acta* **2002**, *330*, 143.

(7) Wasserscheid, P.; Keim, W. *Angew. Chem., Int. Ed.* **2000**, *39*, 3772.

(8) Reynolds, J. L.; Erdner, K. R.; Jones, P. B. *Org. Lett.* **2002**, *4*, 917.

(9) Welton, T. *Chem. Rev.* **1999**, *99*, 2071.

(10) Nara, S. J.; Harjani, J. R.; Salunkhe, M. M. *Tetrahedron Lett.* **2002**, *43*, 2979.

(11) Yao, Q. *Org. Lett.* **2002**, *4*, 2197.

(12) Fletcher, K. A.; Pandey, S.; Storey, I. K.; Hendricks, A. E.; Pandey, S. *Anal. Chim. Acta* **2002**, *453*, 89.

(13) Grodkowski, J.; Neta, P. *J. Phys. Chem. A* **2002**, *106*, 5468.

(14) Handy, S. T.; Zhang, X. *Org. Lett.* **2001**, *3*, 233.

(15) Huddleston, J. G.; Rogers, R. D. *Chem. Commun.* **1998**, 1765.

(16) Dai, S.; Ju, Y. H.; Barnes, C. E. *J. Chem. Soc., Dalton Trans.* **1999**, 1201.

(17) Carda-Broch, S.; Berthod, A.; Armstrong, D. W. *Anal. Bioanal. Chem.* **2003**, *375*, 191.

(18) Dickinson, V. E.; Williams, M. E.; Hendrickson, S. M.; Masui, H.; Murray, R. W. *J. Am. Chem. Soc.* **1999**, *121*, 613.

(19) Armstrong, D. W.; Zhang, L.-K.; He, L.; Gross, M. L. *Anal. Chem.* **2001**, *73*, 3679.

(20) Huppert, D.; Ittah, V.; Kosower, E. M. *Chem. Phys. Lett.* **1989**, *159*, 267.

(21) Ittah, V.; Huppert, D. *Chem. Phys. Lett.* **1990**, *173*, 496.

(22) Chapman, C. F.; Maroncelli, M. *J. Phys. Chem.* **1991**, *95*, 9095.

(23) Karmakar, R.; Samanta, A. *J. Phys. Chem. A* **2002**, *106*, 6670.

(24) Karmakar, R.; Samanta, A. *J. Phys. Chem. A* **2002**, *106*, 4447.

(25) Karmakar, B.; Samanta, A. *J. Phys. Chem. A* **2003**, *107*, 7340.

(26) Ingram, J. A.; Moog, R. S.; Ito, N.; Biswas, R.; Maroncelli, M. *J. Phys. Chem. B* **2003**, *107*, 5926.

(27) Ito, N.; Arzhantsev, S.; Maroncelli, M. *Chem. Phys. Lett.* **2004**, *396*, 83.

(28) Ito, N.; Arzhantsev, S.; Heitz, M.; Maroncelli, M. *J. Phys. Chem. B* **2004**, *108*, 5771.

(29) Arzhantsev, S.; Ito, N.; Heitz, M.; Maroncelli, M. *Chem. Phys. Lett.* **2003**, *381*, 278.

(30) Arzhantsev, S.; Hui, J.; Baker, G. A.; Naoki, I.; Maroncelli, M. "Solvation dynamics in ionic liquids, results from ps and fs emission spectroscopy."; Femtochemistry VII, 2005.

(31) Arzhantsev, S.; Hui, J.; Naoki, I.; Maroncelli, M. *Chem. Phys. Lett.* 2006, In press.

(32) Hyun, B.-R.; Dzyuba, S. V.; Bartsch, R. A.; Quitevis, E. L. *J. Phys. Chem. A* **2002**, *106*, 7579.

(33) Giraud, G.; Gordon, C. M.; Dunkin, I. R.; Wynne, K. *J. Chem. Phys.* **2003**, *119*, 464.

(34) Cang, H.; Li, J.; Fayer, M. D. *J. Chem. Phys.* **2003**, *119*, 13017.

(35) Shirota, H.; Funston, A. M.; Wishart, J. F.; Castner, E. W., Jr. *J. Chem. Phys.* **2005**, *122*, 184512/1.

(36) Rajian, J. R.; Li, S.; Bartsch, R. A.; Quitevis, E. L. *Chem. Phys. Lett.* **2004**, *393*, 372.

(37) Shirota, H.; Castner, E. W., Jr. *J. Phys. Chem. A* **2005**, *109*, 9388.

(38) Weingartner, H.; Knocks, A.; Schrader, E.; Kaatze, U. *J. Phys. chem. A* **2001**, *105*, 8646.

(39) Wakai, C.; Oleinikova, A.; Ott, M.; Weingartner, H., Submitted.

(40) Ito, N.; Huang, W.; Richert, R. *J. Phys. Chem.* **2006**, Submitted.

(41) Chowdhury, P. K.; Halder, M.; Sanders, L.; Calhoun, T.; Anderson, J.; Armstrong, D. W.; Song, X.; Petrich, J. W. *J. Phys. Chem. B* **2004**, *108*, 10245.

(42) Fee, R. S.; Maroncelli, M. *Chem. Phys.* **1994**, *183*, 235.

(43) Jordanides, X. J.; Lang, M. J.; Song, X. Y.; Fleming, G. R. *J. Phys. Chem. B* **1999**, *103*, 7995.

(44) Mertz, E. L.; Tikhomirov, V. A.; Krishtalik, L. I. *J. Phys. Chem. A.* **1997**, *101*, 3433.

(45) Kumar, P. V.; Maroncelli, M. *J. Chem. Phys.* **1995**, *103*, 3038.

(46) Song, X.; Chandler, D. *J. Chem. Phys.* **1998**, *108*, 2594.

(47) Muhlpfordt, A.; Schanz, R.; Ernsting, N. P.; Farztdinov, V.; Grimme, S. *Phys. Chem. Chem. Phys.* 1999, *1*, 3209.

(48) Margulis, C. J.; Stern, H. A.; Berne, B. J. *J. Phys. Chem. B* **2002**, *106*, 12017.

(49) Shim, Y.; Duan, J.; Choi, M. Y.; Kim, H. J. *J. Chem. Phys.* **2003**, *119*, 6411.

(50) Znamenskiy, V.; Kobrak, M. N. *J. Phys. Chem. B* **2004**, *108*, 1072.

(51) Kobrak, M. N.; Znamenskiy, V. *Chem. Phys. Lett.* **2004**, *395*, 127.

(52) Hansen, J. P.; McDonald, I. R. *Theory of simple liquids.*, 2nd ed.; Academic: London, 1986.

(53) Bradaric, C. J.; Downard, A.; Kennedy, C.; Robertson, A.; Zhou, Y. *Green Chem.* **2003**, *5*, 143.

(54) Seddon, K. R.; Stark, A.; Torres, M.-J. Viscosity and density of 1-alkyl-3-methylimidazolium ionic liquids. In *Clean Solvents: Alternative Media for Chemical Reactions and Processing.*; ACS Symposium Series, 2002; Vol. 819; pp 34.

CHAPTER 5. EXPERIMENTAL AND THEORETICAL INVESTIGATIONS OF SOLVATION DYNAMICS OF IONIC FLUIDS: APPROPRIATENESS OF DIELECTRIC THEORY AND THE ROLE OF DC CONDUCTIVITY

A paper submitted to *The Journal of Physical Chemistry B*[1]

Mintu Halder, Lindsay Sanders Headley, Prasun Mukherjee,
Xueyu Song[2], and Jacob W. Petrich[2]

Abstract

An analysis is provided of the subnanosecond dynamic solvation of ionic liquids in particular and ionic solutions in general. It is our hypothesis that solvation relaxation in ionic fluids, in the nonglassy and nonsupercooled regimes, can be understood rather simply in terms of the dielectric spectra of the solvent. This idea is suggested by the comparison of imidazolium ionic liquids with their pure organic counterpart, butylimidazole (*J. Phys. Chem. B*, **2004,** *108*, 10245.) It is borne out by a calculation of the solvation correlation time from frequency dependent dielectric data for the ionic liquid, ethylammonium nitrate, and for the electrolyte solution of methanol and sodium perchlorate. Very good agreement is obtained between these theoretically calculated solvation relaxation functions and those obtained from fluorescence upconversion spectroscopy. Our comparisons suggest that translational motion of ions may not be the predominant factor in short-time solvation of ionic fluids and that many tools and ideas about solvation dynamics in polar solvents can be adapted to ionic fluids.

---

[1]Reproduced with permission from *J. Phys. Chem. B*, submitted for publication.

Copyright 2006 American Chemical Society.

[2]Author to whom correspondence should be addressed.

Introduction

The problem of understanding solvation by room-temperature ionic liquids (RTILs) is a specific aspect of the more general problem of understanding solvation in ionic fluids. RTILs are becoming an increasingly rich area of study.[1-4] Their growing utility has stimulated studies to understand the fundamentals of their behavior. For our current investigation, particularly relevant experimental studies have been based upon fluorescence techniques [5-16] and those obtaining the dielectric spectrum.[17,18] In particular, Weingärtner et al.[17] have investigated the dielectric relaxation of ethylammonium nitrate (EAN) in the 3 MHz to 40 GHz range, and their data stimulated much of the work discussed here.

On the theoretical side, several simulations have been performed to study solvation dynamics in RTILs. The initial rapid solvation events have been the object of computer simulations: Shim et al.,[19] placing a dipolar excitation on a model diatomic solute in a RTIL, observe a fast initial relaxation and suggest that it arises from translations of the anions. Given the small size of the model solute and the large changes in net charge, the motions of the resulting concentrated anionic charges may dominate the relaxation. In the experimental solvation dynamics studies of organic dye molecules such as coumarin 153 (C153) in RTILs, the charge distribution change is scattered across the whole probe molecule, which is most likely well solvated by the bulky organic cations given the hydrophobic nature of C153 in the ground state. We have suggested, therefore, that the most probable scenario is that the cation motions dominate the contribution of the initial fast relaxation upon excitation.[20] In order to elucidate the nature of the fast relaxations, a realistic model of C153 in RTILs will be needed.

Znamenskiy and Kobrak have recently performed molecular dynamics simulations of the dye betaine-30 in $[BMIM^+][PF_6^-]$.[21] They obtain radial distribution functions indicating the proximity of the 1-butyl-3-methylimidazolium ring to the dye, which is consistent with

our experimental observations for coumarin. As in experimental studies the nature of solvation relaxation is argued to be from the translation and diffusional motion of ions.

A fundamental problem, then, in the study of ionic liquids is assessing the relative importance of translational motion of ions,[15,16,22] which can roughly be identified with DC conductivity, and the dielectric relaxation of dipoles. More specifically, an alternative view of the origin of solvation by ionic fluids, that we propose, is it arises from the dielectric relaxation of dipoles resulting from ion pairs due to local neutrality and permanent dipoles carried by the ions. For electrolyte solutions and molten salts, this point of view has been used fruitfully to interpret the experimental dielectric spectra.[23-27] Our recent work on the dynamic aspects of solvation by RTILs using Stokes shift data of the fluorescent probe, coumarin 153, from the picosecond to the nanosecond time regimes[20] already suggested such a connection. In that work, we investigated four RTILs based on the 1-butyl-3-methylimidazolium cation, $BMIM^+$. A major conclusion was that the rapid initial phase of solvation arises from the cations, which are the major carriers of permanent dipoles.

In this report the solvation relaxation measured from fluorescence upconversion experiments is compared with that calculated from the dielectric spectra of the neat ionic liquids. Our results suggest that the time dependent solvation relaxation from solvation dynamics experiments is indeed directly related to the dielectric spectra, $\epsilon(\omega)$, of the ionic liquids just as in the case of dipolar fluids. Furthermore, at least for one solvent studied, the agreement between theory and experiment is much better when DC conductivity is eliminated from the dielectric spectra. The justification for omitting the conductivity at times probed in our experiments is that there is a time scale separation between the dielectric relaxation processes and the conductive processes in an ionic fluid. The latter can be described by a contribution of $\sigma/i\omega$ to the total dielectric response function, where σ is the DC conductivity.[28] The former is given by the dielectric relaxation via much higher frequency processes (> 1 GHz for the subnanosecond processes in solvation dynamics) as

shown by a significant body of experimentally measured dielectric spectra of electrolyte solutions[23] and ionic liquids.[24]

Materials and Methods

Preparation of EAN. Ethylammonium nitrate (EAN, Et-$NH_3^+NO_3^-$) was made by adding a limiting amount of concentrated nitric acid dropwise to a solution of 70% ethylamine in water at 0°C with constant stirring. The mixture was allowed to stir for 30 minutes to ensure complete consumption of the acid. Excess ethylamine and water were removed by rotary evaporation. To remove small traces of water, the ethylammonium nitrate was dried under vacuum at 323 K for 72 hours, using P_2O_5 as a drying agent. After drying, the ethylammoninum nitrate was sealed in a dessicator under argon. Before use, the salt was passed through a micro-scale silica gel column to ensure dryness. The column was constructed using a glass pipette sealed with cotton, and the salt was passed through the silica under pressure from a pipette bulb.

Steady-state Measurements. Steady-state excitation and emission spectra were recorded with a SPEX Fluoromax with a 4-nm bandpass and were corrected for detector response. A 1-cm pathlength quartz cuvette was used for the measurements. The steady-state spectra can be used to compute the reorganization energy, λ, by means of[29]:

$$\lambda = \hbar \frac{\int_0^\infty d\nu[\sigma_a(\nu) - \sigma_f(\nu)]\nu}{\int_0^\infty d\nu[\sigma_a(\nu) + \sigma_f(\nu)]} \tag{5.1}$$

The $\sigma_{a,f}(\nu)$ are the absorption (or excitation) and emission spectra, respectively, on a wavenumber scale.

Fluorescence Upconversion Measurements. Fluorescence upconversion measurements were performed using a homemade unamplified Ti:sapphire laser system.[20,30,31] The cross-correlation functions of its pulses have a FWHM of ~300 fs. Upconversion profiles were used to construct time- resolved emission spectra. They were typically collected over a range of wavelengths from 480 nm to 560 nm at intervals of 10 nm. Nine transients were used to construct the time-resolved emission spectra by normalizing to the steady state spectra.[20,32] We have employed the traditional approach of fitting the time-dependent spectra to a lognormal lineshape function, from which we extract the peak frequency, ν(t). The solvation dynamics were described by the normalized correlation function:

$$C(t) = \frac{\nu(t) - \nu(\infty)}{\nu("t = 0") - \nu(\infty)} \tag{5.2}$$

ν("t = 0") is the frequency at zero time, calculated using the method described by Fee and Maroncelli.[33,34] ν(∞) is the frequency at "infinite time," the maximum of the steady-state fluorescence spectrum. ν(t) is determined by taking the maxima from the lognormal fits of the emission spectra. In most cases, however, the spectra are broad, so there is some uncertainty in the determination of the emission maxima. Thus, we took a range of the raw data points in the neighborhood of the maximum to estimate an error for the maximum obtained from the lognormal fit. Depending on the width of the spectrum (i.e., "zero-time", steady-state, or time-resolved emission spectrum), we determined the uncertainties as follows: "zero-time" ~ steady-state (~ ± 100 cm^{-1}) < time-resolved emission (~ ± 200 cm^{-1}).

Calculation of the Solvation Relaxation Function. The theoretical solvation spectral density was calculated using a dielectric continuum theory developed by one of us.[35,36] To model the solvation dynamics for C153, we used the geometry and charge distribution change that we employed elsewhere.[35] The frequency dependent dielectric function of the ionic fluid in

question is obtained from experimental data. For EAN, the dielectric spectrum at frequencies below 90 GHz is from Weingärtner et al.;[17] higher frequencies are estimated by extending this spectrum via an analytical function. The dielectric spectrum of methanol/$NaClO_4$ for frequencies lower than 90 GHz is from the tabulation by Barthel and Neueder;[37] the spectrum for higher frequencies is obtained from the data for pure methanol scaled at 90 GHz. Figure 5.1 gives the dielectric spectra used in our calculations. These data were used to calculate the total solvation energy E(ω) of C153 in an ionic fluid. A relationship between the imaginary part of the solvation energy and the solvation correlation function, C(t), can be derived

$$C(t) = \frac{\hbar}{\lambda}\int_0^\infty d\omega \frac{E''(\omega)}{\omega}\cos(\omega t) \tag{5.3}$$

where E″(ω) is the imaginary portion of the total solvation energy and λ is the reorganization energy, which is obtained from solving the Poisson equation with a complex dielectric function $\epsilon(\omega)$.[35]

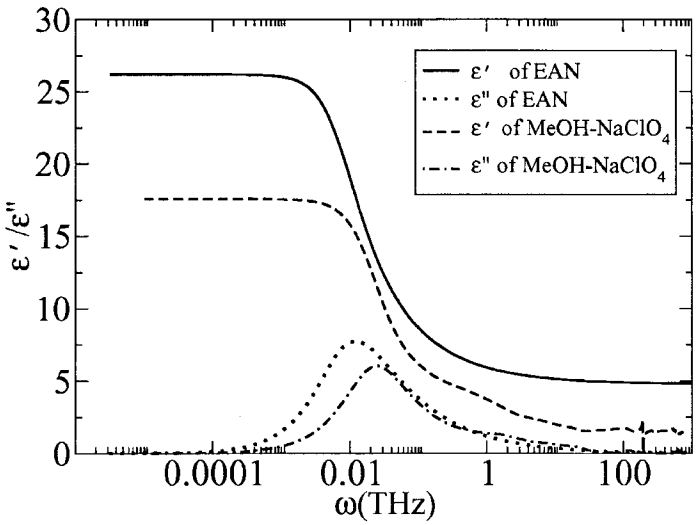

Figure 5.1: Dielectric spectra (without conductivity contributions) used to obtain the solvation energies, and ultimately the solvation relaxation functions, via Equation 5.3.

Results and Discussion

Solvation data are compiled in Table 5.1. The experimentally obtained solvation relaxation functions for EAN and the 1.05-M $NaClO_4$/methanol solution are presented on 10- and 200-ps time scales in Figures 5.2 and 5.3, respectively, along with the corresponding theoretical relaxation functions obtained using Equation 5.3, including and excluding the DC conductivity.

There are several important results. Approximately 30% of the solvation has already been accomplished in 300 fs for both systems. The C(t)s are fit to a sum of exponentials, but we attribute no special significance to this functional form. The agreement between the experimental and theoretical curves is very good, especially when several points are taken into account. At early times (10-ps time scale), the theoretical curve for MeOH/perchlorate corresponds very well with the experimental curve—especially when the DC conductivity has been eliminated. On the other hand for EAN, the theoretical curves, both with and without conductivity, while very similar to each other, deviate from the experimental curve. This divergence for EAN should not be surprising since the high frequency portion of $\epsilon(\omega)$ is obtained by extrapolation. When the comparison is made on the 200-ps time scale, it is clear that for MeOH/perchlorate exclusion of the conductivity is required to superpose theory and experiment. On the other hand, for EAN, the two theoretical curves, both with and without conductivity, lie within the uncertainty of the measurement.

The good agreement between experiment and theoretical calculation clearly indicates that the solvation relaxation in ionic liquids comes from the dielectric relaxation of the fluid.

Table 5.1. Spectral parameters for ionic solvation of coumarin 153.

Solvent system	σ (S cm^{-1})	$\lambda_{t=0}$ (cm^{-1})	$\lambda_{t=\infty}$ (cm^{-1})	$f_{300\ fs}$ [a]	$\langle\tau\rangle_{expt}$ (ps)[b]	$\langle\tau\rangle_{-\sigma}$ (ps)	$\langle\tau\rangle_{+\sigma}$ (ps)
EAN	0.028 [c]	1660	2560 ± 15	0.33	26	17	33.2
1.05-M $NaClO_4$/MeOH	0.0387 [d]	1770	2616 ± 15	0.30	9.8	7.5	27.6

All the experiments were done at room temperature. For the steady-state data, the samples were excited at 420 nm. For the excitation spectra, the emission monochromator was set at 600 nm. The steady-state reorganization energies are based on the average of four measurements.

[a] f(t) = 1 – C(t), where C(t) is obtained from Equation 5.2.

[b] $\langle\tau\rangle = \int_0^\infty C(t)_{fit}\,dt = \int_0^\infty \sum_i A_i \exp(-t/\tau_i)\,dt$. The C(t) are fit to sums of three exponentials.

[c] From Ref. 17 at 298.15 K.
[d] From Ref. 37 at 298.15 K.

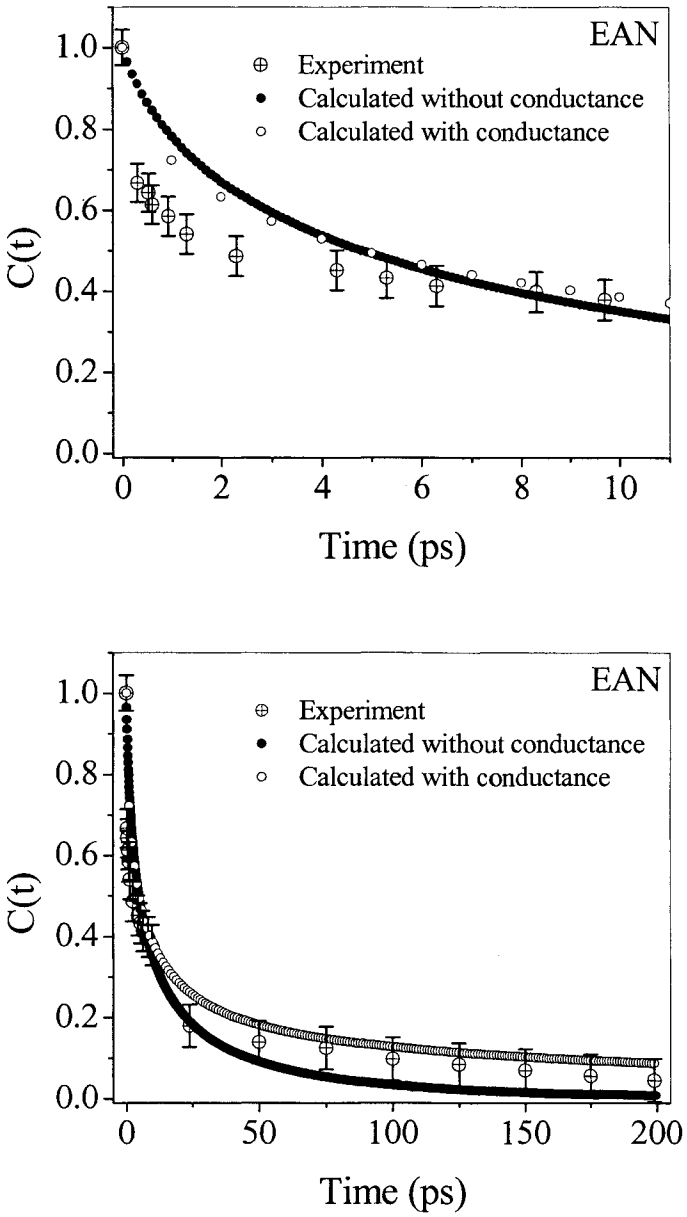

Figure 5.2: Comparison of the spectrally resolved solvation correlation function for EAN, 10-ps full scale (top) and ~200-ps full scale (bottom) obtained from fluorescence upconversion experiments (⊕). The C(t)s obtained from simulation are shown by solid circles (without conductance) and open circles (with conductance).

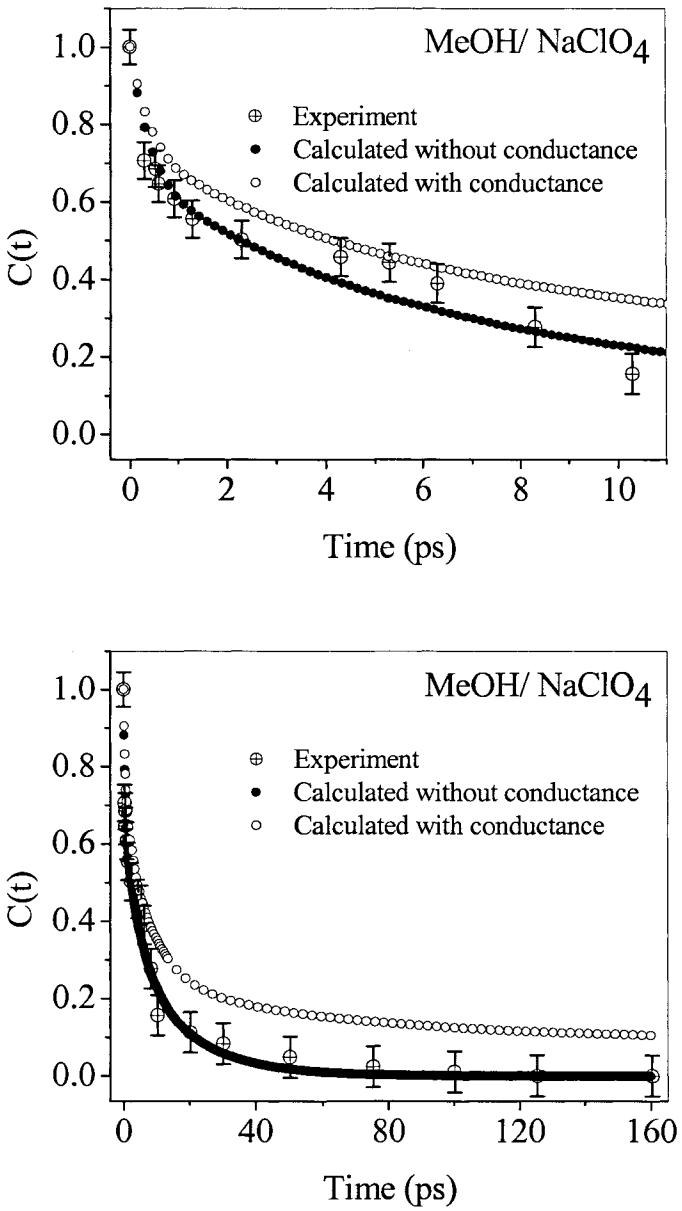

Figure 5.3: Comparison of the spectrally resolved solvation correlation function for MeOH/perchlorate, 10-ps full scale (top) and ~160-ps full scale (bottom) obtained from fluorescence upconversion experiments (⊕). The C(t)s obtained from simulation are shown by solid circles (without conductance) and open circles (with conductance).

Conclusions

In summary, it is our hypothesis that solvation relaxation in ionic fluids, in the nonglassy and nonsupercooled regimes, can be understood rather simply in terms of the dielectric spectra of the solvent. This idea was initially suggested by our comparison of imidazolium RTILs with their pure organic counterpart, butylimidazole.[20,34] It is supported by a calculation of the solvation relaxation function obtained from frequency dependent dielectric data for the RTIL, ethylammonium nitrate, and for the electrolyte solution of methanol and sodium perchlorate. Further experimental and theoretical work is required to understand ionic liquids. A larger spectrum of solvents needs to be studied to test the ideas presented here, detailed measurements of the higher frequency dielectric spectra may lead to better agreement between experiments and theoretical calculations, and more work needs to be done to understand the relative contributions to solvation relaxation from ion pairs and the permanent dipoles from the individual ions.

Acknowledgements

XS thanks the NSF for support from grant CHE0303758.

References

(1) Seddon, K. R. *Nature (Materials)* **2003**, *2*, 363.

(2) Anderson, J. L.; Ding, J.; Welton, T.; Armstrong, D. W. *J. Am. Chem. Soc* **2002**, *124*, 14247.

(3) Poole, C. F. *J. Chromatogr. A* **2004**, *1037*, 49.

(4) Pandey, S. *Analytica Chimica Acta* **2006**, *556*, 38.

(5) Huppert, D.; Ittah, V.; Kosower, E. M. *Chem. Phys. Lett.* **1989**, *159*, 267.

(6) Ittah, V.; Huppert, D. *Chem. Phys. Lett.* **1990**, *173*, 496.

(7) Chapman, C. F.; Maroncelli, M. *J. Phys. Chem.* **1991**, *95*, 9095.

(8) Karmakar, R.; Samanta, A. *J. Phys. Chem. A* **2002**, *106*, 6670.

(9) Karmakar, R.; Samanta, A. *J. Phys. Chem. A* **2002**, *106*, 4447.

(10) Karmakar, B.; Samanta, A. *J. Phys. Chem. A* **2003**, *107*, 7340.

(11) Ingram, J. A.; Moog, R. S.; Ito, N.; Biswas, R.; Maroncelli, M. *J. Phys. Chem. B* **2003**, *107*, 5926.

(12) Ito, N.; Arzhantsev, S.; Maroncelli, M. *Chem. Phys. Lett.* **2004**, *396*, 83.

(13) Ito, N.; Arzhantsev, S.; Heitz, M.; Maroncelli, M. *J. Phys. Chem. B* **2004**, *108*, 5771.

(14) Arzhantsev, S.; Ito, N.; Heitz, M.; Maroncelli, M. *Chem. Phys. Lett.* **2003**, *381*, 278.

(15) Arzhantsev, S.; Hui, J.; Naoki, I.; Maroncelli, M. *Chem. Phys. Lett.* **2006**, In press.

(16) Arzhantsev, S.; Hui, J.; Baker, G. A.; Naoki, I.; Maroncelli, M. "Solvation dynamics in ionic liquids, results from ps and fs emission spectroscopy." Femtochemistry VII, 2005.

(17) Weingärtner, H.; Knocks, A.; Schrader, E.; Kaatze, U. *J. Phys. chem. A* **2001**, *105*, 8646.

(18) Ito, N.; Huang, W.; Richert, R. *J. Phys. Chem.* **2006**, Submitted.

(19) Shim, Y.; Duan, J.; Choi, M. Y.; Kim, H. J. *J. Chem. Phys.* **2003**, *119*, 6411.

(20) Chowdhury, P. K.; Halder, M.; Sanders, L.; Calhoun, T.; Anderson, J.; Armstrong, D. W.; Song, X.; Petrich, J. W. *J. Phys. Chem. B* **2004**, *108*, 10245.

(21) Znamenskiy, V.; Kobrak, M. N. *J. Phys. Chem. B* **2004**, *108*, 1072.

(22) Kobrak, M. N.; Znamenskiy, V. *Chem. Phys. Lett.* **2004**, *395*, 127.

(23) Bruesch, P.; Pietronero, L.; Zeller, H. R. *J. Phys. C: Solid State Physics* **1976**, *9*.

(24) Happ, H.; Boehm, H.; Kasemann, A.; Neuerbourg, R. *J. Phys C: Solid State Physics* **1987**, *20*, 5889.

(25) Barthel, J. M. G.; Krienke, H.; Kunz, W. *Topics in Phys. Chem.* **1998**, *5*, 1.

(26) Kasemann, A.; Happ, H.; Wienpahl, U. *J. Phys.: Condensed Matter* **1989**, *1*,

5253.

(27) Wegdam, G. H.; Te Beek, J. B.; Van der Linden, H.; Van der Elsken, J. *J. Chem. Phys.* **1971**, *55*, 5207.

(28) Böttcher, C. J. F. *Theory of Electric Polarization*, Second ed.; Elsevier: Amsterdam, 1973; Vol. 2.

(29) Jordanides, X. J.; Lang, M. J.; Song, X. Y.; Fleming, G. R. *J. Phys. Chem. B* **1999**, *103*, 7995.

(30) Das, K.; Smirnov, A. V.; Wen, J.; Miskovsky, P.; Petrich, J. W. *Photochem. Photobio.* **1999**, *69*, 633.

(31) Smirnov, A. V.; Das, K.; English, D. S.; Wan, Z.; Kraus, G. A.; Petrich, J. W. *J. Phys. Chem. A* **1999**, *103*, 7949.

(32) Maroncelli, M.; Fleming, G. R. *J. Chem. Phys.* **1987**, *86*, 6221.

(33) Fee, R. S.; Maroncelli, M. *Chem. Phys.* **1994**, *183*, 235.

(34) Headley, L. S.; Mukherjee, P.; Anderson, J. L.; Ding, R.; Halder, M.; Armstrong, D. W.; Song, X.; Petrich, J. W. *J. Phys. Chem. A* **2006**, Submitted.

(35) Song, X.; Chandler, D. *J. Chem. Phys.* **1998**, *108*, 2594.

(36) Song, X. *AIP Conference Proceedings* **1999**, *492*, 417.

(37) Barthel, J.; Neueder, R. *Electrolyte data collection : tables, diagrams, correlations, and literature survey*; DECHEMA: Frankfurt am Main, Germany, 1995.

CHAPTER 6. THE COMPLEX OF APOMYOGLOBIN WITH THE FLUORESCENT DYE, COUMARIN 153

A paper published in the journal *Photochemistry and Photobiology*[1]

Pramit K. Chowdhury[2], Mintu Halder[2], Lindsay Sanders[2], Randy A. Arnold[2], Ying Liu[2], Daniel W. Armstrong[2], Suman Kundu[3], Mark S. Hargrove[3], Xueyu Song[2], and Jacob W. Petrich[2,4]

Abstract

Understanding a protein's dielectric response requires both a theoretical model and a well-defined experimental system. The former has already been proposed by Song (*J. Chem. Phys.* **116**, 9359 (2002)). We suggest that the latter is provided by the complex of coumarin 153 (C153) with apomyoglobin. C153 has been exhaustively studied and has proven to be an excellent probe of the solvation dynamics of polar solvents. Myoglobin is one of the most thoroughly studied proteins. Myoglobins from a wide range of species have been subject to X-ray structural analysis and site-directed mutagenesis. Here we demonstrate the existence of a robust C153-apomyglobin system by means of molecular dynamics simulations, equilibrium binding studies using a Job's plot and capillary electrophoresis, circular dichroism, and time-resolved fluorescence. The reorganization energy of C153 bound to

---

[1]Reproduced from P.K. Chowdhury et al., *Photochemistry and* Photobiology, **2004**, *79*(5), 440 with the permission of the American Society for Photobiology.

[2]Department of Chemistry, Iowa State University, Ames, IA 50011

[3]Department of Biochemistry, Biophysics and Molecular Biology, Iowa State University, Ames, IA 50011.

[4]Author to whom correspondence should be addressed.

apomyoglobin is compared with that of C153 in bulk solvent using the method of Jordanides et al. (*J. Phys. Chem. B* **103**, 7995 (1999)).

Introduction

In the past decade, it has been well established by numerous experimental and theoretical studies that solvation dynamics in polar solvents can be described by linear response theory [1-10]. In general, the full frequency dependent dielectric function of the polar solvent gives a good description of the solvation dynamics from the ultrafast regime to that of diffusive relaxation. Some direct comparisons between theory and experiments have been established [11-14]. The success is largely attributable to the dielectric fluctuations of polar solvents being described accurately by simple linear response models, such as the dielectric continuum model [14-16]. On the other hand, the dielectric response in proteins is more complicated. There exist many length scales due to the structural constraints created by the carbon back bone. Some studies indicate that a linear response model may be valid from atomistic simulations [17, 18]. A simple dielectric continuum description of the protein is clearly insufficient, even though such a description has been widely used to correlate experimental data [19-22]. A full atomistic description is very time consuming for large proteins and may also hinder the distillation of transparent physical pictures [23, 24].

We have previously proposed to seek a physically well-defined middle ground between the continuum and a full atomistic description of the protein's dielectric response in order to develop a new model that recognizes the highly inhomogeneous nature of a protein and at the same time avoids the enormous computational cost of atomistic model simulations. To this end, we proposed a collection of structurally constrained polarizable dipoles embedded in a dielectric continuum solvent to describe the dielectric response of a protein. Other models of solvents can also be used provided that the response function of the solvent

can be obtained from other sources. The main assumption of our model is the existence of a set of frequency-dependent polarizabilities for each residue, portable to all proteins in nature. The polarizabilities can be obtained by performing detailed molecular dynamics simulations for small proteins or by solvation dynamics measurements with various mutations. The dielectric response of large proteins can be computed from these *intrinsic* parameters. Each dipole is located on the center of mass of a residue, and for each such a residue there is a frequency-dependent polarizability $\alpha(\omega)$ (in general a complex quantity such as the dielectric constant function). The total number of polarizable dipoles is thus equal to the total number of residues and their positions are completely specified by the native structure of the protein.

Studies of the solvation dynamics of proteins offer a powerful means to test the validity of models of their dielectric response. In spite of considerable efforts towards the understanding of the dielectric relaxation processes in proteins [25-28], up to now a reliable estimate for the dielectric response function of proteins is still lacking. Early studies indicated that a slow relaxation (~1 ns) indeed exists in myoglobin [29, 30] in contrast to the polar solvents. This is not unexpected due to the structural constraints. But the role of a protein's interior motions in its dielectric relaxation is presently unclear from various experimental studies of solvation dynamics in protein environments. Homoelle et al. have suggested that the dynamical fluctuations observed in phycobiliproteins involve substantial interior motions of the protein [31]. Fraga and Loppnow [32] have shown that the resonance Raman spectra are affected by the different residue compositions of the blue copper proteins from different species. On the other hand, other experimental and theoretical studies of lysozyme seem to suggest that the major contribution of the observed dynamical fluctuations comes from the surrounding water solvent and the water molecules attached on the protein surface [33].

Zewail and coworkers used tryptophan fluorescence to study solvation dynamics in proteins. The solvation dynamics were significantly slower for the surface tryptophan

residues in Subtilisin *Carlsberg* and in monellin than for that of tryptophan in bulk water. They argued that the slow relaxation is due to the water molecules constrained on the protein surface [27, 34, 35]. Given, however, the ~500 cm^{-1} difference in the reorganization energies for the surface tryptophans in the two proteins, it seems that there is also a considerable relaxation arising from the different amino acids neighboring the tryptophans.

These differences in the interpretations of various experiments are in no small part due to the lack of a reliable dielectric response function for the studied proteins from either experiments or computer simulations. The knowledge of the protein dielectric response provided by our model could shed light on this since it presents a residue level dielectric response function of proteins. What is also required, however, is a well-characterized experimental system that facilitates the interpretation of the data. To this end, we propose the complex of coumarin 153 and apomyoglobin. There are three main considerations for the choice of this system. First, coumarins in general, and coumarin 153 (C153) in particular, are well characterized and widely used chromophores for solvation dynamics studies [36-46]. Second, we can produce a broad range of mutant proteins [47, 48] in which one or several amino acids are strategically replaced, so as to test our theoretical model. Third, the structures of many myoglobins and their mutants have been determined to high resolution [49, 50]. We consequently propose that a fruitful system for studying the protein dielectric response is myoglobin in which the heme has been replaced by coumarin 153. The availability of mutant proteins with amino acid replacements near the heme binding site will eventually permit a quantitative evaluation of local contributions of specific residues to the solvation dynamics of proteins.

Previous attempts to exploit the myoglobin system to study the solvation response of proteins have been made [29, 30] using the fluorescent probes, 2,6-ANSDMA and DANCA, respectively (Figure 6.1). The former probe molecule afforded a single exponential response of 9.1 ns; the latter, a more complicated response with both shorter and longer response

times. The discrepancy between the results for these two probe molecules as well as the predominance of the long-lived response time caused us to search for other probes. We thus initially considered the probe molecules 1,8-ANS and biliverdin, both for which there are structures of their complexes with apomyoglobin [51, 52]. Neither of these chromophores is, however, ideal because their absorption spectra are complicated by overlapping electronic states. Even if internal conversion from higher-lying states to the lower fluorescent state is faster than solvation dynamics, as has been suggested to be the case in tryptophan [27, 34, 35, 53], an accurate determination of the reorganization energy based on the steady-state spectra becomes very difficult. We consequently opted for coumarin 153, which not only has been studied in a very wide range of solvents and in the gas phase, but whose excited-state

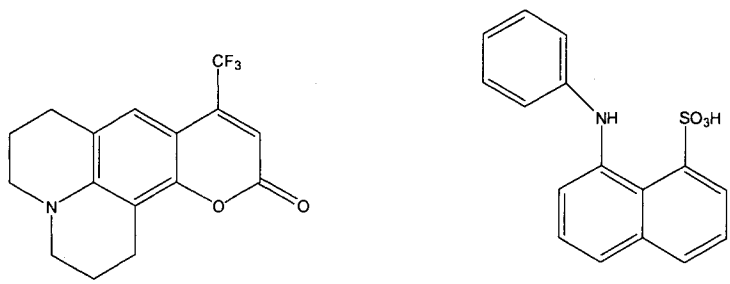

coumarin 153 1,8-ANS

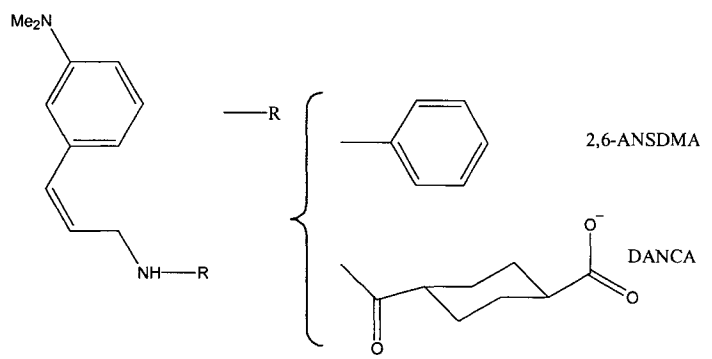

Figure 6.1: Some fluorescent probes.

solvation has been demonstrated not to involve any contributions other than those from S_1 [38]. Hochstrasser and coworkers have studied the solvation of coumarin 343 in calmodulin [41]. These workers attached coumarin 343 to the N-terminus of a tridecapeptide, which was designed to bind tightly to calmodulin. In this system, solvation is complete in 100 ps.

Materials and Methods

Coumarin 153 was purchased from Exciton Inc. (Dayton, OH) and used without further purification. Apomyoglobin was prepared using the procedure described elsewhere [54]. Coumarin 153 has low solubility in water. Consequently, addition of apoprotein providing sufficient time for equilibration (45 minutes) ensured that it was taken up by complex formation. In order to obtain complexes with different C153/apoMb ratios, increasing amounts of C153 were added to a 5 x 10^{-5}-M protein solution. The C153 solution was prepared by adding microliter amounts of a concentrated stock solution of C153 in methanol to water and sonicating for ~1 hour in the dark to ensure complete homogenization of the resulting solution. All the samples were then allowed to equilibrate for 45 minutes prior to the steady-state and time-resolved measurements. Completion of equilibration was checked by recording the steady state spectra at 10-minute intervals after the addition of C153 until no change in Stokes shift was observed.

Binding constant measurements, fluorescence. Two stock solutions were prepared of equal concentration, $5x10^{-5}$ M, of both apoMb and coumarin 153. From these stock solutions, seven 200 μL samples were prepared with an increasing mole fraction, X, of coumarin: 0.1, 0.2, 0.25, 0.5, 0.75, 0.8, and 0.9. After the samples were allowed to stand for approximately 45 minutes to ensure complete equilibration, fluorescence intensities were measured and plotted against mole fraction of coumarin, X, to verify that the maximum intensity occurred at a mole fraction of 0.5, indicating a one-to-one binding stoichiometry. (C153 has very low

solubility in water, and the protein ApoMb by itself has no measurable fluorescence in the region where the complex emits. Thus, the fluorescence is directly proportional to the concentration of the protein-coumarin complex.) Using this maximum intensity and the intensity at one other mole fraction, the binding constant, K_B can be determined [55], where $K_B = (I \times I_0)/(I_0 - I)(I_0[apoMb]_T - I[C153]_T)$. I_0 is the maximum fluorescence intensity at X = 0.5. I is the fluorescence intensity at a given mole fraction, X. $[apoMb]_T$ = total concentration of apoMb at a given X, and the subscript T refers to the total concentration. $[C153]_T$ is the concentration of coumarin 153 at a given X. The dissociation constant for the complex is $K_D = 1/K_B$.

Binding constant measurements, capillary electrophoresis (CE). Frontal analysis CE experiments were performed on a Beckman Coulter P/ACE MDQ capillary electrophoresis system equipped with a 488-nm laser-induced fluorescence (LIF) detector. Untreated fused-silica capillaries with 50 μm ID and 360 μm OD was purchased from Polymicro Technologies, Inc. (Phoenix, AZ). The capillaries were 30 cm in length (20 cm to detection window). When a capillary was first used, it was rinsed for 1 min with water, 5 min with 1 M NaOH, and 1 min with water. Prior to each injection, the capillary was washed for 0.5 min with water, 0.5 min with 1 N NaOH, and 0.5 min with water, followed by 2 min with running buffer. The premixed coumarin-apomyglobin samples were injected at 0.5 psi for 40 seconds to the capillary. Experiments were performed at 10 kV and a temperature of 25°C. Sample emission was monitored at 520 nm. Data were collected by P/ACE system MDQ software. Sodium phosphate and phosphoric acid were purchased from Fisher Scientifics (Fairlawn, NJ). 0.2 M Na-phosphate buffer at pH 9.0 was used. The phosphate buffer was filtered through 0.22 mm Non-pyrogenic filter (Costar, Corp.Corming, NY). In the frontal analysis technique, coumarin 153 and apomyglobin were premixed and injected as a large sample plug onto the capillary column. At pH 9, the apomyglobin is negatively charged. The

electrophoretic mobility of the free coumarin 153 is different from the mobility of the protein and protein-coumarin complex. After injection of large mixed sample plug, the free coumarin will migrate away from the protein. Equilibrium is maintained where the zones temporarily overlap. The equilibrium free coumarin concentration is calculated from the height of the resulting plateau. The height of the free coumarin plateau decreases with the addition of apomyglobin because of its binding to coumarin. The plateau height at [apoMb] = 0 μM was used as the coumarin standard. In this assay, a series of sample mixtures with a fixed protein concentration and increasing coumarin concentrations are injected. Performing such experiments at different coumarin concentrations allows the determination of binding constant according to the following equation: $r/(1-r) = n K_B [C153]_f$, where r is the fraction of bound chromophore, n is the number of binding sites, $[C153]_f$ is the free chromophore concentration in the running buffer, and K_B is the binding constant between apoMb and C153.

Steady-state spectroscopies. Steady-state absorption spectra were recorded on a Perkin-Elmer Lambda-18 double-beam UV-visible spectrophotometer with 1-mm resolution. The concentration of the apoprotein was determined by monitoring the absorbance at 280 nm, where the molar extinction coefficient is 15.2 $mM^{-1}cm^{-1}$. Steady-state fluorescence spectra (both excitation and emission), were obtained on a SPEX Fluoromax with a 4-nm bandpass, and corrected for detector response. For both fluorescence and absorption measurements of the complex, a 3-mm pathlength quartz cuvette was used. Steady-state circular dichroism (CD) spectra were performed on a JASCO CD spectrometer (J-710). A 3-mm pathlength cell was also used for these measurements. The concentration of the samples was kept close to micromolar range to avoid saturation of the detector. The data so presented are an average of 3 scans and were collected at an interval of 1 nm .

Time-resolved spectroscopies. The laser source for the time-correlated single-photon counting measurements was a home-made mode-locked Ti-sapphire laser, tunable from 780 to 900 nm with a repetition rate of 82 MHz. The fundamental from the Ti-sapphire oscillator was modulated by a Pockels cell (Model 360-80, Conoptics Inc) to reduce the repetition rate to about 8.8 MHz and was subsequently frequency doubled by focusing tightly into a 0.4-mm BBO crystal. The blue light, which had a central wavelength of 425 nm, provided the excitation source. Emission from the samples of the complex was collected at $\lambda_{em} > 550$ nm with a bandpass filter in order to reduce the contribution of scattered excitation light interfering with the sample fluorescence. The fluorescence lifetime decays were collected at the magic angle (polarization of 54.7° with respect to the vertical). A half-wave plate was used before the excitation polarizer to ensure vertical polarization of the excitation light. To obtain the rotational dynamics, emission from the samples was collected parallel and perpendicular to the direction of polarization of the excitation pulse. The instrument response function of the apparatus had a full-width–at-half-maximum (FWHM) of 80 ps. The fluorescence lifetime decays were typically collected up to a maximum of 10,000 counts in the peak channel of the multi-channel analyzer (MCA) while for the anisotropy decays, the corresponding maximum value was 12,000 counts. Sample integrity was checked by monitoring the excitation and emission spectra before and after the measurements. The coumarin concentration was kept at ~ 5×10^{-6} M throughout. A 3-mm cell pathlength was used for the time-resolved measurements of the complex.

Molecular dynamics simulations. The starting configuration of horse heart myoglobin is from the protein DATA BANK (PDB id 1WLA) with TIP3P water models. Standard constant pressure-temperature MD was performed using the ORAC package with the Amber force field [56]. In all simulations, short-range non-bonded interactions were calculated up to a 10 Å cutoff, whereas long-range electrostatic interactions were treated by the SPME

method using a very fine grid, 128 point per axis, with periodic boundary conditions, and Ewald convergence parameter of 0.43 $Å^{-1}$. Three different Nosé-Hoover thermostats were coupled to solute, solvent, and total center of mass. An external pressure of 0.1 MPa was applied all along the trajectory. A five time-step rRESPA [57] algorithm with times of 0.5-1.0-2.0-4.0-12.0 fs was used with bond constraints on hydrogen covalent bonds handled by a Shake-Rattle-like algorithm. The final system was first equilibrated with velocity rescaling for 60 ps at 50 K and 80 ps at 300 K. Following this initial equilibration, we ran the system for one additional nanosecond at constant temperature (T = 300 K) and pressure (P = 0.1 Mpa). To achieve full relaxation, the simulation box was entirely flexible for the first 300 ps, whereas for the remainder of the run, only isotropic changes of the box were allowed [58]. Finally, the system was simulated for an additional 10 ns. Shown in Figure 6.2 are snapshots at around 3 ns for the horse heart and the sperm whale apomyoglobin complexes. One might object that the way to find the equilibrium configuration is to raise the temperature and then to cool the system. This is not recommended. Raising the temperature will mostly likely denature the protein, and the heme-pocket may adopt some highly unlikely conformations that would not be present in the native structure. Since the insertion of C153 in our experiments is done with the native myoglobin structure, the method we employ is physically reasonable.

Results and Discussion

The binding of coumarin 153 to apomyoglobin has been characterized by molecular dynamics simulations (which predict tight, stable binding in the heme pocket), measurement of its dissociation constant using two different methods, circular dichroism (which demonstrates no changes in secondary structure for the complex with respect to that of the native holo protein), and its reorientation time using measurements of the polarized fluorescence decay.

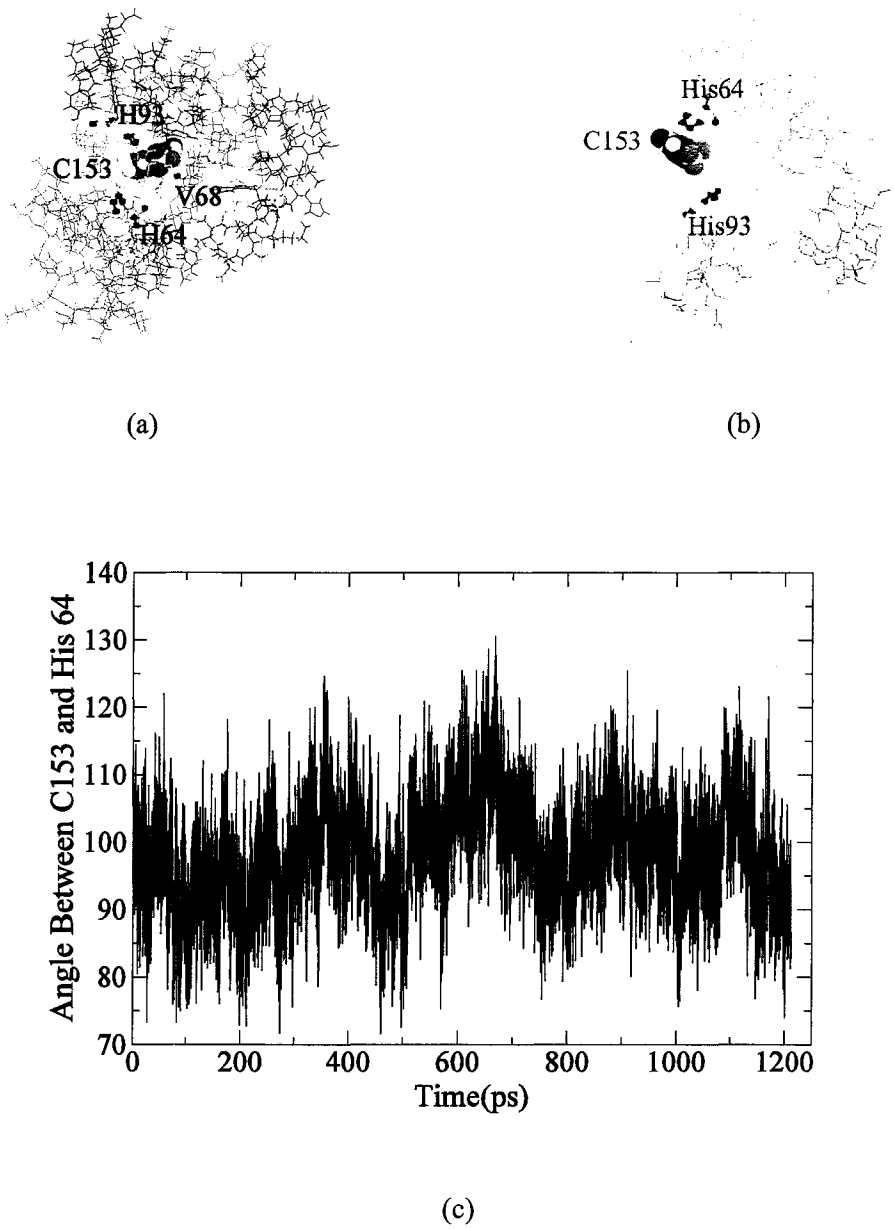

Figure 6.2: Snapshot of equilibrated C153-apomyoglobin in water from 3-ns molecular dynamics simulations using the Amber95 force field: (a) sperm whale apomyoglobin; (b) horse heart apomyoglobin. The C153 is shown in the space-filling models. Key histidine residues in the heme pocket are also shown. Residue Val68 (one of the residues in contact with C153 in the hydrophobic heme-pocket with small nuclear polarizability) is used in one of our mutations [47, 48]. (c) The time dependence of the relative orientation of C153 with respect to His 93 (see text) from the MD trajectory of the horse heart apomyoglobin-C153 complex.

A 10-ns MD simulation using the Amber force field indicates that C153 is stable in the heme-pocket and an equilibrium configuration is found (Figures 6.2 a and b). Also shown in Figure 6.2c is a trajectory of the angle between C153 and His 64, which is defined by the vector from N to ester O of C153 and the vector of two Ns on the His 64 sidechain. This angle is averaged at 98° with a standard deviation of 8°. Similar results are obtained for the angle between C153 and His 93.

Using two different methods, we have obtained dissociation constants of 5.65 ± 0.25 μM (Job's plot) and 13 ± 2 μM (CE) for coumarin 153 and horse heart apoMb, which are comparable to or smaller than those discussed previously for other fluorescent probes [29, 30] (Figures 6.3 and 6.4). The Job's plot of the complex (Figure 6.3) clearly reveals that the maximum of the fluorescence intensity occurs at coumarin mole fraction of 0.5, which is a clear indication of 1:1 stoichiometry for the complex in the given concentration range of protein. One explanation for the difference in the two results is that the CE experiments were performed using a higher C153/apoMb ratio because the detector was equipped with a 488-nm light source, which is not optimal for exciting coumarin 153 fluorescence.

Independent confirmation that the coumarin binds in the heme pocket is provided by the similarity of the circular dichroism (CD) spectra of native myoglobin with that of the C153/apoMb complex (Figure 6.5). A comparison of the fluorescence anisotropy decay of coumarin 153 in solution (DMSO) (Figure 6.6) and bound to apoMb (Figure 6.7) also argues for C153/apoMb complex formation. While the free coumarin exhibits a very fast depolarization time of 100 ps in DMSO, this time is lengthened to 9.2 ns upon binding, the latter time consistent with the rotational correlation time that would be expected for the ~18 kDa protein. More significantly, the anisotropy decay of bound coumarin is single exponential (9.2 ns), within our time resolution. This can be interpreted in terms of a rigidly bound coumarin whose fluorescence is depolarized exclusively by the overall rotational motion of the apomyoglobin itself. A single exponential decay would not be expected for a

surface bound chromophore [59, 60]. That the fluorescence decay of C153 is single exponential also suggests that, within the sensitivity of our experimental apparatus, it binds in the hemepocket in only one conformation.

Finally, there is a significant Stokes shift of bound C153 with respect to C153 in methanol that demonstrates the difference between the hemepocket and the bulk solvent in solvating the fluorescent state. The spectra in Figure 6.8 can be used to compute the reorganization energy, λ, by using the method of Jordanides et al. of [33]:

$$\lambda = \hbar \frac{\int_0^\infty d\varpi [\sigma_a(\varpi) - \sigma_f(\varpi)]\varpi}{\int_0^\infty d\varpi [\sigma_a(\varpi) + \sigma_f(\varpi)]} \tag{6.1}$$

The $\sigma_{a,f}$ are the absorption (or excitation) and emission spectra, respectively on a wavenumber scale. The reorganization energy is widely used as a measure of the strength of interactions between a chromophore and its surrounding dielectric media in solvation dynamics studies. It is usually taken as half of the Stokes shift. This estimation is accurate if the excitation and emission spectra are Gaussian, but it becomes unreliable if the spectra are not Gaussian. The reorganization energy computed using the above expression is 2280 cm^{-1} for C153 complexed with apomyoglobin as opposed to 2800 cm^{-1} for C153 in methanol, which indicates the difference in the probe's environment in these two distinctly different systems.

The preponderance of evidence listed above supports C153 binding to apomyoglobin, specifically in the heme pocket, in a manner illustrated in Figure 6.2. This leaves the dye in a hydrophobic environment consisting of a large number of amino acid side chains that are responsible for stabilizing and isolating the heme prosthetic group to prevent dissociation and oxidation in the native protein. In sperm whale myoglobin, the principal side chains impinging on C153 are two His residues (at positions 64 and 97 in the primary sequence), Phe43, Val68, Leu29, and Leu89.

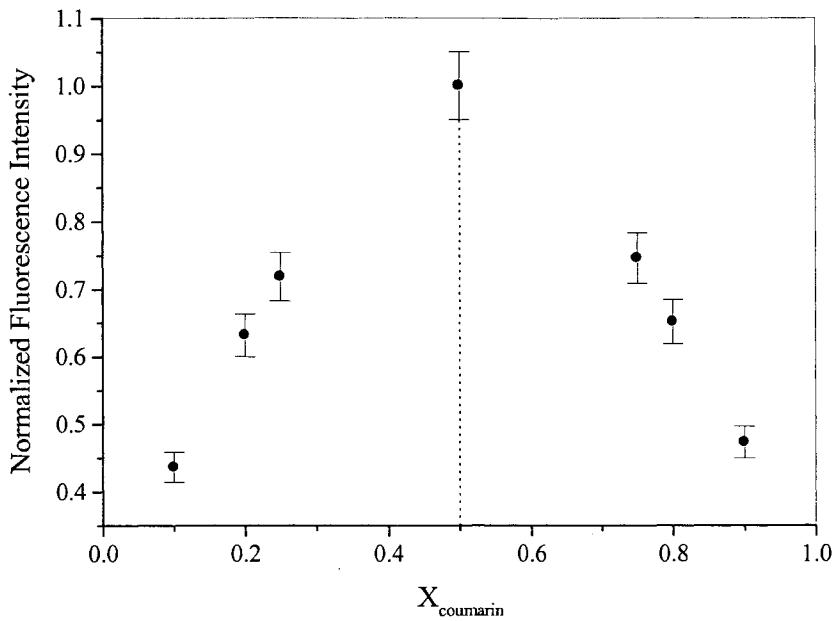

Figure 6.3. Job's plot for the complexation of coumarin-153 with apoMb. That the fluorescence intensity peaks at a mole fraction value of 0.5 (dotted lines) for C153 is a clear indication of a 1:1 complex formed between the probe molecule and the protein. The data presented are an average of four measurements. The calculated dissociation constant for the complex is 5.65 ± 0.25 μM.

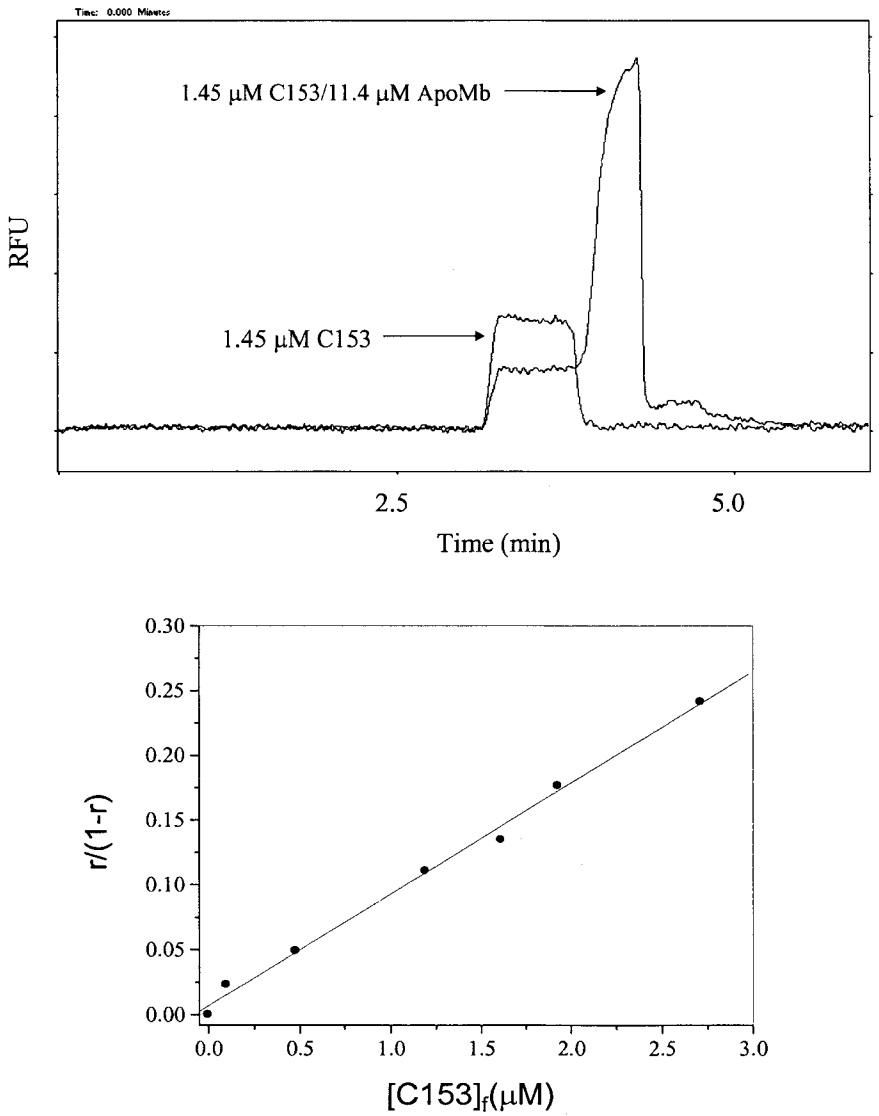

Figure 6.4: Electropherogram (top panel) obtained using the frontal analysis capillary electrophoresis method with coumarin-apoMb. Experimental conditions: pressure injection at 0.5 psi for 40 s; separation voltage, 10 kV; LIF detector with excitation at 488 nm and emission at 520 nm. 0.2 M sodium phosphate buffer at pH 9.0. The first peak plateau is due to the coumarin; the second, to the coumarin-apoMb complex. The final result is based on 3 individual experiments: $K_D = 13 \pm 2$ μM. The ordinate label RFU stands for "relative fluorescence units." The bottom panel is a plot of {r/(1-r)} against free coumarin, where r is the fraction of C153 bound per protein. The slope of a linear fit to the experimental data points gives the binding constant (K_B) of C153 in the complex. The value of K_B obtained from this figure is 0.086 μM^{-1}, which gives $K_D = 11.6$ μM.

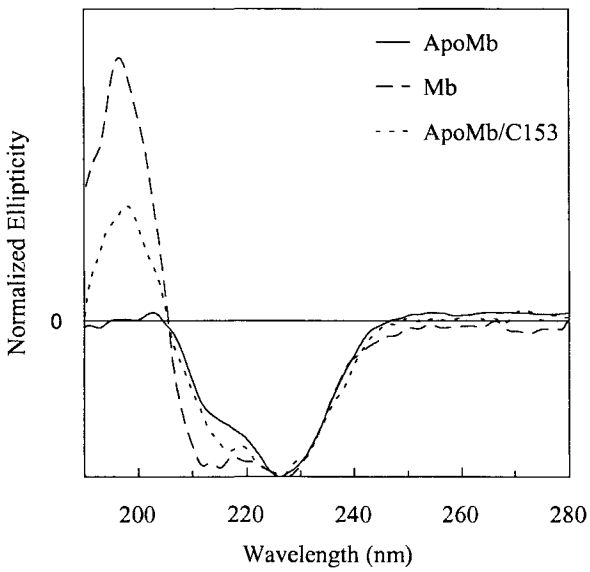

Figure 6.5: The CD spectra of apoMb (solid), Mb (dashed), apoMb/C153 complex (dotted). The figure clearly shows the retention of the native structure of Mb once C153 binds inside the vacant heme pocket of apoMb. Protein concentrations are approximately 10^{-6} M, and the apoMb/C153 complex has a concentration ratio of 2:1. Similar spectra were obtained with other ratios in a range from 9:1 to 2:1.

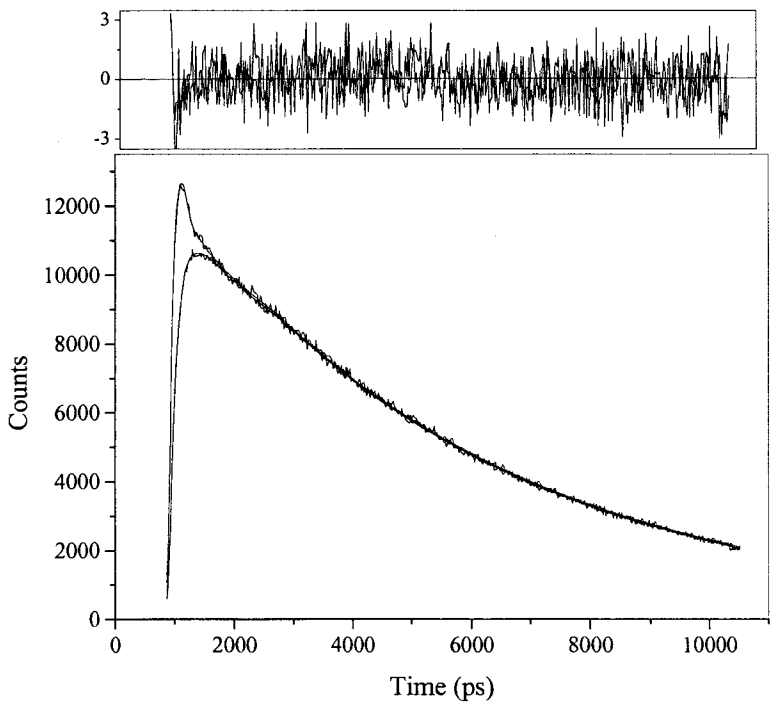

Figure 6.6: Polarized fluorescence decay of C153 in DMSO: $\lambda_{ex} = 420$ nm; $\lambda_{em} > 470$ nm, $\chi^2 = 1.3$; r(t) = 0.32exp(-t/110 ps). The anisotropy measurement was repeated 4 times yielding a reorientation time, $\tau_r = 100 \pm 10$ ps and a limiting anisotropy, r(0) = 0.32 ± 0.02. The fluorescence lifetime was 5300 ± 50 ps. The top panel shows the residual from the fits.

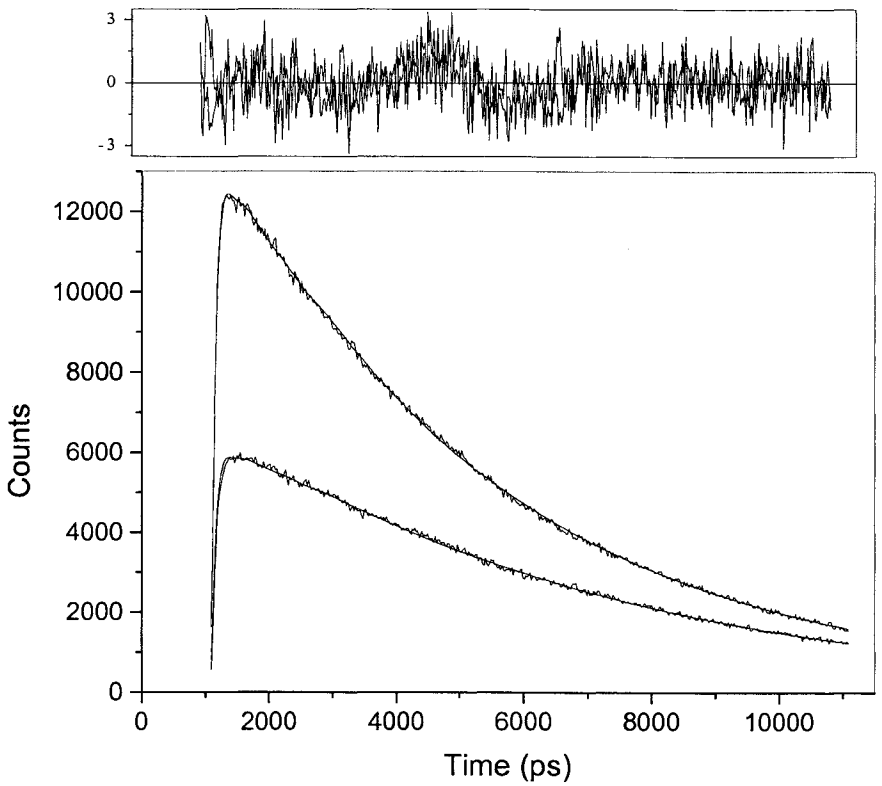

Figure 6.7: Polarized fluorescence decay of the coumarin 153-horse heart apomyoglobin complex. The concentration of protein (5.5×10^{-5} M) is 10 times that of coumarin to eliminate multiple binding of C153 to the protein. $\lambda_{ex} = 425$ nm; $\lambda_{em} > 550$ nm, $\chi^2 = 1.2$; r(t) = 0.29exp(-t/9300 ps). The anisotropy measurement was repeated 3 times. The average value of rotational time is 9200 ± 100 ps and the limiting anisotropy is r(0) = 0.29 ± 0.01. The fluorescence lifetime of coumarin bound to apomyoglobin was 5050 ± 50 ps (3 measurements). For the lifetime measurements, $\lambda_{ex} = 425$ nm; $\lambda_{em} > 550$ nm and $\chi^2 = 1.2$. Fitting the decay to a double exponential gave no improvement over the chi-squared value already obtained from the single exponential fit. The top panel shows the residuals from the fits.

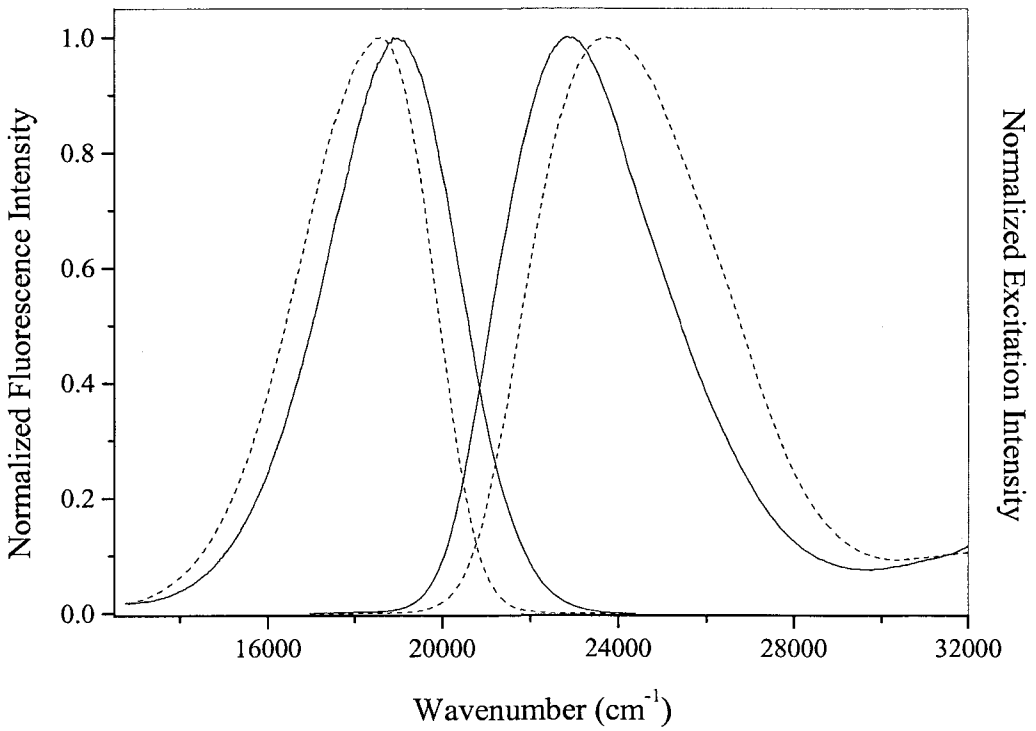

Figure 6.8: Steady state spectra of the horse heart apomyoglobin/coumarin 153 complex (solid lines) and of coumarin 153 in methanol (dashed lines). According to our method of evaluating the reorganization energy [33] the whole excitation or absorption spectrum is needed. If there are more than one electronic excited states close to the fluorescence state it will be very difficult to get an accurate excitation spectrum of that state, which is the case, for example, for ANS, whose excitation spectrum is congested with at least two overlapping peaks in the blue region. The reorganization energy calculated by our method for C153 in the complex was 2280 cm^{-1} while that in methanol was 2800 cm^{-1}.

Conclusions

We have furnished an exhaustive characterization of the complex of the fluorescent probe, C153, with apomyoglobin indicating that it binds moderately strongly and very rigidly in the heme pocket. Since protein is clearly a heterogeneous environment with a spatially dependent polarizability, a precise knowledge of where and how the fluorescence probe binds is crucial to any thorough analysis of the protein dielectric response and our ability to distinguish the protein's response from that of the solvent. Future work will analyze the contribution of the individual amino acid residues in the heme pocket to the dielectric response of the protein.

Acknowledgements

This work was partially supported by NSF grant MCB-0077890 to MSH and JWP. XS acknowledges the financial support provided by a grant from the Petroleum Research Fund, administrated by the American Chemical Society. Mr. J. Graboski assisted with the preparation of the apomyoglobin samples. We thank Conoptics, Inc. for their generous loan of the Pockels cell to reduce the repetition rate of our Ti:sapphire system. We also thank Tijana Grove for assisting us with the CD measurements.

References

(1) Simon, J.D. (1988) Time-resolved studies of solvation in polar media. *Acc. Chem. Res.* **21**, 128.

(2) Bagchi, B., A. Chandra and G. R. Fleming (1990) Dynamic solvent effects in adiabatic electron-transfer reactions - role of translational modes. *J. Phys. Chem.* **94**, 5197-5200.

(3) Maroncelli, M. (1993) The dynamics of solvation in polar liquids. *J. Mol. Liq.* **57**, 1-37.

(4) Hynes, J. T. (1994) Charge transfer reactions and solvation dynamics. In *Ultrafast Dynamics of Chemical Systems*,Volume **7**, 345-381.

(5) Stratt, R. M. and M. Maroncelli (1996) Nonreactive dynamics in solution: The emerging molecular view of solvation dynamics and vibrational relaxation. *J. Phys. Chem.* **100**, 12981-12996.

(6)Fleming, G.R. and M. Cho (1996) Chromophore-solvent dynamics. *Ann. Rev. Phys. Chem.* **47**, 109-134.

(7) DeBoeij, W. P., M. S. Pshenichnikov and D. A. Wiersma (1998) Ultrafast solvation dynamics explored by femtosecond photon echo spectroscopies. *Ann. Rev. Phys. Chem.* **49**, 99-123.

(8) Mukamel, S (1995) *Principles of Nonlinear Optical Spectroscopy*. Oxford University Press, New York.

(9) Song, X. (1999) Theoretical studies of dielectric solvation dynamics. In *Treatment of Electrostatic Interactions in Computer Simulations of Condensed Media*, Volume **492** (G. Hummer and L. R. Pratt, eds), AIP Conference Proceedings, American Institute of Physics 417-428.

(10) Bhattacharyya, K. and B. Bagchi (2000) Slow dynamics of constrained water in complex geometries. *J. Phys. Chem. A* **104**, 10603-10613.

(11) Hsu, C.P., X. Y. Song and R. A. Marcus (1997) Time-dependent Stokes shift and its calculation from solvent dielectric dispersion data. *J. Phys. Chem. B* **101**, 2546-2551.

(12) Song, X., D. Chandler (1998) Dielectric solvation dynamics of molecules of arbitrary shape and charge distribution. *J. Chem. Phys.* **108**, 2594-2600.

(13) Lang, M. J., X. J. Jordanides, X. Song and G. R. Fleming, G (1999) Aqueous solvation dynamics studied by photon echo spectroscopy. *J. Chem. Phys.* **110**, 5884-5892.

(14) Marcus, R. A. and N. Sutin (1985) Electron transfers in chemistry and biology. *Biochim. Biophys. Acta* **811**, 265-322.

(15) King, G. and A. Warshel (1990) Investigation of the free energy functions for electron transfer reactions. *J. Chem. Phys.* **91**, 3647.

(16) Bader, J. S., R. A. Kuharski and D. Chandler (1990) Role of nuclear tunneling in aqueous ferrous ferric electron-transfer. *J. Chem. Phys.* **93**, 230-236.

(17) Zheng, C., C. F. Wong, J. A. McCammon and P. G. Wolynes (1989) Classical and quantum aspects of ferrocytochrome c. *Chem. Scripta* **29A**, 171-179.

(18) Simonson, T (2002) Gaussian fluctuations and linear tesponse in an electron transfer protein. *Proc. Natl. Acad. Sci. USA* **99**, 6544-6549.

(19) Warshel, A. and S. T. Russel (1984) Calculation of electrostatic interactions in biological systems and in solutions. *Q. Rev. Biophys.* **17**, 283-422.

(20) Sharp, K.A. and B. Honig (1990) Electrostatic interactions in macromolecules: theory and applications. *Ann. Rev. Biophys. Chem.* **19**, 301-332.

(21) Schutz, C.N. and A. Warshel (2001) What are the dielectric "constants" of proteins and how to validate electrostatic models? *Proteins: Struc. Func. Gen.* **44**, 400-417.

(22) Simonson, T. (2001) Macromolecular Electrostatics: Continuum models and their growing pains. *Curr. Opin. Struc. Biol.* **11**, 243-252.

(23) Nakamura, H. (1996) Roles of electrostatic interaction in proteins. *Q. Rev. Biophys.* **29**, 1-90.

(24) Brooks, C.L., M. Karplus and B. M. Pettitt (1987) Proteins: A theoretical perspective of dynamics, structure, and thermodynamics. *Adv. Chem. Phys.* **71**, 1-.

(25) Sheppard, R.J., E. H. Grant and G. P. South (1978) *Dielectric Behavior of Biological Molecules, first edition.* Oxford University Press, Clarendon.

(26) Pethig, R. (1992) Protein-water interactions determined by dielectric methods. *Ann. Rev. Phys. Chem.* **43**, 177-205.

(27) Pal, S.K., J. Peon, B. Bagchi and A. H. Zewail (2002) Biological water: Femtosecond dynamics of macromolecular hydration. *J. Phys. Chem. B* **106**, 12376-12395.

(28) Nandi, N., K. Bhattacharyya and B. Bagchi (2000) Dielectric relaxation and solvation dynamics of water in complex chemical and biological systems. *Chem. Rev.* **100**, 2013-2045.

(29) Pierce, D.W. and S. G. Boxer (1992) Dielectric-relaxation in a protein matrix. *J. Phys. Chem.* **96**, 5560-5566.

(30) Bashkin, J.S., G. Mclendon, S. Mukamel and J. Marohn (1990) Influence of medium dynamics on solvation and charge separation reactions - comparison of a simple alcohol and a protein solvent. *J. Phys. Chem.* **94**, 4757-4761.

(31) Homoelle, B.J., Edington, M.D., Diffey, W.M. and W. F. Beck (1998) Stimulated photon-echo and transient-grating studies of protein-matrix solvation dynamics and interexciton-state radiationless decay in phycocyanin and allophycocyanin. *J. Phys. Chem. B* **102**, 3044-3052.

(32) Fraga, E. and G. R. Loppnow (1998) Proteins as Solvents: Blue copper proteins as a molecular ruler for solvent effects on resonance raman intensities. *J. Phys. Chem. B* **102**, 7659-7665.

(33) Jordanides, X.J., M. J. Lang, X. Y. Song and G. R. Fleming (1999) Solvation dynamics in protein environments studied by photon echo spectroscopy. *J. Phys. Chem. B* **103**, 7995-8005.

(34) Pal, S.K., J. Peon and A. H. Zewail (2002) Biological water at the protein surface: Dynamical solvation probed directly with femtosecond resolution. *Proceedings of the National Academy of Sciences of the United States of America* **99**, 1763-1768.

(35) Peon, J., S. K. Pal and A. H. Zewail (2002) Hydration at the surface of the protein Monellin: Dynamics with femtosecond resolution. *Proceedings of the National Academy of Sciences of the United States of America* **99**, 10964-10969.

(36) Maroncelli, M. and G. R. Fleming (1987) Picosecond solvation dynamics of coumarin-153 - the importance of molecular aspects of solvation. *J. Chem. Phys.* **86**, 6221-6239.

(37) Horng, M.L., J. Gardecki, A. Papazyan and M. Maroncelli (1995) Subpicosecond measurements of polar solvation dynamics: Coumarin 153 revisited. *J. Phys. Chem.* **99**, 17311-17337.

(38) Lewis, J.E. and M. Maroncelli (1998) On the (uninteresting) dependence of the absorption and emission transition moments of coumarin 153 on solvent. *Chem. Phys. Lett.* **282**, 197-203.

(39) Kovalenko, S.A., J. Ruthmann and N. P. Ernsting (1997) Ultrafast Stokes shift and excited-state transient absorption of coumarin 153 in solution. *Chem. Phys. Lett.* **271**, 40-50.

(40) Muhlpfordt, A., R. Schanz, N. P. Ernsting, V. Farztdinov and S. Grimme (1999) Coumarin 153 in the gas phase: optical spectra and quantum chemical calculations. *Phys. Chem. Chem. Phys.* **1**, 3209-3218.

(41) Changenet-Barret, P., C. T. Choma, E. F. Gooding, W. F. DeGrado and R. M. Hochstrasser (2000) Ultrafast dielectric response of proteins from dynamic Stokes shifting of coumarin in calmodulin. *J. Phys. Chem. B* **104**, 9322-9329.

(42) Jiang, Y., P. K. McCarthy and D. J. Blanchard (1994) The role of multiple electronic states in the dissipative energy dynamics of coumarin 153. *Chem. Phys.* **183**, 249-267.

(43) Flory, W.C. and D. J. Blanchard (1998) Excitation energy-dependent transient spectral relaxation of coumarin 153. *App. Spect.* **52**, 82-90.

(44) Palmer, P.M., Y.Chen and M. R. Topp (2000) Simple water clusters of coumarins 151 and 152A studied by IR-UV double resonance spectroscopy. *Chem. Phys. Lett.* **318**, 440-447.

(45) Chen, Y., P. M. Palmer and M. R. Topp (2002) Infrared spectroscopy of jet-cooled, electronically excited clusters of coumarin 151: Excited-state interactions and conformational relaxation. *Int. J. Mass. Spec.* **220**, 231-251.

(46) Agmon, N. (1990) Dynamic Stokes shift in coumarin: Is it only relaxation? *J. Phys. Chem.* **94**, 2959-2963.

(47) Kundu, S., B. Snyder, K. Das, P. K. Chowdhury, J. Park, J. W. Petrich and Hargrove, M.S. (2002) The leghemoglobin proximal heme pocket directs oxygen dissociation and stabilizes bound heme. *Proteins-Struc. Fun. Gen.* **46**, 268-277.

(48) Kundu, S. and M. S. Hargrove (2003) Distal heme pocket regulation of ligand binding and stability in soybean leghemoglobin. *Proteins-Struc. Fun. Gen.* **50**, 239-248.

(49) Quillin, M.L., R. M. Arduini, J. S. Olson and G. N. Phillips, Jr. (1993) High-resolution crystal structures of distal histidine mutants of sperm whale myoglobin. *J. Mol. Biol.* **234**, 140-155.

(50) Quillin, M.L., T. Li, J. S. Olson, G. N. Phillips, Jr., Y. Dou, M. Ikeda-Saito, R. Regan, M. Carlson, Q. H. Gibson and H. Li (1995) Structural and functional effects of apolar mutations of the distal valine in myoglobin. *J. Mol. Biol.* **245**, 416-436.

(51) Cocco, M.J. and J. T. J. Lecomte (1994) The native state of apomyoglobin described by proton NMR spectroscopy: Interaction with the paramagnetic probe HyTEMPO and the fluorescent dye ANS. *Protein Sci.* **3**, 267-281.

(52) Wagner, U.G., N. Muller, W. Schmitzberger, H. Falk and C. Kratky (1995) Structure determination of the biliverdin apomyoglobin complex - crystal-structure analysis of 2 crystal forms at 1.4 and 1.5 angstrom resolution. *J. Mol. Bio.* **247**, 326-337.

(53) Shen, X. and J. R. Knutson (2001) Subpicosecond fluorescence spectra of tryptophan in water. *J. Phys. Chem. B* **105**, 6260-6265.

(54) Hargrove, M.S., E. W. Singleton, M. L. Quillin, L.A. Ortiz, G. N. Phillips, J. S. Olson and A. J. Mathews (1994) His(64)(E7)-]Tyr apomyoglobin as a reagent for measuring rates of hemin dissociation. *J. Bio. Chem.* **269**, 4207-4214.

(55) Williams, K.R., B. Adhyaru, R. Pierce and S. G. Schulman (2002) The binding constant of complexation of bilrubin to bovine serum albumin. *J. Chem. Ed.* **79**, 115-116.

(56) Procacci, P., T. A. Darden, E. Paci and M. Massimo (1997) ORAC: a molecular dynamics program to simulate complex molecular systems with realistic electrostatic interactions. *J. Comput. Chem.* **18**, 1848-1862.

(57) Tuckerman, M.E., B. Berne and G. J. Martyna (1992) Reversible multiple scale molecular dynamics. *J. Chem. Phys.* **97**, 1990-2001.

(58) Marchi, M. and P. Procacci (1998) Coordinate scaling and multiple time step algorithms for simulation of solvated proteins in the NPT ensemble. *J. Chem. Phys.* **109**, 5194-5202.

(59) Petrich, J.W., J. W. Longworth and G. R. Fleming (1987) Internal motion and electron transfer in proteins: a picosecond fluorescence study of three homologous azurins. *Biochemistry* **26**, 2711-2722.

(60) Das, K., A. V. Smirnov, J. Wen, P. Miskovsky and Petrich, J.W. (1999) Photophysics of hypericin and hypocrellin A in complex with subcellular components: Interactions with human serum albumin. *Photochem. Photobio.* **69**, 633-645.

CHAPTER 7. THE SEPARATION OF HYPERICIN'S ENANTIOMERS AND THEIR PHOTOPHYSICS IN CHIRAL ENVIRONMENTS

A paper published in *Photochemistry and Photobiology*[1]

Lindsay Sanders, Mintu Halder, Tom Ling Xiao, Jie Ding,
Daniel W. Armstrong, and Jacob W. Petrich[2]

Abbreviations: BBO, β-barium borate; DMSO, dimethylsulfoxide; FWHM, full-width at half-maximum; HSA, human serum albumin; GST, glutathione S-transferase; LBO, lithium triborate

Abstract

We report the first separation of the enantiomers of hypericin. Their steady-state optical spectra and ultrafast primary photoprocesses are investigated in chiral environments. Within experimental error, there is no difference between the two enantiomers in any of the systems considered. This is consistent with the emerging picture that the rich and extended absorption spectrum of hypericin is not a result of ground-state heterogeneity. It is also consistent with the observation that the spectra and photophysics of hypericin are generally insensitive to environments in which it does not aggregate.

---

[1]Reproduced from L. Sanders et al., *Photochemistry and Photobiology*, **2005**, *81*(1) with the permission of the American Society for Photobiology.

[2]Author to whom correspondence should be addressed.

Introduction

This article focuses on the fluorescence spectroscopy of the two enantiomers of hypericin in chiral environments. Hypericin (Figure 7.1) is a naturally occurring perylene quinone that has gained great interest recently owing to its biological activity [1-20]—in particular, its light-induced biological activity [21-25]. The importance of light for its function has motivated our study of the photophysics of hypericin and its analogs [26-36]. Two notable features of the steady-state spectra of hypericin are the mirror image symmetry between the absorption and emission spectra and the extended absorption from the visible to the ultraviolet with no gaps of zero absorbance. Our first attempt to explain these features was to suggest that the ground state of hypericin was populated with at least one other species, for example, a monotautomer [27]. Temperature-dependant ^{1}H NMR and 2D-ROESY studies of hypericin, however, indicate that there is only one conformer/tautomer for hypericin in the ground state [37]. *Ab initio* quantum mechanical calculations are consistent with this observation [38]. In the spirit of continuing to search for instances of ground-state heterogeneity, we have separated hypericin's enantiomers (Figure 7.1): the methyl and hydroxyl groups in the so-called "bay region" impose right- and left-handed twists about the axis containing the carbonyl groups. We have investigated their steady-state spectra and ultrafast primary processes.

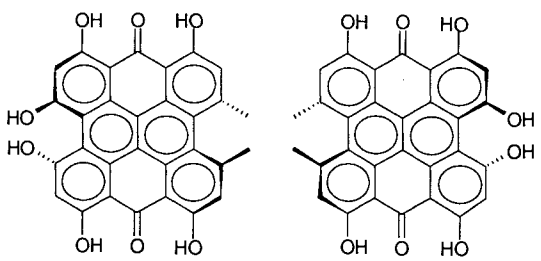

Figure 7.1: Structures of hypericin enantiomers.

Materials and Methods

Separation of hypericin enantiomers. Separations and collections of enantiomers of hypericin were achieved using a HP 1050 HPLC system with UV detector, auto injector, and a computer controlled Chem-station data processing software. The chiral stationary phase, trade named Chirobiotic TAG (TAG) column (250 x 4.6 mm I.D.) was obtained from Advanced Separation Technologies, Inc. (Astec, Whippany, NJ, USA). The chiral stationary phase was prepared by bonding the chiral selector to a 5-μm spherical porous silica gel through linkage chains. Detection wavelengths were varied between 220 nm and 254 nm to confirm the same absorption ratio of the two enantiomers. The semipreparative separation conditions used to isolate mg quantities (overall) of the pure enantiomers of hypericin are as follows. The racemates of hypericin were dissolved in neat methanol to a concentration of 1mg/ml. Up to 50μL of sample was injected onto an analytical scale Chirobiotic TAG column and eluted with 100% methanol, adding 1% triethylamine (TEAA)(v/v). Fractions of the individual enantiomers (from successive injections) were manually collected and concentrated by evaporation at room temperature using continuously flowing air (21°C). All mobile phases were premixed and degassed before use. The flow rate was 0.4 ml/min under isocratic conditions. We did not determine the absolute configurations of the separated enantiomers, which are referred to as hypericin 1 (13.83-min elution time) and 2 (16.65-min elution time) (Figure 7.2).

Sample preparation for optical measurements. A tightly-closed 3-mm pathlength quartz cuvette (instead of a traditional 10-mm cell) was used for all spectroscopic measurements owing to the limited amount of sample available to us. All measurements were taken at ambient temperature. Steady-state excitation and emission spectra were recorded with a SPEX Fluoromax with a 4-nm bandpass and were corrected for detector response. The excitation wavelength for the emission spectra presented in Figure 7.3 was 550 nm.

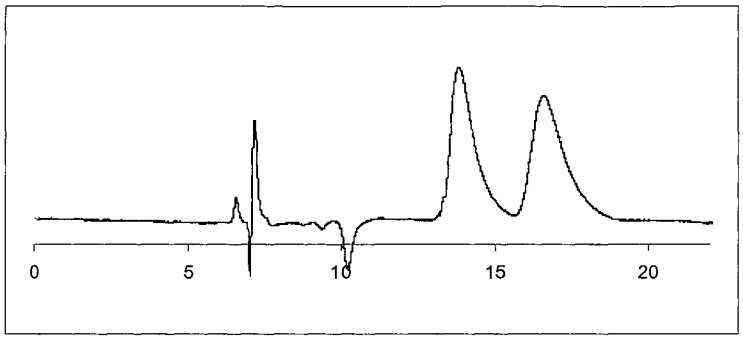

Figure 7.2: Chromatogram obtained using 100% MeOH, 1% TEAA(v/v), 0.4mL/min on Chirobiotic TAG column for separation of racemic hypericin.

5.0 x 10^{-7} M solutions of each hypericin enantiomer were prepared in (S)-(+)-2-butanol (99%) purchased from Aldrich. A concentrated γ-cyclodextrin (99%, Sigma) solution was prepared in water. The chiral hypericins were dissolved in aliquots of this solution and diluted to 1.0 x 10^{-7} M. Human serum albumin (99%) was purchased from Sigma. Solutions of 1.0 x 10^{-6} M hypericin with 5.0 x 10^{-6} M HSA were prepared in a 7-mM phosphate buffer (pH 7) using concentrated stock solutions of hypericin in DMSO. Microliter quantities of hypericin in DMSO were used to keep the final DMSO concentration below 0.8%. The solutions were allowed to equilibrate for 24 hours at 4°C in the dark. Solutions of 5.0 x 10^{-6} M hypericin with 2.5 x 10^{-5} M GST were prepared in 7-mM phosphate buffer (pH 7) with 2-mM EDTA. Concentrated stock solutions of hypericin in DMSO were added in microliter quantities so that the final DMSO concentration remained below 3%. The solutions were left to equilibrate for 24 hours at 4°C in the dark.

Fluorescence upconversion measurements. The fundamental output from a homemade Ti:sapphire amplified system [39, 40] (815 nm) is doubled by a type-I LBO crystal (2 mm). The frequency-doubled blue pulses (407 nm) are separated from the fundamental by a dielectric mirror coated for 400 nm and are focused onto a rotating cell containing the sample

using a 5-cm convex lens. The remaining fundamental was used as the gate to upconvert emission. Fluorescence was collected by an LMH-10x microscopic objective (OFR Precision Optical Products) coated for near UV transmission. The gate and the emission are focused by a quartz lens (12 cm) onto a type-I 0.4-mm BBO crystal (MgF_2 coated, cut at 31° and mounted by Quantum Technology, Inc). The polarization of both the gate and excitation source was controlled with a set of zero-order half-wave plates for 800 nm and 400 nm, respectively. The upconverted signal is then directed into an H10 (8 nm/mm) monochromator (Jobin Yvon/ Spex Instruments S. A. Group) with a 5-cm convex lens coupled to a Hamamatsu R 980 PMT equipped with a UG11 UV-pass filter and operated at maximum sensitivity. The PMT output was amplified in two stages (total by a factor of 25, 5 for each stage) by a Stanford research Systems SR-445 DC-300 MHz amplifier with input terminated at 500 Ω and was carefully calibrated after a long (1-2 hours) warm-up. Photon arrival events were registered with SR-400 gated photon counter operated in CW mode with a threshold level of -100 mV. This signal was fed into a boxcar averager. A part of blue pulse train was used to normalize pump beam fluctuations. A translation stage (Compumotor) with a resolution of 0.06 mm/step was used to delay the exciting pulses, and a computer with Keithley Metrabyte (DAS 800) interfacing card drove the motor. The instrument response function was obtained by collecting the cross-correlation function of the blue and red pulses; the resulting third harmonic intensity was plotted against delay time. The cross-correlation functions typically have a FWHM of ~1 ps. This instrument response is a little over three times as broad as that obtained with our unamplified system [34, 41]. We attribute this to the absence of compensating prisms after frequency doubling, the presence of the rotating sample cell, and perhaps a nonideal optical geometry, which nevertheless permits the facile interchange between pump-probe transient absorption and fluorescence upconversion measurements. All curves were fit and deconvoluted from the instrument function using an iterative convolute-and-compare least-squares algorithm.

Results and Discussion

The steady-state spectra (Figure 7.3) of the hypericin enantiomers were obtained in the following chiral environments: (S)-(+)-2-butanol, γ-cyclodextrin, human serum albumin, and glutathione S-transferase. The latter two are of particular biological interest. Human serum albumin (HSA) is a transport protein in the blood plasma. It binds a wide variety of substances, such as metals, fatty acids, amino acid, hormones, and a large number of therapeutic drugs [42]. Because of its clinical and pharmaceutical importance, the interaction of HSA with ligands has been studied [43, 44]; and, in particular, the interaction of hypericin with HSA has been investigated [45-49]. Glutathione S-transferases (GSTs) are a family of detoxification enzymes that are known to bind nonsubstrate hydrophobic anions such as hemes and porphyrins [50]. It has recently been demonstrated that two forms of GST bind hypericin very tightly: the form studied here, A1-1, binds hypericin with K_D = 70 nM. Although there are slight differences in the hypericin spectra with respect to the four different environments, within experimental error, the two hypericin enantiomers yield identical spectra when they are in the *same* chiral environment.

Figure 7.4 presents the fluorescence upconversion traces for hypericin in S-2-butanol on a 100-ps time scale. The rising component is the signature we have attributed to excited-state intramolecular H-atom transfer [51]. Within experimental error, this component is present for racemic hypericin in DMSO and for the hypericin enantiomers in S-2-butanol in the same amount and with the same time constant. This is in stark contrast to the recent study where it has been shown that 5,8-dicyano-2-naphthol has different emission spectra and excited-state proton transfer kinetics in either R- or S-2-butanol than in racemic 2-butanol [52].

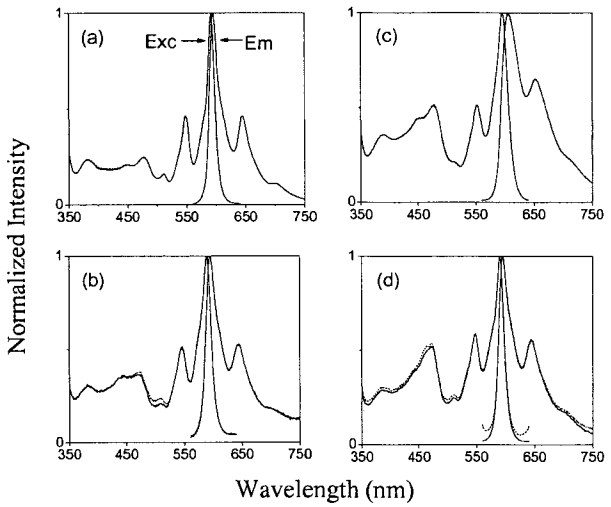

Figure 7.3: Steady state excitation (left column) and emission (right column) spectra of hypericin 1 (solid line) and hypericin 2 (dashed line) in (a) (s)-2-butanol; (b) γ-cyclodextrin; (c) HSA; and (d) GST. For all excitation spectra, the emission was collected at 650 nm; and for all emission spectra, the excitation monochromator was set at 550 nm.

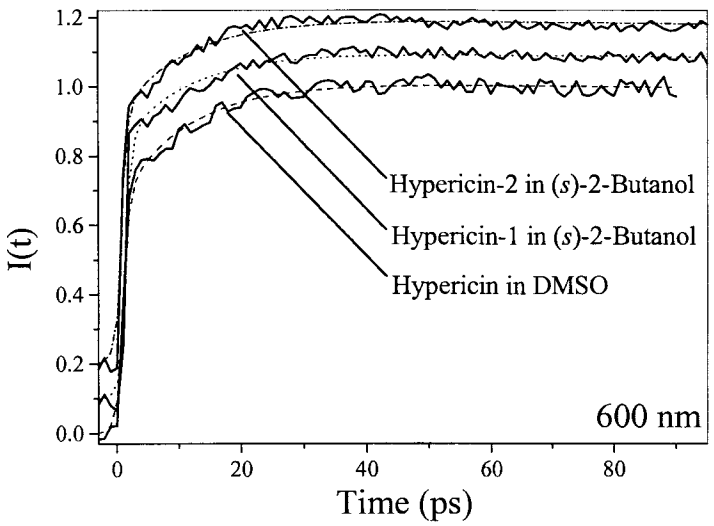

Figure 7.4: Fluorescence upconversion trace for hypericin in DMSO and for the two hypericin enantiomers in *S*-2-butanol at 600 nm. λ_{ex} = 407 nm. The traces are offset vertically with respect to each other to facilitate visual comparison. They can be fit globally with a rising component of 11 ps. This component represents about 30% of the signal.

Conclusions

Falk and coworkers have separated diastereomeric derivatives of hypericin and have discussed the barrier to their interconversion [53-55]. We present here the first direct separation of the enantiomers depicted in Figure 7.1. This study was motivated by the question of whether the rich and complicated spectra of hypericin can be attributed to ground-state heterogeneity. *Ab initio* quantum mechanical calculations [38] and NMR experiments [37, 56] suggest that there is only one species in the ground state. Within experimental error, there is no difference between steady-state spectra of the two enantiomers in any of the systems considered: (S)-(+)-2-butanol, γ-cyclodextrin, HSA, and GST. Nor is there any difference in the excited-state H-atom transfer kinetics of the two enantiomers in (S)-(+)-2-butanol. This is consistent with the emerging picture that the rich and extended absorption spectrum of hypericin is not a result of ground-state heterogeneity. It is also consistent with the observation that the spectra and photophysics of hypericin are generally insensitive to environments in which it does not aggregate.

Acknowledgements

DWA was supported by the National Institutes of Health, NIH R01 GM53825-06. We thank Mr. Pramit Chowdhury for technical assistance. We thank Professor W. Atkins and Mr. Doug Lu for samples of the GST and for furnishing its binding constant with hypericin.

References

(1) Meruelo, D., Lavie, G., Lavie, D. (1988) Therapeutic agents with dramatic antiretroviral activity and little toxicity at effective doses: Aromatic polycyclic diones hypericin and pseudohypericin. *Proc. Natl. Acad. Sci. USA* **85**, 5230-5234.

(2) Lenard, J., Rabson, A., Vanderoef, R. (1993) Photodynamic inactivation of infectivity of human immunodeficiency virus and other enveloped viruses using hypericin and rose

bengal: Inhibition of fusion and syncytia formation. *Proc. Natl. Acad. Sci. USA* **90**, 158-162.

(3) Hudson, J.B., Zhou, J., Chen, J., Harris, L., Yip, L., Towers, G.H.N. (1994) Hypocrella Bambuase is phototoxic to human immunodeficiency virus. *Photochem. Photobiol.* **60**, 253-255.

(4) Couldwell, W.T., Gopalakrishna, R., Hinton, D.R., He, S., Weiss, M.H., Law, R.E., Apuzzo, M.L. (1994) Hypericin: A potential sntiglioma therapy. *Neurosurgery* **35**, 705-710.

(5) Anker, L., Gopalakrishna, R., Jones, K.D., Law, R.E., Couldwell, W.T. (1995) Hypericin in adjuvant brain tumor therapy. *Drugs Fut.* **20**, 511-517.

(6) Zhang, W., Law, R.E., Hinton, D.R., Couldwell, W.T. (1997) Inhibition of human malignant glioma cell motility and invasion in vitro by hypericin, a potent protein kinase C inhibitor. *Cancer Lett.* **120**, 31-38.

(7) Linde, K., Ramirez, G., Mulrow, C.D., Pauls, A., Weidenhammer, W., Melchart, D. (1996) St. John's Wort for depression—An overview and meta-analysis of randomised clinical trials. *Br. Med. J.* **313**, 253-257.

(8) Suzuki, O.K., Oya, M., Bladt, S., Wagner, H. (1984) Inhibition of monoamine oxidase by hypericin. *Planta Medica* **50**, 272-274.

(9) Takahashi, I.N.S., Kobayashi, E., Nakano, H., Suziki, K., Tamaoki, T. (1989) Hypericin and pseudohypericin specifically inhibit protein kinase C: Possible relation to their antiretroviral activity. *Biochem. Biophys. Res. Commun.* **165**, 1207-1212.

(10) Andreoni, A., Colasanti, A., Colasanti, P., Mastrocinique, M., Riccio, P., G., R. (1994) Laser photosensitization of cells by hypericin. *Photochem. Photobiol.* **59**, 529-533.

(11) Thomas, C., MacGill, R.S., Miller, G.C., Pardini, R.S. (1992) Photoactivation of hypericin generates singlet oxygen in mitochondria and inhibits succinoxidase. *Photochem. Photobiol.* **55**, 47-53.

(12) Vandenbogaerde, A.L., Delaey, E.M., Vantieghem, A.M., Himpens, B.E., Merlevede, W.J., de Witte, P.A. (1998) Cytotoxicity and antiproliferative effect of hypericin and derivatives after photosensitization. *Photochem. Photobio.* **67**, 119-125.

(13) Agostinis, P., Donella-Deana, A., Cuveele, J., Vandenbogaerde, A., Sarno, S., Merlevede, W., de Witte, P. (1996) A comparative analysis of the photosensitized inhibition of growth-factor regulated protein kinases by hypericin-derivatives. *Biochem. Biophys. Res. Commun.* **220**, 613-17.

(14) Vandenbogaerde, A.L., de Witte, P.A. (1996) Hypericin as a natural photosensitizer with cytotoxic and antitumor effects. *Phytother. Res.* **10**, S150-S152.

(15) Vandenbogaerde, A.L., Cuveele, J.F., Proot, P., Himpens, B.E., Merlevede, W.J., deWitte, P.A. (1997) Differential cytotoxic effects induced after photosensitization by hypericin. *J. Photochem. Photobio. B-Biology* **38**, 136-142.

(16) Mirossay, A., Mirossay, L., Tothova, J., Miskovsky, P., Onderkova, H., Mojzis, J. (1999) Potentiation of hypericin and hypocrellin-induced phototoxicity by omeprazole. *Phytomedicine* **6**, 311-317.

(17) Mirossay, L., Mirossay, A., Kocisova, E., Radvakova, I., Miskovsky, P., Mojzis, J. (1999) Hypericin-induced phototoxicity of human leukemic cell line HL-60 is potentiated by omeprazole, an inhibitor of H^+K^+-ATPase and 5'-(N,N-dimethyl)-amiloride, an inhibitor of Na^+/H^+ exchanger. *Phys. Res.* **48**, 135-141.

(18) Mirossay, A., Mojzis, J., Tothova, J., Hajikova, M., Lackova, A., Mirossay, L. (2000) Hypocrellin and hypericin-induced phototoxicity of HL-60 cells: apoptosis or necrosis? *Phytomedicine* **7**, 471-476.

(19) Mirossay, A., Onderkova, H., Mirossay, L., Sarissky, M., Mojzis, J. (2001) The effect of quercetin on light-induced cytotoxicity of hypericin. *Phys. Res.* **50**, 635-637.

(20) Mirossay, A., Mirossay, L., Sarissky, M., Papp, P., Mojzis, J. (2002) Modulation of the phototoxic effect of hypericin in human leukemia CEM cell line by N-ethylmaleimide, amiloride and omeprazole. *Phys. Res.* **51**, 641-644.

(21) Duran, N., Song, P.S. (1986) Hypericin and its photodynamic-action. *Photochem. Photobio.* **43**, 677-680.

(22) Lown, J.W. (1997) Photochemistry and photobiology of perylenequinones. *Can. J. Chem.* **75**, 99-119.

(23) Diwu, Z. (1995) Novel therapeutic and diagnostic applications of hypocrellins and hypericins. *Photochem. Photobiol.* **61**, 529-539.

(24) Kraus, G.A., Zhang, W.J., Fehr, M.J., Petrich, J.W., Wannemuehler, Y., Carpenter, S. (1996) Research at the interface between chemistry and virology: Development of a molecular flashlight. *Chem. Rev.* **96**, 523-535.

(25) Falk, H. (1999) From the photosensitizer hypericin to the photoreceptor stentorin - The chemistry of phenanthroperylene quinones. *Ang. Chem.-International Edition* **38**, 3117-3136.

(26) Gai, F., Fehr, M.J., Petrich, J.W. (1993) Ultrafast excited-state processes in the antiviral agent hypericin. *J. Am. Chem. Soc.* **115**, 3384-3385.

(27) Gai, F., Fehr, M.J., Petrich, J.W. (1994) Role of solvent in excited-state proton-transfer in hypericin. *J. Phys. Chem.* **98**, 8352-8358.

(28) Gai, F., Fehr, M.J., Petrich, J.W. (1994) Observation of excited-state tautomerization in the antiviral agent hypericin and identification of its fluorescent species. *J. Phys. Chem.* **98**, 5784-5795.

(29) Das, K., English, D.S., Fehr, M.J., Smirnov, A.V., Petrich, J.W. (1996) Excited-state processes in polycyclic quinones: The light-induced antiviral agent, hypocrellin, and a comparison with hypericin. *J. Phys. Chem.* **100**, 18275-18281.

(30) Das, K., English, D.S., Petrich, J.W. (1997) Deuterium isotope effect on the excited-state photophysics of hypocrellin: Evidence for proton or hydrogen atom transfer. *J. Phys. Chem. A* **101**, 3241-3245.

(31) Das, K., English, D.S., Petrich, J.W. (1997) Solvent dependence on the intramolecular excited-state proton or hydrogen atom transfer in hypocrellin. *J. Am. Chem. Soc.* **119**, 2763-2764.

(32) Das, K., Smirnov, A.V., Snyder, M.D., Petrich, J.W. (1998) Picosecond linear dichroism and absorption anisotropy of hypocrellin: Toward a unified picture of the photophysics of hypericin and hypocrellin. *J. Phys. Chem. B* **102**, 6098-6106.

(33) Das, K., Dertz, E., Paterson, J., Zhang, W., Kraus, G.A., Petrich, J.W. (1998) Hypericin, hypocrellin, and model compounds: Steady-state and time-resolved fluorescence anisotropies. *J. Phys. Chem. B* **102**, 1479-1484.

(34) Das, K., Smirnov, A.V., Wen, J., Miskovsky, P., Petrich, J.W. (1999) Photophysics of hypericin and hypocrellin A in complex with subcellular components: Interactions with human serum albumin. *Photochem. Photobio.* **69**, 633-645.

(35) Das, K., Ashby, K.D., Wen, J., Petrich, J.W. (1999) Temperature dependence of the excited-state intramolecular proton transfer reaction in hypericin and hypocrellin A. *J. Phys. Chem. B* **103**, 1581-1585.

(36) English, D.S., Das, K., Ashby, K.D., Park, J., Petrich, J.W., Castner, E.W.J. (1997) Confirmation of excited-state proton transfer and ground-state heterogeneity in hypericin by fluorescence upconversion. *J. Am. Chem. Soc.* **119**, 11585-11590.

(37) Smirnov, A., Fulton, D.B., Andreotti, A., Petrich, J.W. (1999) Exploring ground-state heterogeneity of hypericin and hypocrellin A and B: Dynamic and 2D ROESY NMR study. *J. Am. Chem. Soc.* **121**, 7979-7988.

(38) Petrich, J.W., Gordon, M.S., Cagle, M. (1998) Structure and energetics of ground-state hypericin: Comparison of experiment and theory. *J. Phys. Chem. A* **102**, 1647-1651.

(39) English, D.S., Zhang, W., Kraus, G.A., Petrich, J.W. (1997) Excited-state photophysics of hypericin and its hexamethoxy analog: Intramolecular proton transfer as a nonradiative process in hypericin. *J. Am..Chem. Soc.* **119**, 2980-2986.

(40) English, D.S., Das, K., Zenner, J.M., Zhang, W., Kraus, G.A., Larock, R.C., Petrich, J.W. (1997) Hypericin, hypocrellin, and model compounds: Primary photoprocesses of light-induced antiviral agents. *J. Phys. Chem. A.* **101**, 3235-3240.

(41) Smirnov, A.V., Das, K., English, D.S., Wan, Z., Kraus, G.A., Petrich, J.W. (1999) Excited-state intramolecular H atom transfer of hypericin and hypocrellin A investigated by fluorescence upconversion. *J. Phys. Chem. A* **103**, 7949-7957.

(42) Peters, T. (1985) Serum albumin. *Adv. Protein. Chem.* **37**, 161-245.

(43) Fehske, K.J., Muller, W.E., Wollertt, U. (1979) The lone tryptophan residue of human serum albumin as part of the specific warfarin binding site. *Mol. Pharmacol.* **16**, 778-779.

(44) Davila, J., Harriman, A. (1990) Photochemical and radiolytic oxidation of a zinc porphyrin bound to human serum albumin. *J. Am. Chem. Soc* **112**, 2686-2690.

(45) Miskovsky, P., Jancura, D., Sanchez-Cortes, S., Kocisova, E., Chinsky, L. (1998) Antiretrovirally active drug hypericin binds the IIA subdomain of human serum albumin: Resonance Raman and surface-enhanced Raman spectroscopy study. *J. Am. Chem. Soc.* **120**, 6374-6379.

(46) Miskovsky, P., Hritz, J., Sanchez-Cortes, S., Fabriciova, F., Ulicny, J., Chinsky, L. (2001) Interaction of hypericin with serum albumins: Surface-enhanced Raman spectroscopy, resonance Raman spectroscopy and molecular modeling study. *Photochem. Photobio.* **74**, 172-183.

(47) Senthil, V.L.J.W.G.C.A.G.L.I. (1992) Photosensitization of aqueous model systems by hypericin. *Biochem. Biophys. Acta.* **1115**, 192-200.

(48) Kohler, M., Gafert, J., Friedrich, J., Falk, H., Meyer, J. (1996) Hole-burning spectroscopy of proteins in external fields: Human serum albumin complexed with the hypericinate ion. *J. Phys. Chem.* **100**, 8567-8572.

(49) Falk, H., Meyer, J. (1994) On the homo- and heteroassociation of hypericin. *Monatsh. Chem.* **125**, 753-62.

(50) Adman, E.T., Le Trong, I., Stenkamp, R.E., Nieslanik, B.S., Dietze, E.C., Tai, G., Ibarra, C., Atkins, W.M. (2001) Localization of the C-terminus of rat glutathione S-transferase A1-1: Crystal structure of mutants W21F and W21F/F220Y. *Proteins: Struc. Func. Gen.* **42**, 192-200.

(51) Petrich, J.W. (2000) Excited-state intramolecular H-atom transfer in nearly symmetrical perylene quinones: hypericin, hypocrellin, and their analogues. *Int. Rev. Phys. Chem.* **19**, 479-500.

(52) Solntsev, K.M., Tolbert, L.M., Cohen, B., Huppert, D., Hayashi, Y., Feldman, Y. (2002) Excited-state proton transfer in chrial environments. 1. Chiral solvents. *J. Am. Chem. Soc* **124**, 9046-9047.

(53) Tran, H.T.N., Falk, H. (2002) Concerning the chiral discrimination and helix inversion barrier in hypericinates and hypericin derivatives. *Monatshefte Fur Chemie* **133**, 1231-1237.

(54) Altmann, R., Etzlstorfer, C., Falk, H. (1997) Chiroptical properties and absolute configurations of the hypericin chromophore propeller enantiomers. *Monatshefte Fur Chemie* **128**, 785-793.

(55) Altmann, R., Etzlstorfer, C., Falk, H. (1997) Concerning the enantiomerization barrier of hypericin. *Monatshefte Fur Chemie* **128**, 361-370.

(56) Wen, J., Chowdhury, P., Fulton, D.B., Datta, A., Das, K., Andreotti, A.H., Petrich, J.W. (2003) Does solvent influence the ground-state tautomeric population of hypericin? *Photochem. Photobio.* **77**, 5-9.

CHAPTER 8. CONCLUSIONS

The major theme of this dissertation has been solvation dynamics, especially as pertains to room temperature ionic liquids. The studies presented here (Chapters 3-5) of these increasingly important and useful solvents have advanced the description of their dynamic solvation behaviors and how best to model them. Chapter 3 studies a number of RTILs sharing the same cation, 1-butyl-3-methylimidazolium. The major result is the comparison of an RTIL's rapid initial solvation component with that of butylimidazole, a neutral organic counterpart of the cation. At early times, the correlation function curves overlap, and this result is qualitatively reproduced with two different ultrafast spectroscopy techniques, stimulated emission and fluorescence upconversion. This leads to the conclusion that the rapid initial solvation of the probe molecule coumarin 153 is dominated by the cation. Although previous studies had indicated that the generally smaller anion was more likely to respond first,[1] it is intuitively reasonable that the polar cation will respond to a dipole more than the spherical charges of the anions will. Of the four RTILs studied here, the only one without high spherical symmetry is the bis[trifluoromethane-sulfonimide]. More work needs to be done to elucidate the contributions of this and similar anions to the overall solvation response.

Another important result of this work is the quantitative difference between the stimulated emission and upconversion techniques. Comparison between the resultant spectra suggests that there is an absorbing species contributing to the stimulated emission response. This excited state absorbance slows the decay and rise times of the measured response, artificially lengthening the observed solvation time scale. Upconversion is the more reliable technique for these types of measurements and will be used exclusively in the future.

Chapter 4 is an extension of the study in Chapter 3. A wider range of RTIL cations were studied here, all based on alkylimidazolium cations. Again, an initial fast time

component of solvation is seen, consistent with the previous data. We attempted a comparison of a bulky tetraalkylphosphonium ionic liquid previously examined elsewhere[2] with a neutral counterpart, tributylphosphine. We did not, however, see a correlation between the two as we had with butylimidazole and a 1-butyl-3-methylimidazolium. This is probably because the tributylphosphine is significantly more polar than the tetraalkylphosphonium, and it is therefore not a good predictor of the RTIL's behavior. We also report a method of determining the contribution of coumarin 153's intramolecular reorganization energy to the reorganization energy of the entire system. This is accomplished by a linear regression of experimentally measured reorganization energies in solvents with a wide range of polarities and dielectric constants. This method is an alternative to calculating the "time-0" emission.[3]

Chapter 5 asks whether dielectric relaxation, representing nuclear vibrations and electron cloud readjustments, can predict solvation behaviors without including conductivity effects, representing translational motions of the ions. Two model systems with known dielectric spectra were investigated: the room temperature ionic liquid ethylammonium nitrate[4] and the aqueous ionic solution of 1.05 M sodium perchlorate.[5] Correlation functions were calculated based on dielectric information with and without conductivity and compared to experimental correlation functions. For both systems, the calculated functions using only dielectric information were accurate within experimental error. Furthermore, neglecting conductivity resulted in a more accurate result for the perchlorate solution and a slightly more accurate result for the ethylammonium nitrate. This suggests that room temperature ionic liquids can be modeled using simple dielectric continuum models. Investigation of more systems needs to be done to further explore this conclusion.

In Chapter 6, the focus shifts from room temperature ionic liquids to proteins. We were able to characterize a complex of coumarin 153 and apomyoglobin that appears to be a viable system for studying protein solvation dynamics. Molecular dynamics simulations,

circular dichroism, and polarized fluorescence decay measurements all suggest that coumarin 153 strongly binds in the active pocket of apomyoglobin, replacing the heme. We obtained dissociation constants of 5.65 ± 0.25 μM and 13 ± 2 μM using a Job's plot and capillary electrophoresis, respectively, again indicating tight binding. Furthermore, the Job's plot indicates a 1:1 stoichiometry in the coumarin 153 and apomyoglobin complex. This complex will be used in future experiments to study protein solvation dynamics and to compare with theory.

The final chapter, Chapter 7, reports the first separation of hypericin's enantiomers and a study of their photophysics in chiral environments. The initial purpose for this study was to use the enantiomers to investigate chiral room temperature ionic liquids. Unfortunately, we were unable to obtain optically pure chiral RTILs, so we looked at traditional chiral environments instead. Within experimental error, no differences between the enantiomers' steady-state spectra were observed in any of the four chiral environments. Also, there is no difference in their excited-state H-atom transfer kinetics in (S)-(+)-2-butanol. Although this study diverges from its original purpose, its results can be used to support earlier conclusions about hypericin. Consistent with previous experimental[6] and theoretical results,[7] the lack of a difference between the two enantiomers suggests that the unusual extended absorption spectrum of hypericin is not due to ground state heterogeneity.

References

(1) Karmakar, R.; Samanta, A. *J. Phys. Chem. A* **2002**, *106*, 6670.

(2) Arzhantsev, S.; Ito, N.; Heitz, M.; Maroncelli, M. *Chem. Phys. Lett.* **2003**, *381*, 278.

(3) Fee. R. S.; Maroncelli, M. *Chem. Phys.* **1994**, *183*, 235.

(4) Weingartner, H.; Knocks, A.; Schrader, W.; Kaatze, U. *J. Phys. Chem. A* **2001**, *105*, 8646.

(5) Barthel, J.; Neueder, R. *Electrolyte data collection: tables, diagrams, correlations,*

and literature survey; DECHEMA: Frankfurt, Germany, 1995.

(6) Smirnov, A.; Fulton, D. B.; Andreotti, A.; Petrich, J. W. *J. Am. Chem. Soc.* **1999**, *121*, 7979.

(7) Petrich, J. W.; Gordon, M. S.; Cagle, M. *J. Phys. Chem. A* **1998**, *102*, 1647.

ACKNOWLEDGEMENTS

It goes without saying that none of the work included here would have been possible without my major professor, Dr. Jacob Petrich. It has been a pleasure to know and work with him, and I am grateful for how he challenged me yet allowed me the flexibility to pursue my own interests at my own pace. I will always appreciate and admire how he treats each student as an individual. His guidance and encouragement will be remembered throughout my career.

My gratitude goes out to all my committee members: Dr. Mei Hong, Dr. Hans Stauffer, Dr. Mark Hargrove, and Dr. Xueyu Song. I am happy to have selected such a wonderful group of professors to help guide my progress and keep me in line.

This work could not have been completed without my lab mates. Most of our research projects have been completed as a team, and they have all been wonderful team players. Our postdoc, Dr. Mintu Halder, has been absolutely invaluable in keeping the lab up and running. It constantly amazes me how he can fix in five minutes what I've been working on for an hour, as well as his willingness to do so! The graduate student who has been here with me the longest, Prasun Mukaherjee, has demonstrated endless enthusiasm for the work, and is always willing to pick up the slack if I am running behind, and for that I am truly grateful. It has been my pleasure to meet the newest additions to our lab, Sayantan Bose and Ram Adhikary. I am confident that many wonderful things will come out of our lab while they are working here. I also want to thank our current undergraduate students, Alice Hurd and Alex Reynolds, for bringing a breath of fresh air into the lab.

Members of the lab group who have moved on have also been invaluable in my education. Dr. Pramit Chowdhury, from whom I "inherited" the lab, was a patient teacher with a gift for encouragement. I cannot imagine having started my graduate career without him. Tessa Calhoun and Erin Campbell were two amazing undergraduate students with gifts

for research which will almost certainly surpass my own. Their energy and dedication has been an inspiration for me. My thanks also goes to two postdocs who have come and gone, Dr. Ranjan Das and Dr. Govindarajan Krishnamoorthy (GK). Although our time together was limited, I appreciate their support.

Much of my research could not have been done (or could not have been done as well) without collaborations and help from others. Dr. Daniel Armstrong and his students supplied many of the room temperature ionic liquids, as well as sharing their knowledge of the subject. Special thanks goes to Dr. Jared Anderson, Dr. Jie Ding, and Jeffrey Crank for their synthesis and purification efforts. Jared especially deserves my gratitude for fielding an endless supply of questions from me and for sharing his passion for RTILs. Another member of their group, Dr. Tom Lin Xiao, did excellent work separating hypericin enantiomers for us.

Dr. Xueyu Song has single-handedly provided much of the theoretical data included in this dissertation, and I thank him for sharing his expertise in molecular dynamics simulations with me. He has been very kind in answering questions and being supportive throughout my graduate career.

Dr. Mark Hargrove and his research group have been our protein specialists, and I appreciate all the time and effort they have expended. I have worked with them on projects beyond what appears here, and they have always been very accommodating. I especially thank Dr. Suman Kundu for the hours he spent making and purifying protein.

I also offer my thanks to everyone not listed here who has allowed me to invade their space and use their equipment. Your time, patience, and generosity are greatly appreciated.

Finally, I have to thank the chemistry department as a whole, especially all the wonderful secretaries, the chemistry store, and the machine shop. You are the ones who truly keep the department running.